UNIVERSITÀ DEGLI STUDI DI PALERMO

DIPARTIMENTO DI FISICA E CHIMICA

DOTTORATO DI RICERCA IN FISICA – XXIII CICLO

ROLE OF WATER IN SACCHARIDE BASED BIOPRESERVATION

SSD FIS/07

DR. SERGIO GIUFFRIDA

TUTOR: PROF. A. CUPANE

COORDINATORE: PROF. A. CUPANE

Contents

Chapter 1

Introduction

In this thesis a study, both experimental and computational, on saccharide–based biopreservation is presented, with a particular focus on the role of water in the process. Experiments and simulations have been performed on model systems constituted by a protein (myoglobin) embedded in amorphous solid saccharide–water matrices, which may contain also cosolutes to alter their properties. This study has a dual aim:

(a) The understanding of the role of the hydrogen–bond (HB) network present in the saccharide matrix, and its modifications induced by solute content and nature, in the process of biopreservation. Many, among the hypotheses currently discussed to explain the effectiveness of sugars on preservation of biomolecules, attribute a outstanding relevance to water present in the matrix and its relation with the sugar. The hypothesis here supported is that the HB network, its strength and its relation with the embedded biomolecules, plays the leading role in the biopreservation mechanism. The different properties of the HB networks generated by different saccharides would be also at the basis of the peculiar efficiency of trehalose with respect to the other sugars. To this aim, experiments have been performed with variable water content and protein–sugar ratio, as well as by including cosolutes able to perturb the HB network properties in the system. Particular attention has been paid in the evaluation of the matrix properties along with those of the embedded protein.

(b) The deepening of the knowledge on the mechanism of protein preservation, in particular with respect to trehalose efficiency, by a combined set of studies, which explore different spatial and temporal scales. Many results have been reported in the literature for model systems studied with a lot of techniques. This resulted in a bunch of hypotheses, of which many are likely to hold true only in the systems they have been formulated. At variance,

adopting a multi–technique approach would enable to draw a consistent picture of trehalose biopreservation process.

From an experimental point of view, the study was performed with Fourier–Transform Infrared Spectroscopy (FTIR) and Small Angle X–Ray Scattering (SAXS). FTIR gives information about the structure of the sample at atomistic level and on the strength of intermolecular interactions, as probed by alteration of molecular vibration frequencies. Classical FTIR spectroscopy is not generally used for the study of protein dynamics. Here, the dynamics information is conveyed by the alteration of band shapes and position upon perturbation of the sample. As such, it can be studied by analysing the behaviour of infrared bands as a function of temperature.

FTIR measurements were performed in trehalose–water and myoglobin–trehalose–water systems containing various cosolutes with the aim to characterise how they alter the relative populations of different classes of water molecules present in the samples, hence how the HB network is influenced. The knowledge acquired from the study of cosolute–containing trehalose samples has been applied to study the behaviour of other saccharide matrices (sucrose, maltose, lactose, raffinose) both in the presence and in the absence of proteins and at different protein sugar ratios. FTIR measurements as a function of temperature has been performed to complete previous studies and to allow a better comparison with simulative and experimental data on analogous systems present in literature.

Classical, state of the art, Molecular Dynamics (MD) simulation have been performed on binary trehalose–water and ternary myoglobin–trehalose–water systems at different temperatures, in the range 50-400 K. A deeper understanding of the different roles of sugar and water molecules is obtained by comparing the outcomes of simulations of the above ternary systems with those of the same systems in which the dynamics of one of the components (water) has been constrained. This has been made either by blocking both the translational and the rotational motions of the molecules, or by blocking only translations, while allowing the water molecule to rotate, or by restraining the water motions by means of a harmonic potential.

The results from MD and FTIR allow to study the relation between protein and matrix structure and dynamics at molecular level. However these techniques are not really suitable to obtain information on larger structural alterations and in particular, because of their spatial scale, they are not able to mark the presence of micro- or mesoscopic inhomogeneities. We therefore performed SAXS measurements on binary (saccharide-water) and ternary (MbCO-

saccharide-water) systems with the aim to detect the effects of the embedded protein on a larger spatial scale. SAXS was chosen since it is a most suitable technique to investigate micro-nano structures having electronic densities that differ from their surrounding.

This thesis is structured as follow. After a general introduction on the preservation of biological molecules and on the actual state of affairs with biopreservation by saccharides (chapter 2), a presentation on the chemical and biological properties of the biomolecules utilised is given (chapter 3), which includes also a discussion on the effects of cosolutes on solutions and hydrated matrices containing biological structures (Hofmeister effects, section 3.3). The experimental and simulative techniques are presented (chapter 4), and then the results for each technique are shown and discussed (chapters 5 for FTIR, 6 for MD and 7 for SAXS). Chapter 8 is a global discussion on the results, where also some general conclusions are drawn.

Chapter 2

Biopreservation and role of saccharides

Preservation of biological matter (biopreservation) is a relevant topic, in particular for its implications in food industry, pharmaceutics and medicine. Food preservation, in particular, has been an important issue for mankind since the beginning of civilisation, and sugars have been identified quite early as effective preservers (think about candies or fruit jams). Nowadays the traditional sugar preservation is relevant mainly for the organoleptic properties it bestows on the preserved product, while industrial preservation has moved to more efficient additives and techniques.

The interest on saccharide–based preservation has indeed shifted from rough storage to the recovery of biological molecules in functionally active forms. This has been triggered by the discovery that many organisms, both vegetal and animal, can overcome extreme stress conditions by putting themselves in a state of suspended animation (*cryptobiosis*). While entering in this state, an increase of sugar concentration in their tissues can be observed. In particular some plants (called resurrection plants like the rose of Jericho, gen. *Selaginella* and *Anastatica*, see fig. 2.1 a) and animals (tardigrades, see 2.1 b) use to produce large quantities of a particulare sugar, trehalose (see 3.1), which appears to be most effective in biostructure stabilisation following exposition to drought or extreme temperatures [1, 2].

Trehalose is effective in the protection of various biological molecules and tissues: it has been profitably used to preserve proteins, both structural and enzymes, lipidic membranes and more complex structures like whole cells and vaccines [2–5]. Notwithstanding this particular effectiveness of trehalose, a lot of sugars do have bioprotective properties and are used as bioprotectant by different organisms. Actually, this could be expected due to the rather homogeneous chemical structure of the saccharides, hence their similar hydrogen bonding capability.

(a) *Anastatica* in active (right) and dormant (left) form

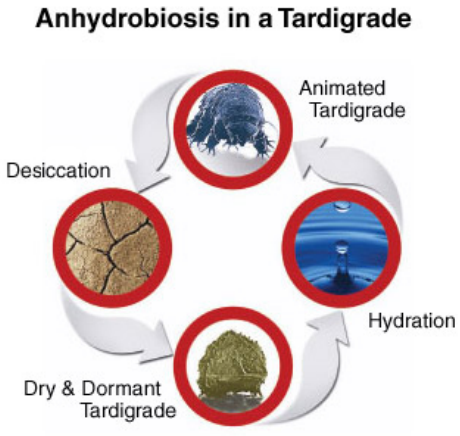

(b) Vital cycle of a tardigrade

Figure 2.1: Two organisms able to go in anhydrobiosis: Rose of Jericho (a) and tardigrade (b)

The differences with other sugars are however evident in condition of extreme stress: while all the sugars have protective properties, only trehalose is able to preserve in the limit conditions [6].

Actually, the mechanism of bioprotection by trehalose is not clearly elucidated. Large efforts are currently addressed to understand it and, more in general, the mechanisms regulating the biopreservation by saccharides, both *in vivo* and *in vitro*, leading to some hypotheses. Taking into account that biopreservation is more efficient in glassy matrices, trehalose action has been related to the higher value of its glass transition temperature (T_g) in comparison with other disaccharides [7]. The relationship between water, sugar and biomolecules has been widely investigated, attributing the preserving effects to specific interactions between sugar and biological systems in the dry state (*Water Replacement* hypothesis [8]) or among sugar, protein and residual water at the interface, preserving the native solvation (*Water Entrapment* or sugar preferential exclusion) [9, 10]. It has also been proposed that the high viscosity of sugar matrices could be at the basis of a reduction of large–scale internal protein motions, which leads to loss of structure and denaturation [11]. It has been suggested that the rigid carbon skeleton of the disaccharides impose sterical restraints which may influence the dynamic properties of the embedded molecule, revealing the importance of the spatial configuration of each disaccharide [12]. The above hypotheses are not mutually exclusive. The formation of a glassy state does not imply hydrogen bonding, as evidenced by measurements on dextran [13]. The efficiency of trehalose may be due to the ability of forming glassy structures in a wide hydration

range, along with the hydrogen bond capability. Actually, trehalose was found more effective than other disaccharides at high temperatures, when direct interactions with the macromolecule play a stronger role [14]. However, this is not consistent with results on raffinose, which is less effective than other sugars [15], although it has a glass transition temperature comparable with that of trehalose, along with larger hydrogen bonding potential [16].

An approach based on structural studies of trehalose-water binary systems, proposes that the polymorphism of trehalose, both in the crystalline and amorphous states, is at the basis of its effectiveness [17]. The slow formation of dihydrate trehalose crystals, by water evaporation at high temperature and low moisture, would keep water molecules in the same HB network as in the solvated trehalose, capturing the residual water molecules without disrupting the native structure of the biological systems; further slow dehydration would produce anhydrous trehalose, hence protecting the biostructures by inhibiting translational motions, preserving the active molecular conformations. This process has bioprotective effects because of the existence of reversible paths among the different states, avoiding at the same time water crystallisation.

The very strong trehalose-water interaction may play a role in determining trehalose effectiveness. Raman and neutron scattering experiments [18, 19] on binary systems revealed the disruption of the tetrahedral network of water molecules on addition of trehalose, with a consequent reordering of water molecules around the saccharide, which impairs ice formation and improves preservation. The same authors reported the formation of long–lived water bridges in very concentrated saccharide solutions, which slow water dynamics [20]. Despite being a phenomenon common to many saccharides, above a definite concentration trehalose appears to reduce the water diffusion [20] and increase the water residence time to a larger extent than its homologues [21, 22].

Incoherent neutron scattering experiments showed that the amplitude of the local, high frequency dynamics of the glass correlates with the ability to impart protein stability. Local relaxations are suppressed and collective vibrations, which occur with timescales of a nanosecond and faster, are “stiffened”, in correspondence with the coupling of dynamics of the protein and the glass [23]. This relationship suggested that a time–dependent friction approach is valuable in understanding the effect of solvent dynamics on protein motions. An effective preservation medium will strongly suppress the local, fast motions that appear to be precursors for protein denaturation or other deactivation pathways [23].

Raman scattering experiments were performed also on protein-sugar solutions [24–28]. By

comparing trehalose, sucrose and maltose containing systems, it was found out how trehalose is the most effective in stabilising the folded secondary structure of the protein [24]. The experiments were carried out both in the low-frequency range and in the amide I band region, both providing a microscopic description of the process of thermal denaturation. In particular, amide I band is very sensitive to the unfolding of the secondary structure, whereas the low-frequency range provides significant information on protein dynamics and on coupling of protein and hydration-water dynamics. By comparing protein-trehalose solutions at different composition [24, 25, 29], it has been observed that the main effect of trehalose is related, once again, to its capabilities to perturb the tetrahedral organization of water molecules and to strengthen intermolecular O-H interactions responsible for the stability of tertiary structure [27]. In this way, the thermal stability of the HB network of water contributes to the stabilisation of the native tertiary structure and inhibits the first stage of denaturation, that is, the transformation of the tertiary structure into a highly flexible state with intact secondary structure. Trehalose was also observed to be the best stabiliser of the folded secondary structure, in the transient tertiary structure, leading to a high–temperature shift of the unfolding process (i.e. the second stage of denaturation) [24].

Proteins embedded in saccharide amorphous matrices at very high sugar concentration have been so far extensively studied by Neutron Scattering, Mössbauer spectroscopy, Flash Photolysis, MD simulations [30–39]. At high sugar concentration, the dynamics of a protein is highly inhibited; moreover, the inhibition is markedly dependent on the traces of residual water [32]. In particular, MD simulations in protein–containing systems suggested that the protein surface is directly connected to an HB network including trehalose and water, in which the fraction of water molecules involved increases upon dehydration, so as the average number of hydrogen bonds in which each water molecule is involved. These observations suggest that the water replacement and water entrapment hypotheses need not be mutually exclusive, as pointed out also by recent MD simulations showing that trehalose molecules assemble in distinctive clusters on the surface of the protein; the flexibility of the protein backbone is then reduced due to the presence of these sugar patches [40].

These findings, together with FTIR results on carboxy-myoglobin (MbCO) embedded in trehalose matrices at different water content [41–43] suggested that the rigidity of the HB network increases on drying and that this network is mainly responsible for coupling the internal dynamics of the protein to that of the low–water matrix [43]. The inhibition of internal pro-

tein dynamics under extreme dryness was therefore explained in terms of a tight anchorage of the protein surface to a stiff matrix: saccharide protect biomolecules not simply by preserving their native solvation, but rather by locking their surface either directly or through bridging water molecules, thus hindering motions. Accordingly, when a strong, extended HB network forms, as in glassy trehalose–water–protein systems, the energy penalty associated with the solvent re-arrangements, needed for large-scale protein internal motions, increases sizably [44], as supported by vibrational echo experiments performed on different hemeproteins in trehalose glasses [45]. In sections 5.2 and 6.1 the relation between protein and solvent dynamics will be discussed in the light of the new results obtained in this work.

The formation of extended HB networks has been rationalized by Terahertz Spectroscopy, an useful tool for probing the collective modes of the water network. In particular, it has been reported that each solute affects in a peculiar way the fast collective network motions of the solvent well beyond the first solvation layer and the total THz absorption depends on both saccharide concentration and number of HB formed with water [46]. This suggests that, under suitable solutes concentration, large-scale collective modes involving wide regions of the sample can set up, such long-range coherence failing if solute particles reduce their participation in hydrogen bonding. The presence of anisotropic structuring of water extending up to three solvation shells away from the sugar has been confirmed also by MD studies [47]. In this respect, light scattering spectra on aqueous solutions of trehalose, recorded in a very wide frequency range [48], indicate the presence of two separate solvent relaxation processes: a slow one, related to the solute dynamics, ascribed to hydrating water, and a fast one ascribed to bulk solvent. These results were confirmed by MD simulations [49] and in presence of protein [50].

From the thermodynamic point of view, the efficiency in bioprotection has been related to the T_g of sugar–water systems [7], although this has been challenged by studies on long term storage, which showed that it is much more important to have a system unable to form crystals than a system with T_g well above the storage temperature [51].

Differential Scanning Calorimetry (DSC) results have shown that the ability of disaccharides to produce a homogeneous glass is independent of the cooling rate [52]. This independence is achieved above a definite critical water/sugar mole ratio, whose value has been found to be 20, 18, and 15 for trehalose, maltose, and sucrose respectively, i.e. the same order reported for the perturbation of the HB network by sugars [18, 19, 24]. It is noteworthy that trehalose binary matrices can exist in a wider hydration range as an homogenous glass, while phase separation

and crystallisation might occur in sucrose also at relatively low water content.

Similar DSC data for various dry protein–saccharide–water systems showed that the presence of protein decrease the T_g extrapolated at zero water content. This would indicate that looser water/disaccharide interactions are present: the protein, competing for water with disaccharide molecules, would reduce the strength of the HB network encompassing the sample, in line with what shown by structural techinques [37,41,52]. At variance, at high–to–intermediate hydration ($\geq$ 5 water/sugar mole ratio), it has been observed that the glass–liquid transition line shifted toward higher hydration, i.e. an increased T_g is present at constant water/saccharide mole ratio. This effect has been found small for small proteins and large for large proteins, marking it as a size effect, and has been attributed to the confinement experienced by the solvent, much more severe in the case of larger than smaller proteins [53].

The increase of protein denaturation temperature (T_{den}) with dehydration has been found to be monotonous for many proteins, reaching also $\sim$70 K above the T_{den} in solution for the large and/or charged proteins. Therefore the extent of protein stabilisation depends also on charge effects, which would strengthen the matrix HB network due to electrostatic interactions with the protein surface.

Moreover, T_{den} and T_g have been found to be linearly correlated, with correlation lines specific for each protein. Hence, collective properties that regulate the glass transition are linearly correlated to local properties involved in the protein denaturation, the stabilisation extent depending on the specific protein–matrix interactions, in agreement with the proposed coupling between protein stability and matrix dynamics. In this respect, the comparison among $T_{den} \div T_g$ correlation plots for various saccharide matrices showed that trehalose acts as a better stabiliser than sucrose, at equal T_g [52,53].

Chapter 3

Biomolecules and cosolutes

3.1 Saccharides: chemical and biological properties

Saccharides or carbohydrates are simple molecules which constitute one of the building blocks of the biological matter. They are organic compounds consisting only of carbon, hydrogen, and oxygen, with a general empirical formula $C_m(H_2O)_n$. Despite their name, carbohydrates are not, chemically speaking, hydrates of carbon, but polyhydroxy–aldehydes or –ketones, i.e. polyalcohols with an aldehyde or ketone group.

Saccharides can exist both as monomeric molecules (monosaccharides, as glucose or fructose), dimers (disaccharides, as sucrose), oligomers (dextrins) and true polymers (starch, cellulose). Due to the monomer structure, which present many possible connection points, oligosaccharides and polysaccharides can be both linear and branched, with a plurality of possible structures, which yield macromolecules able to play a wide number of roles. Polysaccharides serve for energy storage (starch in plants and glycogen in animals), as structural components (cellulose in plants and chitin in arthropod exoskeleton), for cellular identification (antibodies/antigens) or filler/lubricant in the extracellular matrix (proteoglycans). Saccharide monomers are also part of the structure of nucleic acids and coenzimes [54].

Saccharides are also one of the basilar components of food both in the polymeric form, as starch–rich foods (such as cereals, bread, pasta), and in mono– or dimeric form, as sugar–rich food (candies, jams, desserts, soft drinks). Many oligomeric (dextrins) and polymeric saccharides (pectins, alginates, agar) are used as additives to alter the rheology of food. They acts as gelling, thickening or stabilising agents because of their ability to absorb and hold large amounts of water [55].

The work presented in this thesis has been performed mainly with trehalose matrices, whose bioprotective properties have been discussed in chapter 2. Trehalose (α,α–1,1–D–glucopyranosyl–D–glucopyranoside, see fig. 3.1) is a non–reducing disaccharide, whose two glucose subunits are bound through both the anomeric hydroxyls (1,1–bond), giving a symmetric molecule. It was firstly discovered in *ergot*, a parasitic fungus growing on rye, and was long considered a simple energy storage sugar, until it was discovered its widespread presence in many organisms able to undergo anhydrobiosis (see chapter 2). Trehalose is edible for all the organisms which express the enzyme *trehalase*. This latter is designed to hydrolise the α,α–1,1–glycosidic bond, one among the most stable natural glycosidic bond. This great stability confers trehalose a noteworthy resistance against thermal degradation: it can withstand temperatures above 100 °C for months, while e.g. sucrose in the same conditions degrades with caramelisation [1].

Trehalose crystallises in a dihydrate form. These two water molecules are strongly bound bridging the two subunits, which conversely have no direct hydrogen bond between themselves. The need of structural water to attain the crystalline form has an useful side effect: trehalose need moisture to crystallise and in extermely dry environments it preserves very well the amorphous state. The substitution of these water molecules with HB deriving from other source allow trehalose to adapt to different environments, keeping high flexibility and stability with no tendency to fold and separate in nanocrystals. This has been suggested as a factor contributing to the bioprotective effect, because of higher pliability of trehalose to the surface of biostructures, with respect to other sugars [1].

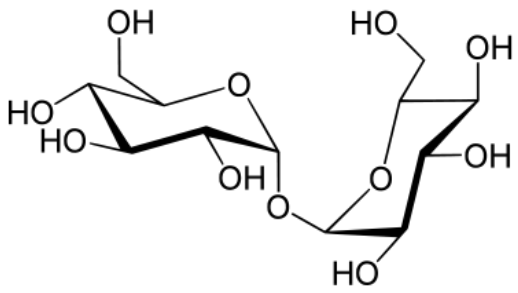

Figure 3.1: Molecular structure of trehalose.

Although most of the present study is performed on trehalose matrices, a comparison with other saccharides is needed to point out how the different matrices influence the behaviour, and the protection, of the embedded protein. For the comparison, three disaccharides (sucrose, maltose and lactose) have been chosen alongside a trisaccharide (raffinose).

Sucrose (α,β–1,2–D–glucopyranosyl–D–fructofuranoside, see fig. 3.2) is disaccharide composed by one glucose and one fructose. It is the most commonly found sugar in human environments, being the well known table sugar, widely used as sweetener. Its biological role is energy storage in plants. From a structural point of view sucrose, as trehalose, has a glycosidic bond

between the anomeric hydroxyls, hence it is not reducing.

However the asymmetric glycosidic bond of sucrose is about 25-fold less stable than the trehalose one, hence sucrose can be broken in monomers and can easily undergo browning and caramelisation above 100 °C. Sucrose crystallise in anhydrous form, therefore in very dry environments it tends toward nanocrystallisation and separation, at variance with trehalose.

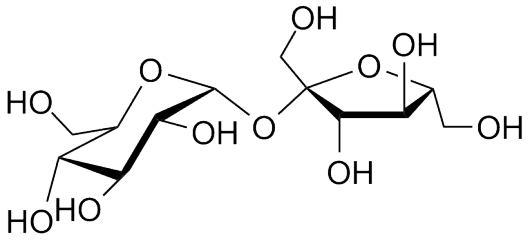

Figure 3.2: Molecular structure of sucrose.

Maltose (4–O–α–D–glucopyranosyl–D–glucose, see fig. 3.3) is a reducing dimer of glucose; it represents the fundamental unit of starch or dextrins. It has neither a definite role in nature, nor a wide use in technology. It is only used as a degradation product of starch in the brewing process and in the sweetening of processed products. Maltose molecule has a quite large dipole moment for a disaccharide: 5.2 D to be compared with 2.5 D for sucrose and 1.5 D for trehalose, calculated at DFT level (BLYP/6–31G**) from the crystalline structure [43]. It has been reported that this large dipole moment could be at the basis of clustering of maltose in solid amorphous state, which lead to inhomogeneous structures [56].

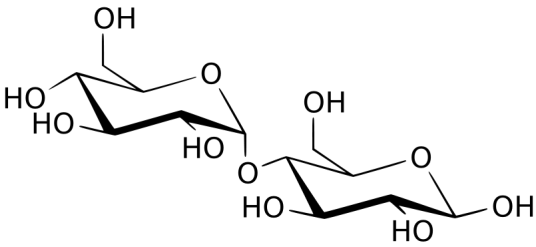

Figure 3.3: Molecular structure of maltose.

Lactose (4–O–β–D–galactopyranosyl–D–glucose, see fig. 3.4) is a reducing disaccharide composed by two different subunits. It is found essentially in milk and milk–derived products. It has bland flavour and weak sweet taste, thus it is used as a carrier and stabiliser of aromas and pharmaceutical products. Being reducing, lactose, as well as maltose, is not resistent to high temperature treatment, and undergoes Maillard reaction in the presence of proteins together with caramelisation. These sugars are not a proper choice for preservation against high temperatures, although they can be used to stabilise systems against other types of stress [55].

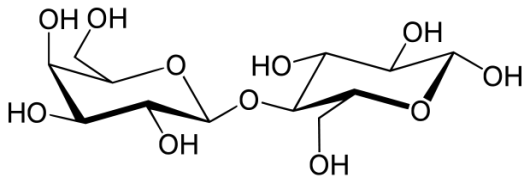

Figure 3.4: Molecular structure of lactose.

Raffinose (α–O–D–galactopyranosyl–(1→6)–α,β–1,2–D–glucopyranosyl–D–fructofuranoside, see fig. 3.5) is a trisaccharide found in various vegetables and legumes, beside being a by–product of sugar refinement, whose the name comes from. Structurally it is similar to a junction of a sucrose and a lactose molecule, sharing the central ring. Its importance, besides some technological applications related to hydrogen production, concerns in the preserving effect it has shown in biomedical applications [57]. Raffinose has a noteworthy high glass transition temperature (112 °C) and crystallises in hydrated form (pentahydrated), both properties in common with trehalose and contributing to the protective effectiveness [16].

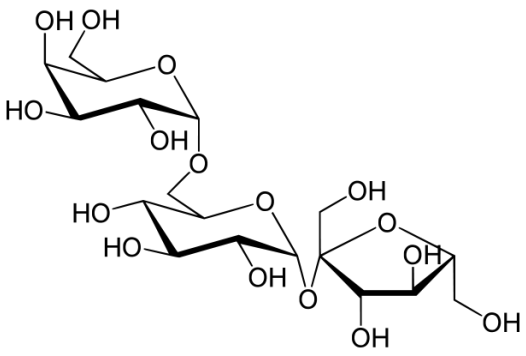

Figure 3.5: Molecular structure of raffinose.

3.2 Proteins as probe molecules

Proteins are biological macromolecules consisting of one or more polymeric chains of aminoacids. Proteins are essential parts of organisms and participate in virtually every process within the cell. Many proteins are enzymes that catalyse metabolic reactions, others have structural or mechanical functions, such as actin and myosin in muscle, or the proteins of the cytoskeleton, which maintains cell shape; others partecipate in a number of processes which includes cell signalling, adhesion, responding to stimuli and transporting molecules from one location to another.

Proteins differ from one another in their specific sequence of amino acids, which usually results in folding of the protein into a specific three–dimensional structure that, in turn, determines its function. The shape into which a protein naturally folds is known as its native conformation. This process is spontaneous, and triggered by the chemical properties of the amino acids, even if some of them require the aid of molecular chaperones o peculiar conditions of macromolecular crowding to fold into their native states [54]. Protein structure is generally classified in four level of organisation:

1. The primary structure is the amino acid sequence, i.e. the single linear polymer chain of aminoacids bound together by peptide bonds between the carboxyl and amino groups of adjacent aminoacid residues. Sometimes proteins have non–aminoacidic groups attached,

which are called prosthetic groups or cofactors.

2. The secondary structure is the regular repeat of motifs stabilised by hydrogen bonds. The most common examples for these motifs are the α–helix, β–sheet and turns. These secondary structures are local and many of them can be present in the same protein molecule.

3. The tertiary structure is the overall shape of a protein molecule, which the basic function of the protein depends on. It is generally stabilised by nonlocal interactions such as the partitioning of hydrophobic aminoacids in a core separated from the solvent, salt bridges, hydrogen bonds, disulfide bonds, and even post–transductional modifications.

4. The quaternary structure is formed by several protein chains joined together to function as a single protein complex.

Proteins can be divided into three main classes, depending on their tertiary structures: globular proteins, fibrous proteins, and membrane proteins. Globular proteins are generally soluble and many are enzymes. Fibrous proteins are usually structural, such as collagen, the major component of connective tissue, or keratin, the protein component of hair and nails. Membrane proteins often serve as receptors or provide channels for polar or charged molecules to pass through the cell membrane [58].

3.2.1 Conformational substates and solvent effects

Proteins are not rigid macromolecules: they may change among several related structures while they perform their functions. These are usually referred to as "conformations" or conformational substates, and transitions between them are called conformational intercoversions. Such changes can be induced by substrate binding or alteration in the environment of the protein, or even in solution because of thermal vibration and collision with other molecules [58].

Interconversions among structural substates allow most of the proteins to function, and are responsible of the allosteric regulation of protein function. An example of their role is evident by analysing the crystallographic structure of myoglobin (see section 3.2.2): it lacks any channel joining the heme pocket with the exterior to allow oxygen escape. The O_2 exchange is possible only through temporaneous passages which forms in different conformational substates, producing a "dynamical" channel.

The presence of these substates can be visualized by using a conformational energy landscape plot (see fig. 3.6). The landscape show the principal minimum which defines the thermodynamic stable structure. Going out of this minimum is the process of denaturation. However, the minimum is not unambiguous, but presents many energetically accessible secondary minima, each representing a conformational substate. The presence of multiple minima in the conformational energy landscape of the protein has been stated by different studies, which also pointed out that their presence causes anharmonicity in protein motions. Interconversions can be either reduced or blocked by lowering the temperature.

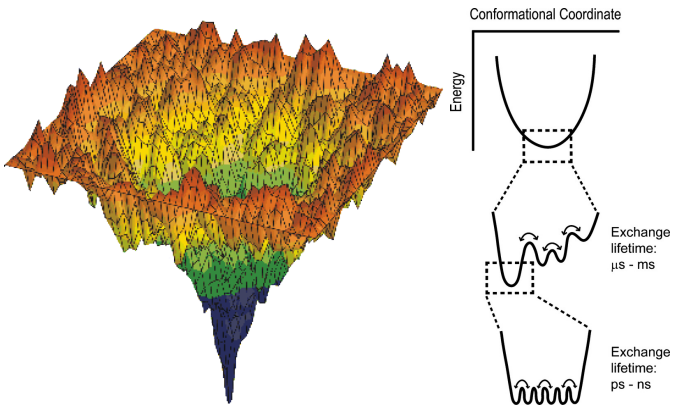

Figure 3.6: Sketch of a conformational energy landscape (*left*) and enlargement of the minimum which evidences the low tier substates (*right*).

Many studies have been devoted to study the influence of the solvent (or external matrix) on protein dynamics and on the substate interconversion. A direct influence of the matrix on protein behaviour has been defined as *slaving* [59]. Most of the studies involving the slaving concept have been performed looking for correspondences between the temperture of the onset of large–scale motion in proteins (*protein dynamical transition*) and transitions in the external medium [60,61]. The study of solid systems with high concentration of protein showed that the concept of slaving can be considered reciprocal, i.e. that a *coupling* of protein and solvent is, in these conditions, a better description than a slaving of the protein by the solvent [41–43].

3.2.2 Myoglobin and its structure

Myoglobin is a globular protein with ellipsoidal shape, with a size of $33\times42\times34$ Å and molecular weight $\sim$18 kDa (see fig. 3.7). It is constituted by 153 aminoacids arranged in 8 α–helices named A to H, each including from 7 to 26 aminoacids, connected by short loops. The helices are packed as to define a hydrophobic core which hosts the active site, the heme prosthetic group. Myoglobin is present in all vertebrates, where its main function is to bind and store molecular oxygen within muscles, although also an enzymatic activity related to denitrification has been reported [54,58].

Figure 3.7: Structure of myoglobin.

The heme group (see fig. 3.8) is a planar molecule, with approximate symmetry D_{4h}, formed by four pyrrole subunits joined by methine bridges placed around a Fe atom, which in the active forms is in the reduced oxydation state II. The Fe(II) atom always binds to a histidine from the polypeptidic chain (H93, F helix), called proximal histidine, anchoring the whole group to the chain. Fe(II) can be penta- or hexa–coordinated: in *deoxymyoglobin* it is pentacoordinated and displaced 0.55 Å out of the heme plane toward proxymal histidine, with a local C_{4v} symmetry.

The possible sixth coordination site is used to bind small ligands such as O_2 in oxymyoglobin, CO in carboxymyoglobin and H_2O in *met*-myoglobin, which has also Fe in the oxydized state III. The exchange of O_2, thus the conversion between the *deoxy* and *oxy* forms, can be considered the main function of myoglobin. These two forms are stabilised by the presence of another histidine residue (H64, E helix) which can either form hydrogen bonds with the bound O_2 or act as proton trap, avoinding Fe(II) oxydation. Moreover the presence of distal histidine reduces the affinity of the heme group for the binding of CO with respect to O_2.

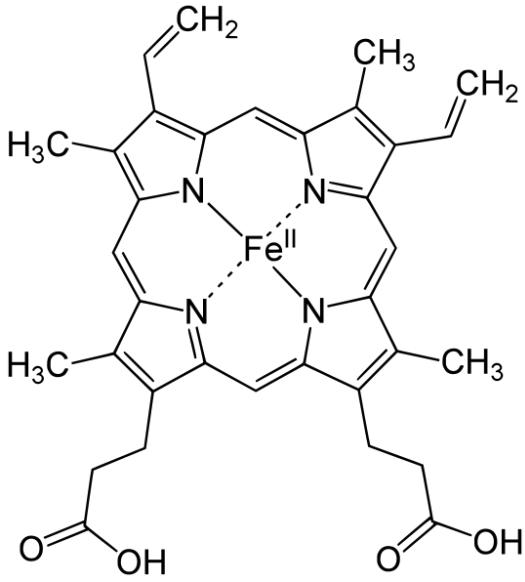

Figure 3.8: Molecular structure of heme group.

Myoglobin has been extensively studied, and its properties are known in detail. For this reason it is widely used as a model protein and as a probe for many studies, including the present [31, 32]. Many studies on myoglobin embedded in saccharides have been already performed with various techniques. They tipicaly make use of carboxymyoglobin because this derivative is particularly useful for the studies of conformational substates interconversion. Particular importance for the present studies can be ascribed to flash–photolysis [62, 63], FTIR

spectroscopy [41–43, 64, 65] and MD simulations [36–39]. These studies and their results will be recalled in the chapter 4, when discussing the respective techniques and in the general discussion of the results.

3.3 Cosolutes: the Hofmeister series

Ion effects are ubiquitous in chemistry and biology, influencing the properties of solutions and condensed systems, often exhibiting recurring trends which cannot be explained with point charge models or simple thermodynamics. These trends were studied towards the end of the nineteenth century by Franz Hofmeister, which published a series of papers describing the effects of salts on the solubility (and other properties) of a variety of biological systems [66]. From him these orderings of salts have been called "Hofmeister series". Since Hofmeister's original work, Hofmeister effects have been noted in countless systems and processes, including salting proteins in and out of solution, water retention in macroscopic systems such as e.g. wool, molecular ordering of surfactants, and modulation of membrane protein conformations [67,68]. These effects appears evident only at relatively high concentration of solutes (> 0.1M), while at lower concentrations short range repulsions and Coulomb interactions suffice to describe the physical chemistry of the aqueous solution, i.e. activity and osmotic coefficients [69].

Hofmeister series generally show a typical sequence order irrespective of the measured quantity, with effects more pronounced for anions than for cations. Only for some similar ions the exact ordering can sometimes be inverted, i.e. the relative positions of phosphate vs. sulfate, of sodium vs. potassium, and of calcium vs. magnesium may switch depending on the nature of the system being studied, but otherwise this ordering is highly reproducible in a wide array of systems [70]. Although anions and cations can be put on the same series, as shown in fig. 3.9, cationic and anionic series are independent form each other, and their relation depend on the specific property measured. Since also many neutral molecules show Hofmeister effects, a third series for neutral molecules can be also conceived [68].

The species to the left of Cl^- are referred to as *kosmotropes*, while those to its right are called *chaotropes*. These terms originally referred to an ion's ability to alter the HB network of water. The kosmotropes, which are believed to be "water structure makers", are strongly hydrated and have stabilising and salting–out effects on proteins and macromolecules. On the other hand, chaotropes ("water structure breakers") are known to destabilise folded proteins and

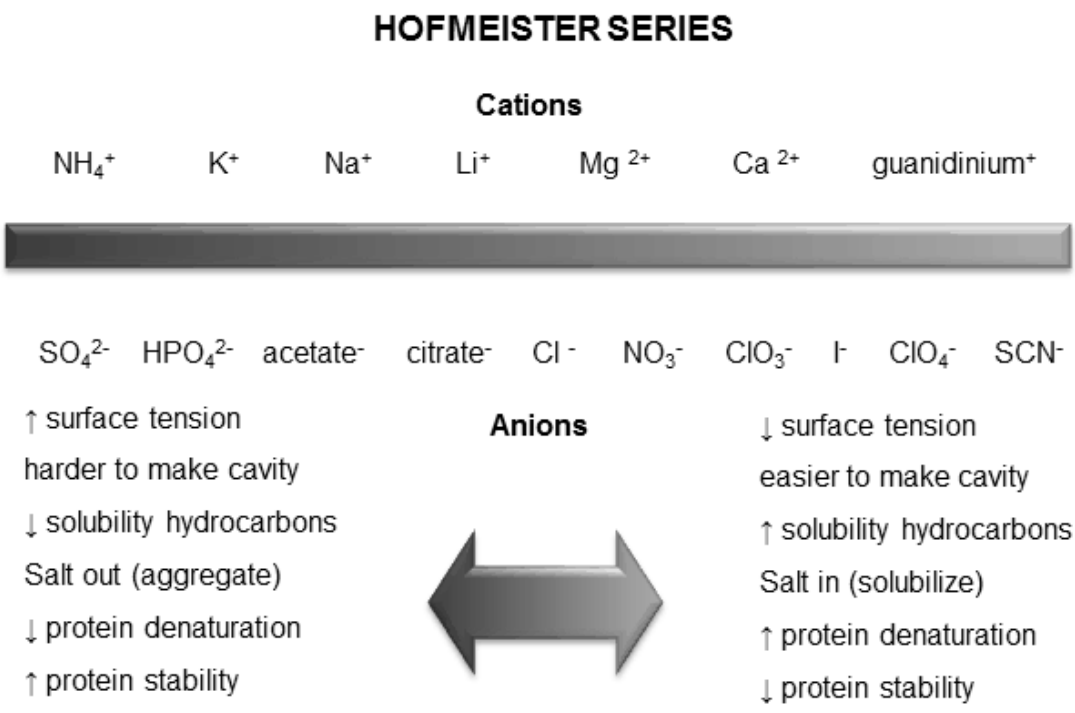

Figure 3.9: Cationic and anionic Hofmeister series.Taken from [71].

give rise to salting–in behaviour [67, 68].

Recently, substantial attention has been paid to Hofmeister phenomena because of their relevance to a broad range of fields: among them enzyme activity, protein stability, and protein–protein interactions. Although Hofmeister effects for macromolecules in aqueous solution are ubiquitous, the molecular–level mechanisms by which ions operate has just begun to be unraveled, and it is widely debated [71]. Detailed theories of aqueous electrolyte solutions have been devised, which can explain many physico–chemical properties, but fail to exploit the underlying mechanism of salt effects on macromolecules.

Current ideas about the nature of specific salt effects vary; many believe that ions act only by modifying the structure of water close to biological interfaces. Others believe that the specific effects consist mainly of water–mediated solubilisation or expulsion of specific surface groups in macromolecules. These arguments cannot fully explain that specific ion effects are present also in electrolyte solutions without proteins [72]. The present theoretical framework fail to solve the complex Hofmeister puzzle because many different interactions (ion–water, surface–water, surface–ion, water–water) need to be taken into account. What seems to be generally accepted is that they come from: 1) changes in water structure (around ions and solvated

surfaces), and 2) specific ion adsorption–exclusion mechanisms at interfaces.

The recent hypothesis formulated by Ninham and collaborators attempts to explain ion specificity by invoking dispersion interactions of ions with solvent and surfaces [73, 74]. In this framework, it possible to explain both the stronger effect of anions and some noteworthy irregularities in the series. Nevertheless, Hofmeister effects cannot be completely understood exclusively in terms of ion polarizability. Basically, this is because water cannot be treated as an unperturbed medium that simply hosts the dissolved entities.

Alternative models argue that ion specificity arises from the balance between ion–water and water–water interactions or from alteration of the hydrogen bond network of water. In this respect the main issue is the extent of the ion effect on the HB network. No consensus exists on this, and it remains largely unclear whether ions act through precisely defined, specific, local interactions, or through more delocalized collective interactions [72].

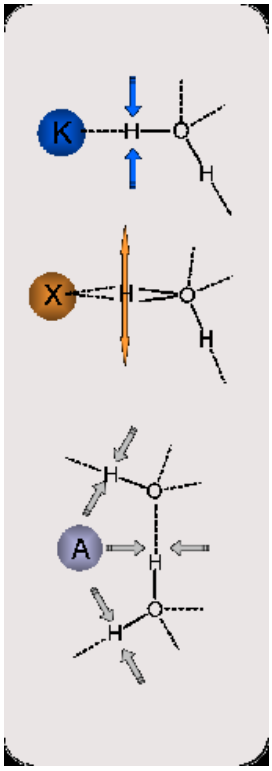

Figure 3.10: Sketch of the interactions with water of a polar kosmotrope (K), a chaotrope (X), and an apolar kosmotrope (A). Blue and grey arrows are meant to represent HB strengthening, orange arrow represents HB weakening.

Several thermodynamic parameters have been correctly predicted by considering effects only on the first hydration layer of the ion. Within this model, it is simple to describe the concepts of chaotropicity or kosmotropicity in terms of loosening or stregthening of the hydrogen bonds in the hydration layer with respect to the bulk water. According to Collins [67]: "binding of chaotropes to water molecules is weaker than binding of water molecules to each other; binding of kosmotropes to water is stronger than binding of water molecules to each other". A sketch of this concept is illustrated in fig. 3.10. Chaotropicity correlate with a low charge density, thus large singly–charged ions tend to be chaotropic: they can set up only weak hydrogen bonds with the surrounding water and have a small tendency to partition out the water HB network. On the contrary kosmotropicity correlates with a high charge density, thus small or multiply–charged ions tend to be kosmotropic: they establish a strong HB network around themselves which stabilises the first hydration shells and competes with water HB network. Recently, it has been pointed out that salts have little or no impact on water hydrogen bonding orientations above the first hydration

layer, while no sharp influence is produced in bulk water [71]. This would rule out long range Hofmeister effects, confirming the hypothesis.

Another view of the same idea can be drawn on the basis of the common, although biased, model for liquid water, as a mixture of hydrogen–bonded clusters and unbounded free–water molecules. In this framework, ions of high charge density have strong electrostatic interactions with water molecules and are structure–makers. They reduce the fraction of free water and increase the viscosity of the solution. On the other hand, ions with low charge densities, which are structure–breakers, decrease the viscosity of the aqueous solution by breaking or weakening hydrogen bonds between water molecules, and thus increase the fraction of free water [75]. The conclusions are valid also if models of water as a random, continuous HB network, without need of intrinsic heterogeneity, are adopted. FTIR studies and MD simulations pointed out that, in this case, a bimodal distribution of HB angles sets up. In this distribution "true" hydrogen bonds, with a certain degree of covalence, are present alongside weakened HB, which can be considered more properly electrostatic or dipole interactions. The effect of salts in these models appears to be the increase of a type of HB with respect to the other [70].

Most experimental techniques do not show a significant change of water structure outside the first solvation shell of the ions. Further confirmations on the importance of local interactions comes from dielectric spectroscopy, which has shown no difference in relaxation times between bulk water and a variety of aqueous salt solutions [76]. At variance, ultrafast IR studies have argued that ions have some effect on water dynamics, but not on equilibrium water–water hydrogen bond geometries [77]. An aqueous salt solution should not be viewed as a homogeneous liquid with a intermolecular interaction, uniformly modified by the presence of the solute, but rather as a colloidal suspension of more–or–less inert particles in pure liquid water, with the particles formed by the ions and their first hydration shells [77].

Some studies have offered alternative mechanistic explanations for Hofmeister effects, including formation of salt bridges which stabilise or destabilise protein structure, and salt–induced changes in solvent surface tension at the protein–solvent interface [78, 79]. The models based on interactions involving (even indirectly) the biomolecule surface received a strong confirmation from their ability to explain the apparent inversion of the Hofmeister effects on those, relatively rare, proteins whose native state is less compact than the denatured state. This would reveal the key role of protein–water interfacial tension on protein structure and dynamics, the latter processes being coupled to (interfacial) solvent fluctuations [79].

The models based only on HB network perturbation are however not exhaustive and directs interactions with the surface need to be taken into account [80]. Generally, cosolutes are unevenly distributed with respect to the biostructure interface. Given that most of biological interfaces are less polar than water, kosmotropes are generally excluded from interface, sequestering water and increasing the insolubility of apolar groups, while chaotropes tend to accumulate at the interface increasing solubility of apolar groups. Chaotropes therefore twarth the hydrophobic stabilisation of proteins, while kosmotropes enhance it [81]. This can also be viewed as a stabilisation by preferential hydration in the presence of kosmotropes and a destabilisation by biomolecule–salt association in the case of chaotropes [72]. This agrees with the strong dependence of the destabilisation on the difference in hydration of the single chaotropes, while the kosmotropes' stabilisation is far less sensitive [82].

Several studies have found both specific ion effects and Hofmeister trends, arguing for the presence of both specific ion interactions with proteins and bulk solvation effects mediated by ion–induced changes in water. The difficulty in separating Hofmeister effects from other, more general, physico–chemical effects, such as those originating from ion strength or osmolarity, makes this type of studies difficult [83].

For what concerns the present work, cosolutes have been used essentially for their undisputable ability to modify the hydrogen bond network of the matrix. The very high concentration of the systems here considered allow to avoid problems regarding the range of effect of the cosolutes: in a very crowded environment, in which trehalose occupy most of the volume, is not conceivable to have a real bulk water, whose properties are independent both on trehalose and on the salts. It is here assumed that water is always in the first or second shell of either trehalose or salt. Chaotropes and kosmotropes are here used to modulate the strength of the HB network, which is however dominated by trehalose. Their effects alter the population of the various types of HB present in the sample, hence the shape of the signals that are observed. By relating the known effect of the solutes with the alterations of the signal, it has been possible to find markers for strong or weak HB, to be used to deepen the knowledge of the various saccharide matrices.

The possible formation of direct ion–trehalose complexes has been seldom reported in the literature, but the main effect of salts in trehalose amorphous matrices seems to be the structuration the residual water, thus altering the hydrogen bonded network [84].

Chapter 4

Methods

This work has been performed making use of three main techniques: FTIR spectroscopy, MD simulation and SAXS. The detail of each technique, the signals and observables taken into consideration and the preparation of the samples (or of the models) are detailed in the following.

4.1 FT-IR Spectroscopy

Infrared spectroscopy is a spectroscopic technique sensitive to molecular vibrations. The frequency of the absorbed radiation that matches vibrational transition energies falls in the infrared region of the electromagnetic spectrum. The frequencies are specifically determined by the tipe of vibration, the masses of the involved atoms and the associated vibronic and rotovibrational couplings. In the Born–Oppenheimer and harmonic approximations, the transition frequencies are associated with the normal modes corresponding to the molecular electronic ground state potential energy surface. Various type of vibration can be observed, the two principal groups being stretching, i.e. the elongation of an interatomic bond, and bending, i.e. the vibration of an angle. While stretching transitions give usually isolated and strong peaks, easy to identify, the bending transitions region is very complex and is further complicated by the presence of band arising from combination or overtones. The pattern of bands in this region is distinctive for each molecule, for this reason it is called “fingerprint region”.

Although first infrared spectrophotometers were dispersive, all the modern instruments utilise a Michelson interferometer (see fig. 4.1). In this arrangement, the incident radiation is directed through the interferometer and then through the sample. In the interferometer the source light is divided in two beams reflected by two mirrors (fixed and mobile), which successively

interfere giving a signal as a function of the difference of optical path, called an "interferogram". Fourier transform turns the latter in the sample spectrum as a function of wavenumber. FTIR are generally single beam instruments, thus it is always needed to subtract a background spectrum obtained measuring the empty sample holder.

For this work a Jasco FTIR–410 has been used to record all the spectra. In this instrument a constant flux of dry nitrogen was always blown within the whole optical path and the measurement chamber to avoid spurious signals from atmospheric moisture or CO_2. All the spectra have been recorded with a 1 cm^{-1} resolution and averaged over 250 scans, to improve the signal/noise ratio. The solid amorphous samples have been deposited on round calcium fluoride (CaF_2) cells (surface $\sim$1.3 cm^2) and put in an Oxford Instruments Optistat CF–V sample holder. This arrangement allow the sample to be put under high vacuum, and the temperature to be controlled in the interval 30-350 K with an Oxford Instruments ITC–503 working by counterbalance an electric resistence and a liquid helium flux.

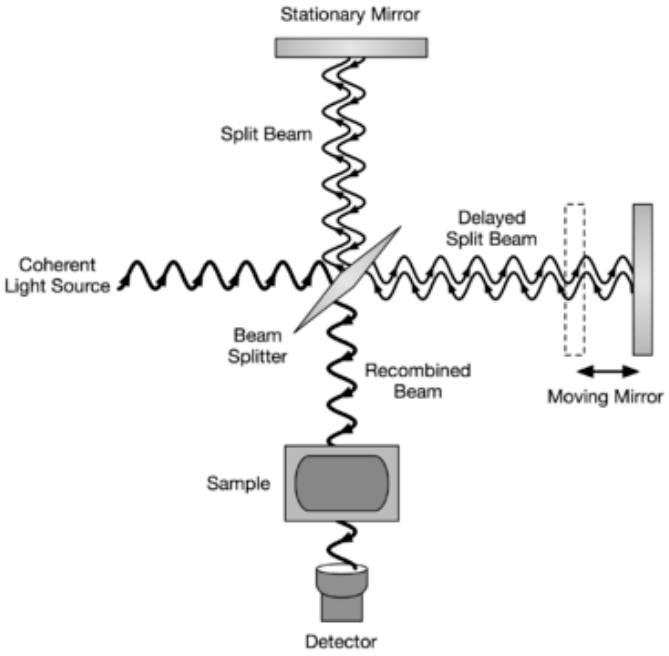

Figure 4.1: Michelson Interferometer.

FTIR spectra has been used for the evaluation of parameters both of the protein and of the matrix, and also to estimate the sample water content. It has indeed been possible to record, in a single measurement, the properties of the protein, through the CO stretching band (COB, $\sim$1900-2000 cm^{-1}) and those of the saccharide matrix through the water association band (WAB, 2000-2400 cm^{-1}), see fig. 4.2.

The CO stretching band

The infrared spectrum of MbCO show a structured band in the $\sim$1900-2000 cm^{-1} frequency range, which is ascribed to the stretching vibration of C–O bond in the iron–bound CO molecule.

The presence of an internal structure in this band stems from the existence of a class of conformational substates, which have been called *taxonomic substates* or A substates [85]. Each of these substates gives rise to a specific sub–band. Three sub–bands are generally reported: A_0 ($\nu \simeq 1966$ cm^{-1}), A_1 ($\nu \simeq 1951$ cm^{-1}), A_3 ($\nu \simeq 1938$ cm^{-1}). A fourth substate (A_2) was introduced in the first studies, but nowadays the analysis in terms of three sub–bands is preferred. This analysis has been performed also on samples of MbCO embedded in saccharide matrices at various hydrations (see fig. 4.2). Although the use of three components correctly describes the band in trehalose [41] and maltose [43], it was found that it is not sufficient to fit the shape of the band in sucrose and raffinose [42,43]. In these two sugars a fourth sub–band has been found at $\sim$1925 cm^{-1} (see inset in fig. 4.2, lower panel), which does not correspond to "A_2", but is instead likely to depend on modification of heme pocket structural modifications induced by sucrose–like units. As previously reported, raffinose is composed by a sucrose molecule with a galactose moiety bound to O6 of the glucose subunit. This feature could even arise from the simple furanoside moiety, present in both the sugars. Indeed, the lower flexibility of the penta–atomic with respect to the hexa–atomic ring might constrain the protein structure in a new substate. However, the COB measured in MbCO embedded in fructose and ribose matrices did not show the above features, ruling out the interaction with

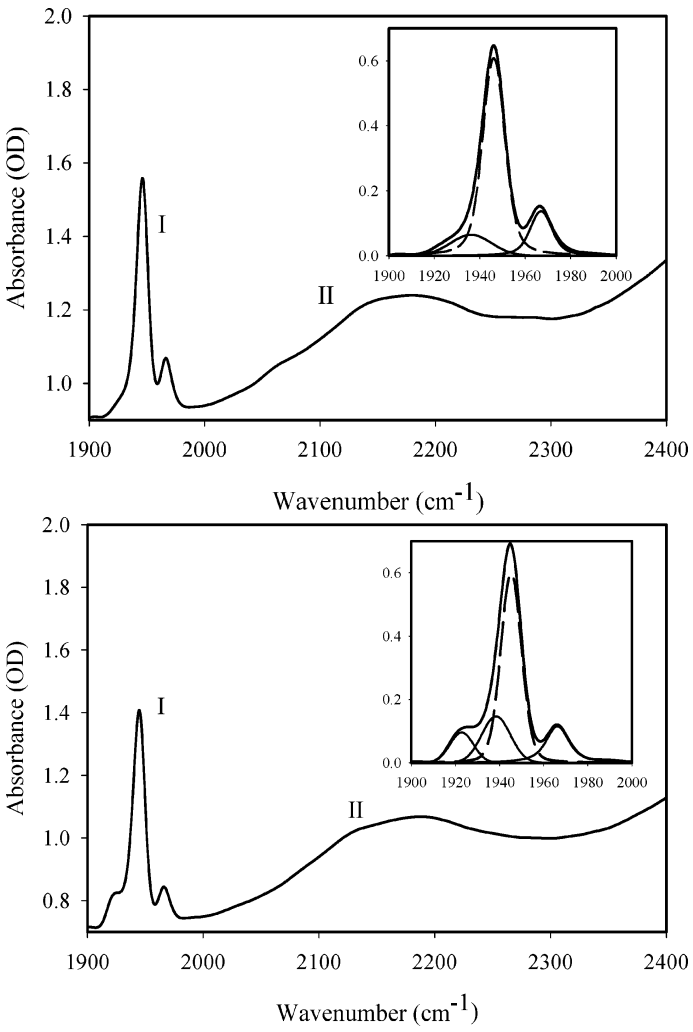

Figure 4.2: COB (I) and WAB (II) in samples of myoglobin embedded in hydrated trehalose (*upper panel*) and sucrose (*lower panel*) matrices at 300 K. In insets the fitting of the COB is shown: please note the presence of the fourth substate in the sucrose sample.

furanose groups. This fourth substate was found in sucrose matrices also with MD simulation, where the distribution of the angle between the local electric field at the oxygen and the CO bond vector exhibits a secondary maximum in sucrose matrices, which is almost absent in the other disaccharide matrices [38].

The COB sub–bands have been fitted using either gaussian or voigtian shapes. A voigtian curve is a gaussian convolution of lorentzian curves:

$$V(\nu) = G(\nu) \otimes L(\nu) = A \frac{\int \frac{e^{-y^2/(2\sigma^2)}}{\Gamma^2+(\nu-\nu_0-y)^2}\,\mathrm{d}y}{\int \frac{e^{-y^2/(2\sigma^2)}}{\Gamma^2+y^2}\,\mathrm{d}y}$$

where A is a scale factor proportional to the population of the absorbing species, while ν_0 is the peak frequency. This curve has both a homogeneous lorentzian broadening Γ, related to the life time of the excited state, and an inhomogenous gaussian broadening σ. Γ is frequently neglectable, giving a gaussian curve, as in A_3 case, while on the contrary σ is never neglectable.

The parameters of the sub–bands are dependent on many variables, among them temperature, pressure, pH. Many studies have been performed to relate the three substates to specific structures of the protein. The key difference appears to be the proximity of partially charged atoms, both forming or not HB with the bound CO molecule. A peculiar role has the distal histidine, which interacts with CO with two different orientations, giving A_1, the most populate substate in standard conditions, and A_3. The substate A_0 is instead related to structures in which the distal histidine is pulled out of the heme pocket [86].

Water association band

The WAB is a unusual broad combination band, which occur in the spectrum of water and hydrated systems in a wavenumber range 2000-2500 cm^{-1}, in a position almost devoid of interferent bands [87].

The origin of this band is still a puzzle. The apparent progression of three broad librational bands of cubic ice, from 835 to 1560 and finally 2255 cm^{-1}, makes likely an assignment of WAB as the second overtone of the librational mode ν_{L2}. This hypothesis works in ice and correctly explains the temperature dependence of the band (frequency increase with lowering T), but fails in liquid water, where the fundamental ν_{L2} is 570 cm^{-1}, which would give a second overtone at 1710 cm^{-1}, far from the actual value of $\sim$2125 cm^{-1} [88].

Another recurring assignment has been to a combination of bending and librational fundamentals [89, 90]. This is likely to be valid for the liquid (1645+570=2215), as compared to the

observed 2125 cm^{-1}, but appears less likely for crystalline ice: with the cubic ice librational frequency established as 835 cm^{-1} and the bending frequency near 1700 cm^{-1}, the uncorrected combination frequency of 2535 cm^{-1} is too high a value. Although a final answer has not been found, both have been considered valid after some modifications such as anharmonic corrections [88] or involvement of translational modes in liquids [91].

Both these interpretations, deriving from modes extremely dependent on the molecule environment, allow to explain the noteworthy area reduction and the shift of the maximum at higher frequencies with decreasing temperature. At high T the interactions with the surroundings and the wavefunction superposition with molecules hydrogen–bonded with water decrease, loosening the HB network, hence making the intensity of the band to fall, as well as the frequency to decrease [92]. Nevertheless, this high variability makes the WAB an ideal marker for species interacting with water. In saccharide matrices, where water molecules are expected to interact strongly with sugar, WAB has been shown to be highly dependent on the specific saccharide and on hydration [41–43, 93–95].

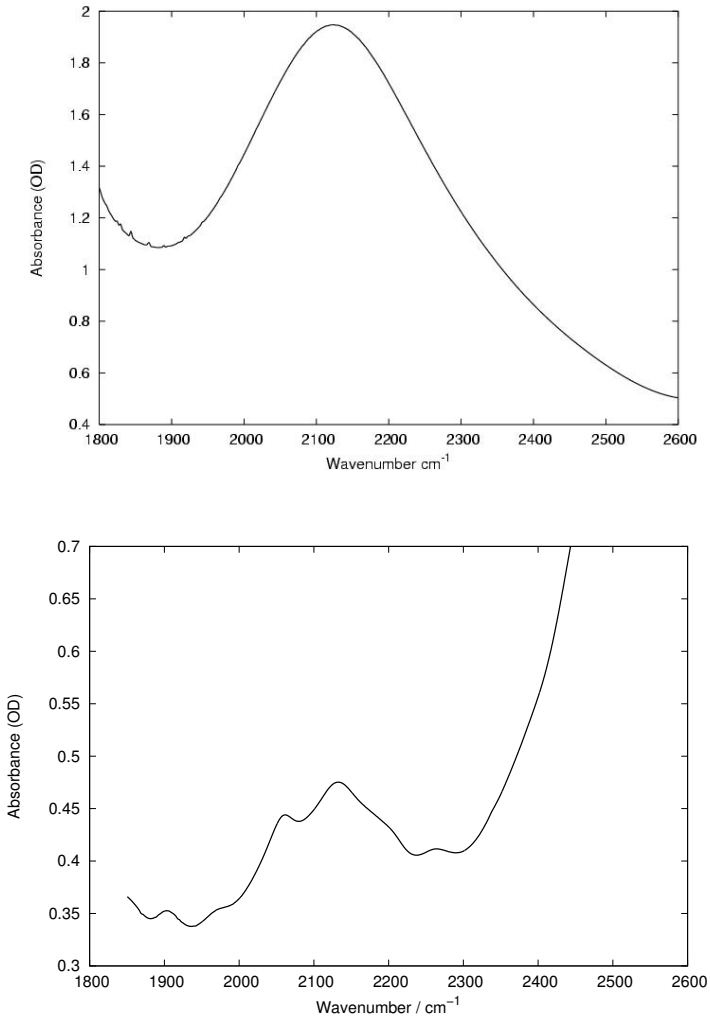

Figure 4.3: Water association band in pure liquid water (*upper panel*) and in trehalose–water matrix (*lower panel*) at 300 K.

WAB looks as a gaussian band in liquid water (see fig. 4.3, upper panel) and maintain approximately the same shape above 30% w/w water content, while it is structured in samples at low water content (see fig. 4.3, lower panel) [96]. From the analysis of the pattern of sub–bands

in the latter systems, it should be possible to have an idea of the properties of HB network in various matrices, as WAB can be considered safely more a marker of the HBs, in which water is involved, than of the water itself[1]. This analysis has been performed in terms of gaussian curves, due to the large inhomogeneity expected for these samples. However, one has to be cautious in the interpretation of these sub–bands: 1) the pattern obtained is sometimes not unique, because of the lack of defined peaks for each sub–band and of a high degree of superimposition among sub–bands; 2) each component is not granted to correspond to a "single IR species"; 3) it is not possible to attribute a particular IR peak to a single given HB pair [97].

By using Hofmeister salts to knowingly modify the HB network of trehalose matrices, it would be possible to characterise WAB as a marker and then use it to analyse matrices containing different sugars, thus deepening the knowledge on the effects on, and their relation with, biopreservation. This work was needed because an established pattern for the analysis of the WAB is not present in the literature; the model here used was derived from the recurring occurrence and position of the single sub–bands in the various samples. In this way five recurring sub–bands have been found. The model will be discussed in 5.1, 5.2 and 5.3.

Thermal behaviour of IR bands

The thermal behaviour of COB and WAB can be related to the dynamics of the protein and the matrix. In particular, information on the thermal interconversion among taxonomic and lower hierarchy substates can be obtained from the COB, through direct decomposition in sub–bands and from the thermal line broadening and peak frequency shifts. The corresponding dynamics of the matrix can be deduced from the WAB, given that water molecules are spread in the saccharide matrix and are therefore an optimal probe.

Temperature variations can modify various parameters of a band. Since the main interest in this work is the global modification of the signal, to have an estimate of the overall *changes* the samples undergo, it has been chosen an integral, although rough, measure of the thermal evolution calculated by using the functional integral distance of the normalized spectra at each temperature from the respective normalized spectrum measured at a reference temperature (Spectra Distance, *SD*). This is defined as [41]:

[1] One must however keep in mind that WAB is a band of water and it cannot sense hydrogen bonds not involving water molecules.

$$SD = \sqrt{\sum_{\nu} \left(A(\nu,T) - A(\nu,T_{ref})\right)^2 \Delta\nu} \tag{4.1}$$

where A(ν) is the normalized absorbance at the frequency ν, $\Delta\nu$ is the frequency resolution and T_{ref} is a reference temperature.

The above quantity represents the deviation of the normalized spectra at temperature T from the normalized spectrum in condition of minimal occurrence of thermal motions, which generally is the lowest temperature measured (20 K), although it has been shown this is not necessarilty so (see section 5.5) [98]. Since, in principle, the sub–bands are each independent from one another, the *SD*s should be calculated independently, but this would introduce an error deriving from the fitting procedure, as the sub–bands have an high degree of superimposition. It is possible however to prove that if the whole band does not undergo huge changes with temperature, the *SD* calculated on the whole band is a good approximation of the sum of *SD*s calculated on the single sub–bands.

The *SD*s calculated on the WAB and COB have been proposed and used to estimate the thermally induced readjustments of either the matrix (SD_{WAB}) or the protein structure, as evidenced by the bound CO molecule (SD_{CO}) [41–43, 65, 98]. Considering that such structural changes imply protein internal motions, SD_{CO} also conveys information on internal protein dynamics. In this respect the thermal behaviour of COB in MbCO embedded in trehalose matrices has been compared with the mean square displacements of hydrogen atoms in the protein as measured by Neutron Scattering experiments. This comparison has been thoroughly discussed in [65].

Water combination band and estimate of water content

Saccharides are very hydrophilic molecules, able to bind several water molecules in their hydration shells. For this reason, the properties of the saccharide matrices strongly depend on water content, and the evaluation, and control, of the hydration play an important role in the study of saccharide matrices. Regrettably, this is one of the main problems in the study of these systems. The most direct absolute method, gravimetry, has proven not very useful: the amount of residual water is too low to obtain an acceptable error using a standard balance. Moreover, due to the strong hygroscopicity of the dried trehalose matrices, the water content could change during the measurements procedures. It would be more advisable a method able to evaluate water concentration during the IR measurement itself.

The most simple answer to this problem is utilising an IR band of water for the estimate.

This idea may be endorsed also because, in this case, it is more important to know the relative variations in water content among different samples than the absolute content of water, making absolute methods not necessary.

However, the chosen band cannot be the WAB itself. As above reported, WAB depends on the water content, but also on the interactions of water molecules with non–water hydrogen bonding groups. Because of the high concentration of sugar (which has 8 HB donor groups and 11 HB acceptor groups, in the case of the disaccharides studied) and the low water concentration in our samples, the ratio between water–water interactions and water–sugar interactions undergoes huge variations, depending on water content [99]. For a band so sensitive to intermolecular HB this means that huge variations in molar absorptivity might be present, making the WAB unuseful to estimate the water content.

Another band has instead been chosen, the water $\nu_2 + \nu_3$ combination band. Also this band lays in a region relatively devoid of interferent bands, at $\sim$5200 cm^{-1}, and originates from the combination of the asymmetric O–H streching mode ($\nu_3, \sim$3540 cm^{-1}) and the HÔH bending mode ($\nu_2, \sim$1650 cm^{-1}). At variance with WAB, which is very sensitive to water environment, the $\nu_2 + \nu_3$ combination band is very weakly dependent on the nature of the hydrogen bonded species [100], showing instead a dependence only on the average number of HB the water molecule establishes [101]. In concentrated saccharide environments, this average number is approximately constant. This is due to the substitution of water–water HB with water–saccharide HB up to the saturation of "HB capacity", and is also confirmed by the substantial similarity of the shape of the $\nu_2 + \nu_3$ band in the various systems. An evaluation of the latter's area can be therefore a satisfactory estimate of the relative water content in the sample, confirming the widespread use of this band for evaluating water content.

Looking at the values of the areas of water $\nu_2 + \nu_3$ band and WAB upon dehydration of a sample, one can notice that $\nu_2 + \nu_3$ band area reduces more steeply and more linearly than WAB area. This could be expected, as the former is due to water loss, while the latter is compensated by the raising number and the strengthening of water–saccharide (or water–protein) HB. This difference could therefore be fruitfully used to have a rough estimate the relative importance of water molecules interacting with non–water H–bonds in the sample. This has been made by defining the ratio $r_A = A_A/A_C$, where A_A is the area of WAB and A_C is the area of $\nu_2 + \nu_3$ combination band. This ratio is higher for samples with lower water content, hence with higher occurrence of water–non-water HB, and it tends to the limit value of 1.8 in very hydrated

samples of amorphous saccharides. In this model, high r_A value at very low water content is an estimate of the stress induced on residual water molecules, which are forced to interact with all the other (HB forming) components of the system. This coud be assumed as an indicator of how much the matrix is perturbed by dehydration [42, 43, 95, 98].

IR sample preparation and measurement

The samples for IR spectroscopy were prepared with: lyophilized ferric horse myoglobin from Sigma (St. Louis, MO, USA) with purity >99.4%, used without purifications; trehalose from Hayashibara Shoji Inc. (Okayama, Japan), used after recrystallisation from acqueous solution; maltose and lactose from Sigma, sucrose and raffinose from Fluka (Buchs, CH), with purity >99%, used without purification; the salts either from Sigma or from Carlo Erba (Milano, I), all of analytical grade, used without purification.

All the samples containing myoglobin, except those for the measurements at different saccharide:protein ratios, were prepared starting from aqueous solutions containing myoglobin ∼5 mM, saccharide 0.2 M (except in the case of raffinose, where a 0.133 M concentration was used, as to match the number of saccharidic units), and phosphate buffer 20 mM (K_2HPO_4 + KH_2PO_4, pH 7). The myoglobin used to prepare these solutions was in oxydized form (*met*–myoglobin). MbCO was prepared by reduction with sodium dithionite ($Na_2S_2O_4$), added up to a final concentration 0.1 M after having equilibrated the solutions with CO to remove dissolved oxygen.

Aliquots (0.1 mL) of the above solutions were layered on CaF_2 windows of a 1.3 cm^2 surface. All samples were initially dried for about 8 h under CO atmosphere in a silica gel desiccator. Further drying proceeded at 353 K for ∼15 h under vacuum. After the above treatments, all samples were in the form of amorphous films, firmly attached to the CaF_2 cell. The amorphous state was confirmed by the very low turbidity detected by measuring the absorbance at 1900 cm^{-1} at 300 K. After desiccation the samples were closed with a second CaF_2 window and measured under vacuum, after stabilisation of the water content evaluated at 300 K with the water combination band (see above). It cannot be excluded that more water could have been extracted at higher temperature or by allowing the sample to crack and crystallise (in particular with sucrose). However, this has been avoided to have reproducible samples dried with a systematic technique, which granted very low water content, still allowing to maintain the amorphous state and the sample macroscopic homogeneity. The hydrated samples discussed

in section 5.3 were prepared from the corresponding dry samples by exposure to 60% relative moisture for 15 h at 300 K. After this treatment the samples, although hydrated, remained in solid state, and did not show CO loss, as instead noticed in samples hydrated at higher relative moisture. For each system 3 to 6 samples have been measured and the results averaged.

All the samples with different saccharide:myoglobin ratios were prepared exactly in the same way, only modifying the concentration of myoglobin and sugar in solution, as to have the requested molar ratio, and a constant myoglobin+saccharide total mass, as to attain films with approximately the same sample thickness. With this method it was possible to obtain reliable samples with ratios down to 10:1 saccharide:protein. Further increase in myoglobin concentration gives unstable samples, unable to form films or withstand high temperatures or high hydrations. The method above described was instead profitably used to prepare samples with high sugar content and even samples without protein, whose mother solution is prepared with double concentration of sugar. Samples with high saccharide content are very stable at low hydration, but become progressively less stable if exposed to excess moisture. For these reasons, only dry samples were studied with variable saccharide:protein ratio and without protein.

As for the samples containing Hofmeister cosolutes, they were prepared with the same method, the only difference being that sodium dithionite was removed and substituted with the suitable concentration of the desired cosolute. A side effect of this preparation was that samples with myoglobin and cosolutes contained *met*–Mb and not MbCO. Therefore for those samples, the COB was not studied.

4.2 Molecular Dynamics

Molecular dynamics (MD) is a numerical technique that allows the study of structure and dynamics of atomic and molecular systems. It is conceptually simple, as it is based on numerical solving the Newton's equations of motion for a system of interacting particles, where forces between the particles are obtained from a potential energy defined by an analytical function of the atomic coordinates, or Force Field. The atoms and molecules are allowed to interact at discrete times, and, after a preliminary equilibration, the stationary evolutions of atoms and molecules are evaluated.

MD is a very flexible technique from the point of view of the level of detail examined: coarse–grained MD allows to calculate properties of large systems which evolve on microsec-

onds time scale, at the expense of the atomic details, while on the other hand atomistic simulation with quantum mechanical evaluation of the potentials allows a high degree of accuracy, but with enormous computational cost. In the field of biophysics and physical chemistry a compromise is generally used, i.e. full atomistic simulations, where the molecular details are explicit, and usually empiric molecular mechanics force fields are employed.

The trajectories from MD simulations may be used to determine structural, dynamics, and thermodynamics properties of the system by measuring time averages of the corresponding observables expressed as a function of particle positions and velocities, by assuming the ergodic hypothesis. Therefore, a MD simulation should be long enough compared to the time scales of the natural processes being studied: to make statistically valid conclusions from the simulations, the simulated time should match at least the dynamics (or kinetics) time scales of the process of interest. Typical time courses for fully atomistic MD simulation of biological macromolecules are of the order of nanoseconds, at least if activated processes are not present.

Previous MD simulations performed on trehalose–water systems [47, 102] and myoglobin–trehalose–water systems [36, 37] have already demonstrated that trehalose remarkably modifies the HB network and water dynamics, as well as the dynamics of the embedded protein. MD has been utilised in this work to provide a better understanding of structure and dynamics of myoglobin and trehalose–water matrix in three different systems:

- A system with a single MbCO molecule embedded in a trehalose–water matrix both with and without constraints added to the water molecules, studied at 300 K; these constraints were:
    1. fixing both translational and rotational motions of water molecules, in the whole matrix or in shells at given distance from the protein;
    2. fixing translational motions of water molecules, but allowing them to rotate;
    3. the application of a suitable harmonic potential to restrain motion of water molecules;
- A system with a single MbCO molecule embedded in a trehalose–water matrix studied at different temperatures (every 50 K in the 50-400 K range) with mobile and fixed (as in the above point 1) water molecules;
- A binary trehalose–water matrix studied at different temperatures (every 50 K in the 50-400 K range) with mobile and fixed (as in the above point 1) water molecules.

All the system contained, beside the MbCO molecule if needed, 830 trehalose and 1909 water molecules.

MD simulations were run with the NAMD program[2] [103], with the CHARMM force field (version 27, [104]), with a parameter set proposed for carbohydrates for trehalose (version 36, [105]); the TIP3P model was used for the water molecules [106].

The trehalose–water matrix was built starting from a crystalline configuration of trehalose dihydrate [107]. A building block of eight unit cells (32 trehalose and 64 trehalose–bound water molecules) was generated and equilibrated at 300 K over an 80 ps simulation. Then, to prepare the trehalose–water system, a rectangular box was built and filled with trehalose and water molecules using the pre–equilibrated configuration as a building block; some water was added, leaving with the above reported numbers of trehalose and water molecules, corresponding to a 89% w/w trehalose–water ratio. A system with such a trehalose–water ratio is in a glassy state at room temperature [7].

As for MbCO–trehalose–water system, a MbCO, whose initial coordinates were obtained from the crystallographic data of sperm whale myoglobin (pdb entry: 2MB5, all hydrogen atoms explicitly included [108]), was placed in a rectangular box filled with sugar and water molecules by using pre–equilibrated sugar–water configuriation as a building block. Molecules whose atoms were within a 1.8 Å from any protein atom were removed, thus leaving the above mentioned number of trehalose molecules. To ensure the neutrality of the box, nine random water molecules were replaced by nine chlorine counterions. Then, water molecules were added up to reach the amount needed to have the protein in a 89% w/w trehalose–water matrix, as above.

The two systems were equilibrated over a variable time interval of .5-2.5 ns in the isotherm–isobaric (NPT) ensemble at P = 1 bar and T = 300 K by using the Langevin piston pressure control as implemented in NAMD [103]. The simulations for data collection were then performed in the canonical (NVT) ensemble at T = 300 K by using Langevin dynamics. Periodic boundary conditions were used [109]. Van der Waals interactions have been cut off beyond a distance of 12 Å. Electrostatic interactions were calculated by the Ewald sum using the PME method [110]. Smoothing functions were applied to both electrostatics and Van der Waals interactions from a distance of 10 Å. All chemical bonds were kept fixed by using the SHAKE

[2]NAMD was developed by the Theoretical and Computational Biophysics Group in the Beckman Institute for Advanced Science and Technology at the University of Illinois at Urbana–Champaign, `http://www.ks.uiuc.edu/Research/namd/`

constraint algorithm [111, 112]. The equations of motion were integrated with the extended Velocity Verlet scheme [113] with a step size of 1 fs, for a total of 10 ns, after equilibration. Coordinate sets were saved every 200 fs for data analysis, which was performed with the help of the VMD software[3] [114].

For temperatures below and above 300 K, a new equilibration was perfomed in the NPT ensamble at P = 1 bar and the requested temperature. Each equilibration started from the last equilibrated configuration at higher (or lower) temperature. Trajectories were recorded for a total time of 10 ns.

The system with fixed translations and/or rotations at each temperature were not re–equilibrated; the trajectories were recorded for 10 ns in the NVT ensemble. The system with water molecules restrained by a harmonic potential need instead a re–equilibration procedure, which lasted 10 ns, after which a 10 ns trajectory at 300 K was recorded.

Information on the atomic motions was obtained through the evaluation the time average deviation of each atom X from its average position or Root Mean Square Fluctuation (RMSF):

$$RMSF(X) = \sqrt{\frac{\sum_{j=1}^{N}(\mathbf{r}_X(t_j) - <\mathbf{r}_X>)^2}{N}} \tag{4.2}$$

where N is the total number of time steps t_j and $<\mathbf{r}_X> = \frac{1}{N}\sum_{j=1}^{N}\mathbf{r}_X(t_j)$, where $\mathbf{r}_X(t_j)$ is the position of the atom, whose RMSF is being calculated.

4.3 Small angle X–Ray Scattering

Small–angle X–ray scattering (SAXS) belongs to a family of scattering techniques widely used in the characterization and study of both structure and dynamics of many different systems, as biological macromolecules or materials. The method is accurate, non–destructive and usually requires only a minimum of sample preparation. Samples for SAXS can be solid or liquid, or even heterogeneous, containing solid, liquid or gaseous domains of the same or another material in any combination. It has the advantages that crystalline samples are not needed and the study of large macromolecules and aggregates is straightforward.

In SAXS experiment, a sample with inhomogeneities in the 1-1000 Å range is exposed to X–rays with a typical wavelength $\lambda \simeq 0.15$ nm. The scattered intensity $I(q)$ is recorded at very low angles (up to 10°), as a function of momentum transfer q ($q = 4\pi\sin(\theta)/\lambda$, where 2θ is

[3] VMD – Visual Molecular Dynamics, `http://www.ks.uiuc.edu/Research/vmd/`

the angle between the incident and scattered radiation). Data in the present work have been recorded in the q range 0.01–0.5 $Å^{-1}$.

SAXS signal originates from a large number of molecules randomly oriented, thus it is inherently averaged and presents a loss of information, if compared e.g. with crystallography. Parameters easily obtained with SAXS are average particle sizes, shapes, distribution, and surface–to–volume ratios. Ordered or partially ordered systems such as porous or fractal–like materials can also be studied.

The random positions and orientations of particles result in an isotropic intensity distribution which, for monodisperse non–interacting particles, is proportional to the scattering from a single particle averaged over all orientations. The net particle scattering is proportional to the squared difference in contrast, i.e. in scattering length density, which for X–rays is electron density, between particle and background. Detailed structural information can be obtained in disordered systems between 50 and 250 Å, while in partially ordered systems up to 0.15 μm [115].

An example of scattering curves for different proteins in solution is reported in fig. 4.4. At low q values the curves carry information on particle shape. Intermediate values are useful to obtain information on the protein folding, while high q values allow to penetrate in the molecular structure. SAXS signal becomes more and more unresolved in the latter region, making SAXS unsuitable to study molecular structure, which instead is the domain of WAXS, Wide–Angle X–Ray Scattering.

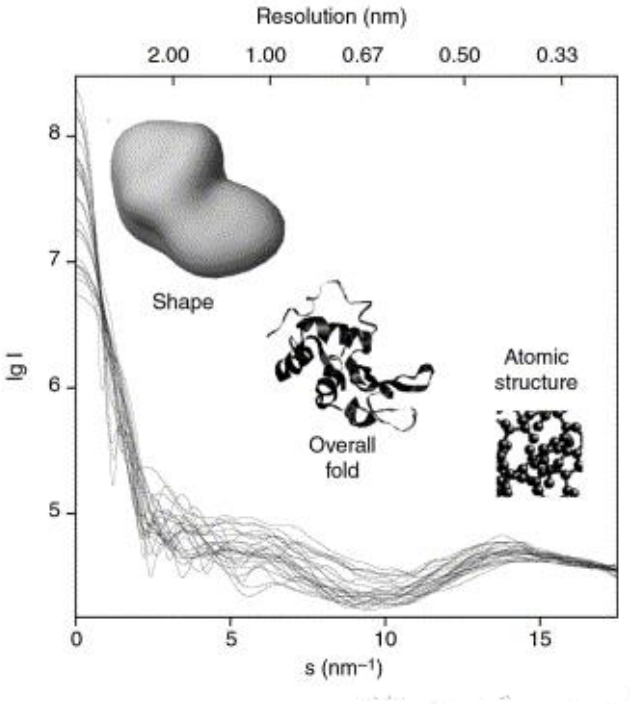

Figure 4.4: SAXS curve for different proteins in solution; s is linearly proportional to q (reproduced from http://en.wikipedia.org, Licence GNU FDL).

In a SAXS instrument, a monochromatic X–Ray beam hits a sample and some intensity scatters, while most is simply transmitted. The scattered X–rays form a scattering pattern which is then detected at bidimensional flat X–ray detector situated behind the sample. The transmit-

ted beam is filtered with a beam stop, which avoids saturation and eventual damage of the detector. Because of the low angle of detection, this technique needs a highly collimated or focussed X–ray beam. For this reason SAXS is often performed at synchrotron radiation sources, in particular if diluted samples or weak scatterers are to be analysed. However also laboratory sources exist and can be fruitfully used for concentrated samples.

Laboratory SAXS instruments are built taking in particular account the beam collimation, and can have either point–collimation or line–collimation geometry. In the present work a laboratory instrument with point–collimation geometry has been used: it has pinholes that shape the X–ray beam to a small circular or elliptical spot that illuminates the sample. Thus the scattering is centro–symmetrically distributed around the primary X–ray beam and the scattering pattern in the detection plane consists of circles around the primary beam. In particular, the utilised instrument is a Bruker Nanostar with multiwire detector HighStar, equipped with a graphite monochromator, which uses Cu–Kα radiation. Dynamic vacuum was maintained in the sample chamber during all the measurements. Due to the small dimension ($\sim$0.1 mm^2) of the beam and the non–homogeneity of the samples, a preliminary scan was performed in order to optimize the X–ray transmission.

Functions for data analysis

In the case of dilute solutions of identical particles with no long–range order and constant electron density ρ, embedded in a medium of electron density ρ_0, the scattering intensity is:

$$I(q) = (\rho - \rho_0)^2 v^2 \int 4\pi R^2 \gamma(R) \frac{\sin(qR)}{qR} \mathrm{d}R \tag{4.3}$$

where $I(q)$ is the single particle scattered intensity, R and v are respectively radius and volume of a single scattering particle, and γ is the normalized correlation function [115]. In the case of spherical particles with constant electronic density and radius R, this equation becomes:

$$I(q) = (\rho - \rho_0)^2 v^2 \left[3 \frac{\sin(qR) - qR\cos(qR)}{(qR)^3} \right]^2 \tag{4.4}$$

where the quantity between square brackets is the so–called Rayleigh function [115]. At variance, for system of random shaped particles, with constant electronic densities, the expression results in the Debye equation:

$$I(q) = \frac{A}{\left(1+(qD)^2\right)^2} \tag{4.5}$$

where A is a proportionality constant and D the average dimension of the object, kept constant [116]. For other geometrical bodies, like ellipsoid cylinders and prisms, semi–analytical expressions can be found. Equation 4.5 has been used to fit random–shaped inhomogeneities in the matrix.

In the limit of very low q the Porod law applies, in which $I(q) \propto q^{-4}$. This describes the presence of large scale interfaces, as e.g. those derived from sample mesoscopic cracking.

For undiluted systems an interference term must be also considered. For spherical particles the overall intensity thus becomes:

$$I(q) = (\Delta\rho)^2 v^2 P(q) S(q) \tag{4.6}$$

where $P(q)$ is the form factor and $S(q)$ is the structure factor of the lattice of interacting particles. For a lattice of spheres of identical size, $P(q)$ assumes the Rayleigh expression reported above, while other expressions have been derived for both $P(q)$ and $S(q)$ for a large variety of systems of particles with different shapes and different lattice arrangements.

In the case of myoglobin embedded in saccharide matrices, the Rayleigh expression, for $P(q)$, and the Percus–Yevick function in the decoupling approximation, for $S(q)$, have been utilised [117, 118]. By approximating the protein as hard spheres, this function assumes an analytical form:

$$PY(q) = \frac{1}{1-24\eta\left(p_1(q)+p_2(q)+p_3(q)\right)} \tag{4.7}$$

where:

$$p_1(q) = \frac{(1+2\eta)^2}{(1-\eta)^4}\frac{2qd\cos(2qd)-\sin(2qd)}{(2qd)^3},$$

$$p_2(q) = \frac{-3\eta(2+\eta)^2}{2(1-\eta)^4}\frac{\left((2qd)^2-2\right)\cos(2qd)-2qd\sin(2qd)+2}{(2qd)^4},$$

$$p_3(q) = \frac{\eta(1+2\eta)^2}{2(1-\eta)^4}\frac{\left((2qd)^4-12(2qd)^2+24\right)\cos(2qd)-\left(4(2qd)^2-24\right)\sin(2qd)-24}{(2qd)^6};$$

in these equations d is the protein–protein average distance and η stands for the volume fraction of the supposedly spherical particles.

SAXS sample preparation and measurement

Four saccharide matrices have been studied with SAXS (trehalose, sucrose, maltose, lactose) both with and without protein. Samples were prepared starting from solutions analogues to those used for FTIR samples, at the same initial concentrations (saccharide:protein ratio 40:1). Beside samples containing sodium ditionite (and MbCO, if with protein), as done for FTIR measurements, also samples without sodium ditionite (and *met*–Mb, if with protein) have been prepared to test the effect of a solute with high electron density.

Each sample was prepared by pouring 30 μL of the above solutions in a truncated cone hole in a steel sample holder, with $\sim$2.5 mm as smaller bottom diameter. The whole sample holder (containing 4 to 6 samples) was initially dried for $\sim$8 h in a silica gel desiccator, under either CO (samples with MbCO) or N_2 atmosphere (either samples with *met*–Mb or reference samples), and then further dried by leaving them for $\sim$15h at 353 K, under vacuum; such high temperature treatment was done to avoid sample micro–crystallisation, although small nano–crystals might form even under such conditions, as observed in some sucrose samples without protein [93]. The samples were then transferred within the measurement chamber, where they were left under vacuum at 298 K for several hours (up to 15 h). The data were then recorded at 298 K. Due to the small dimension ($\sim$0.1 mm^2) of the beam and the non–homogeneity of the samples, a preliminary scan was performed in order to optimize the X–ray transmission. SAXS data were then recorded in the q range 0.01-0.5 Å^{-1}. Several samples (5 to 15) were recorded for each system and the results were averaged.

At a variance with FTIR samples, with SAXS it is not possible to estimate the water content during the measure, hence no confidence on the final amount of water can be obtained. Indeed, water removal at 298 K was found to be a very slow process, and traces of water uptaken during the sample transfer might be not withdrawn. However, the long lasting drying allowed to the SAXS samples should be sufficient to avoid the slight differences in water content between FTIR and SAXS samples to quash the results. Quite large errors on parameters related to the water content, as the inhomogeneity sizes (see chapter 7), could be attributed to this supplementary dehydration.

Hydrated trehalose–myoglobin samples were prepared by progressive exposure to controlled moisture. The first hydrated sample (H1) was obtained by exposing the dry trehalose–myoglobin sample, at the end of the measurement, for $\sim$2 h at 60% relative humidity; the second hydrated sample (H2) by exposing the sample H1 at 75% relative humidity for $\sim$2 h;

the third hydrated sample (H3) was obtained by exposing H2 at 90% relative humidity for $\sim$2 h and the fourth (H4) by exposing H3 at 100% relative humidity for $\sim$2 h. It is worth noting that SAXS measurements must be performed under vacuum, hence the hydrated samples were able to lose water during the measurement, and we could not estimate their exact water content. However the short time needed for the data recording ($\sim$15 min), and the low drying speed in the measurement chamber, granted that the samples would not be fully dried in the process and, thus, that the hydration order (H4 $>$ H3 $>$ H2 $>$ H1 $>$ dry sample) should be preserved.

Chapter 5

FT–IR Results

In this chapter the IR results are presented starting with the characterisation of WAB by studying the samples with Hofmeister cosolutes, and then discussing the applications to systems containing protein and other saccharides.

5.1 The WAB in trehalose–cosolute systems

Sugars, rather than binding free water molecules, insert into existing HB network giving rise to a stable, homogeneous (at a mesoscopic level) system with strong and extensive interactions. With respect to local water HB network, the hydrated sugar matrix, which involves molecules much larger than water, able to interacting among themselves, has a larger amount of broken or weaker HB (structure breaking effect), together with stable domains with less defect areas and less free OHs, which would give an opposite structure–maker effect [119]. Therefore it is not surprising that WAB is structured and presents components typical of both chaotropic and kosmotropic environments.

The analysis of WAB in a wide set of samples containing cosolutes able to alter the HB network of the matrix put in evidence the presence of a recurring set of sub–bands, present in all the samples. The four principal sub–bands have been found in all the samples, with a fifth one seldom present, but recurring in some systems. The frequency interval for each sub–band is reported in table 5.1, alongside a name to identify it. Only in some cases other sub–bands are needed, namely in conditions of high ordering as e.g. incipient crystallisation. It should be noted that the frequency range is quite large for normal IR bands in nearly homogeneous samples, as those here studied. However, this is less surprising if we consider that the unperturbed WAB in

liquid water is a very broad band, with 300 cm^{-1} width.

As the WAB is supposed to originate from a water bending–libration combination, it is conceivable to ascribe the high and low frequency components to water interacting with stronger and weaker HB, respectively. Of the components, the only one with a simple assignment is W2, the unique component clearly present in samples of pure water (see fig. 4.3). Moreover, sample hydration causes essentially W2 growing (see section 5.3 below), with little effect on the other sub–bands. This suggests that it might be assigned to *bulk–like* water. "Bulk–like" water means the water interacting with other water molecules, as in a real bulk, but also water in an environment similar to the bulk water one. It is noteworthy that this band is usually the most populated in most of the samples, indicating that, in sugar amorphous matrices, a quite large amount of water could exists in not strongly strained environment.

Table 5.1: Frequency ranges for recurring sub–bands, utilised for the fitting of the WAB.

W0	2010-2030 cm^{-1}
W1	2050-2070 cm^{-1}
W2	2100-2140 cm^{-1}
W3	2180-2210 cm^{-1}
W4	2240-2270 cm^{-1}

Another component, whose assignment can be deduced with good accuracy, is W4. This sub–band is on the high frequency side of the WAB. The frequency of the maximum in cubic ice (2255 cm^{-1}) falls in its frequency range. Upon crystallisation of a saccharide matrix, an increase of the whole high frequency side, and in particular of the W4 component, is clearly evident (see fig. 5.1). W4 component could therefore be assigned to *ice–like* water, which does not necessarily correspond to crystalline water, but more to water in an ordered environment. It could be also noticed that crystallisation increases also W3 component, so also this sub–band might be related to ordered environments. However W3 is not evident in pure water, and its population

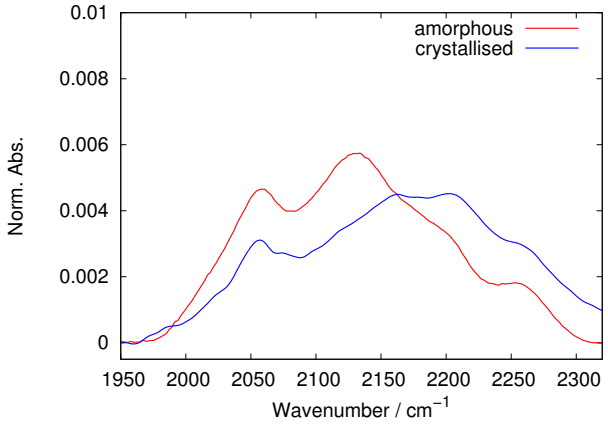

Figure 5.1: Comparison between fully amorphous and partially crystallised trehalose matrix with LiCl with ratio trehalose:salt 2:1. Note the increase in the high–frequency side of the band upon crystallisation.

Table 5.2: Peak positions for WAB components in trehalose matrices containing potassium halides, sodium perchlorate and sodium sulphate with ratio trehalose:salt 2:1.

	KF	KCl	KBr	KI	$NaClO_4$	Na_2SO_4
W0	–	–	–	–	2013	–
W1	2055	2055	2054	2052	2052	2035+2059
W2	2135	2131	2127	2127	2129	2084+2090+2103+2132
W3	2200	2195	2190	2190	2198	2183
W4	2263	2260	2259	2255	2260	2254+2331

is reduced following hydration, so it must depend on the solute presence and it is not likely to arise from structures, which can take place in pure water.

The effect of the presence of simple anions and cations in the trehalose matrix is shown in figures 5.2, 5.3, 5.4 and in table 5.2. In fig. 5.2 the WAB analysis for the series of potassium halides, with a ratio trehalose:salt 2:1, is reported. This concentration has been chosen as a compromise: it is high enough to have the salts to play Hofmeister effects on the matrix, but not so high to have all water in the salt domain. The HB network in these systems is dominated by sugar and water, the salt acting only as a modifier. It could be noticed that, descending in the group, there is a slight reduction of the population of high frequency components, with respect to low frequency ones, and a slight red shift of each peak.

From F^- toward I^-, the Hofmeister effect changes from kosmotrope to chaotrope, with inversion at Cl^-. F^- forms a tight hydration shell with many H_2O molecules, whereas Cl^- forms a very modest hydration shell. Br^- and I^-, on the other hand, can form only weak HB with H_2O. The kosmotropes acts as stabilisation centers, much more for F^- in comparison with Cl^-. The chaotropes, on the other hand, act as weakening agents, and their effect is stronger for I^- than for Br^- [120].

Considering that K^+ has a mild effect and cations should be, in principle, less effective that anions, we might attribute the alteration essentially to the effect of the latter. Therefore, the low frequency W1 component, dominant with more chaotropic salts, can be ascribed to water embedded in a chaotropic environment, while the high frequency W3 component to water in a kosmotropic environment. Also the W4 component is more populated with kosmotropic salts, as it can be expected considering that it should correspond to ice–like water, hence to a structured environment. The large difference between the effect of fluoride and the other anions

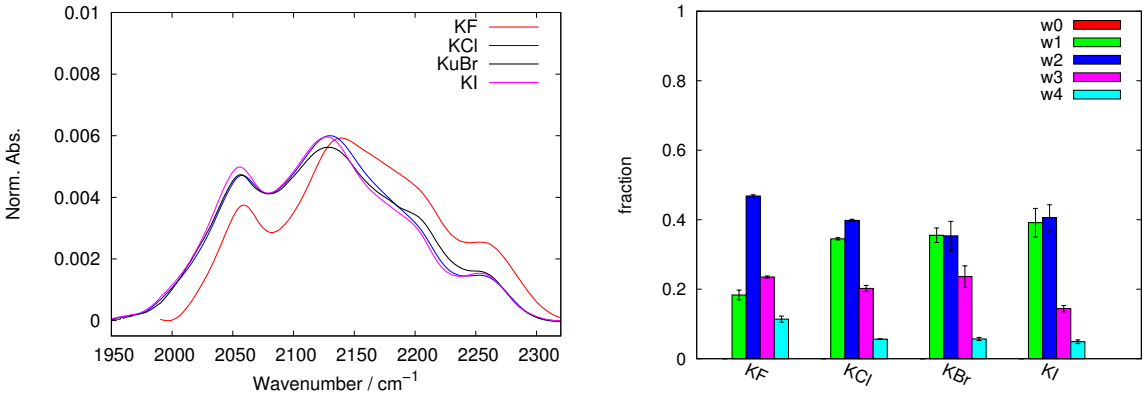

Figure 5.2: Profile of the WAB in trehalose matrices containing potassium halides with ratio trehalose:salt 2:1 (*left*) and population of the sub–bands (*right*). Vertical bars are standard deviations on the population.

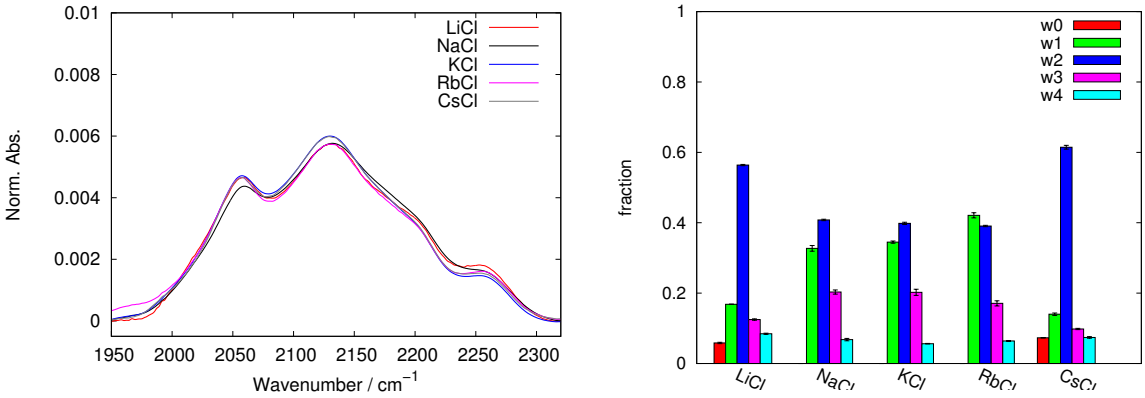

Figure 5.3: Profile of the WAB in trehalose matrices containing alkaline chlorides with ratio trehalose:salt 2:1 (*left*) and population of the sub–bands (*right*).

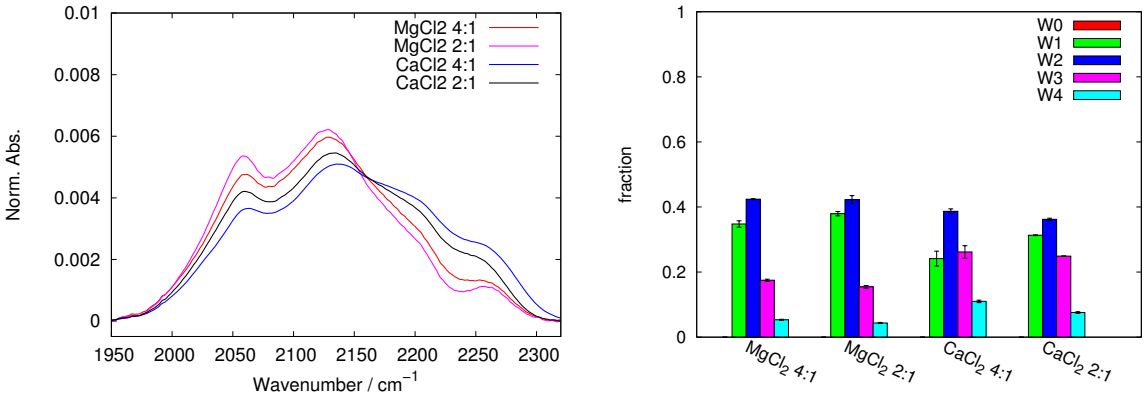

Figure 5.4: Profile of the WAB in trehalose matrices containing alkaline earth chlorides with ratio trehalose:salt 2:1 and 4:1 (*left*) and population of the sub–bands (*right*).

Table 5.3: Peak positions for WAB components in trehalose matrices containing alkaline and alkaline earth chlorides with ratio trehalose:salt 2:1, and trehalose:$CaCl_2$ 4:1.

	LiCl	NaCl	KCl	RbCl	CsCl	$MgCl_2$	$CaCl_2$	$CaCl_2$ 4:1
W0	2015	–	–	–	2017	–	–	–
W1	2054	2056	2055	2053	2053	2056	2056	2057
W2	2129	2133	2131	2130	2129	2130	2137	2137
W3	2201	2197	2195	2196	2201	2193	2197	2206
W4	2258	2261	2260	2260	2258	2261	2264	2264

could be due to the known autoassociation properties of this ion in water, which substantially alters the HB network [74].

In fig. 5.3 the WAB analysis for the series of alkaline chlorides, with a ratio trehalose:salt 2:1, is reported. It can be observed that only small variations are present changing the cation along the alkaline series. All the components have very similar frequencies[1] (see table 5.3), while the populations are very similar except for the two extremes of the series, Li^+ and Cs^+. The two latter induce an higher population of the central W2 component, with a depletion of both W1 and W3, and show also W0 component populated. The little effect observed agrees with the weakness of Hofmeister effect reported for cations, but the deviation for the extremes is not easily explainable, as lithium and caesium should have opposite effect, irrespective of the prevailing chaotropic or kosmotropic effect: their similarity is therefore unexpected. However, it is possible to find a correlation with the salt solubility in organic polar solvents (i.e. alcohols). Both the salts are more soluble than the three other homologues in alcohols, hence a more direct interaction with sugar hydroxyls can be conceived, which would allow water to remain in a less perturbed (more bulk–like) environment, thus increasing W2, or to interact with more hydrophobic part of the trehalose molecule. The latter would be the origin of W0 sub–band, which can be attibuted to water in a chaotropic environment, as confirmed below.

With alkaline earth cations (see fig. 5.4) there is a slightly larger effect on WAB: Mg^{2+} has frequencies and populations comparable with K^+, Na^+, Rb^+ cations, while Ca^{2+} induces a slight blue shift in W2 and W4 bands, leaving the frequencies of the other sub–bands unaltered, and an increase of population the high frequency W3 band. Both the alkaline earth ions

[1]Take notice that the instrumental error for the frequency is 2 cm^{-1}, while the standard deviation is always < 1 cm^{-1} except when indicated.

should be more chaotropic than their alkaline counterparts, with calcium ion more chaotrope than magnesium, this being apparently in opposition with the assignment of W3 to a structured environment proposed above.

A clarification can be obtained from the study of these two salts at a different concentration, 4:1 trehalose:salt ratio. The reduction in salt concentration causes in both the cases a shift of population toward high frequency components, as expected from chaotropic ions. In the case of magnesium the band shape remains very similar to what observed with the alkaline ions. In the case of calcium, at variance, the shape is even more different: this weird behaviour can be explained by taking into account that Ca^{2+} can form hydrated complexes with trehalose [84]. The formation of these complexes is likely to produce a structured environment, justifying the increased W4 at the expense of W1. However, raising Ca^{2+} content still causes the red shift typical of chaotropic solutes. This can explain the alkaline earth chloride behaviour, confirming, at the same time, the proposed assignments for the sub–bands.

To have a further support to these assignments, the effect of trehalose:salt ratio has been analysed for the potassium halides at three different ratios (4:1, 2:1, 2:3). The results are reported in figures 5.5, 5.6, 5.7, 5.8. Two behaviours are evident with respect to WAB shape: matrices containing KCl and KBr show little variations with concentration, while KF and KI show large changes.

The KCl case (see fig. 5.5), in which neglectable changes with concentration are present, well agrees with the "neutral" character of chloride ion, and gives a further confirmation of the idea that WAB sub–bands are related to populations of water in kosmo– and chaotropic local environments, with almost no effect of other quantities, e.g. ion strength. The only effect of

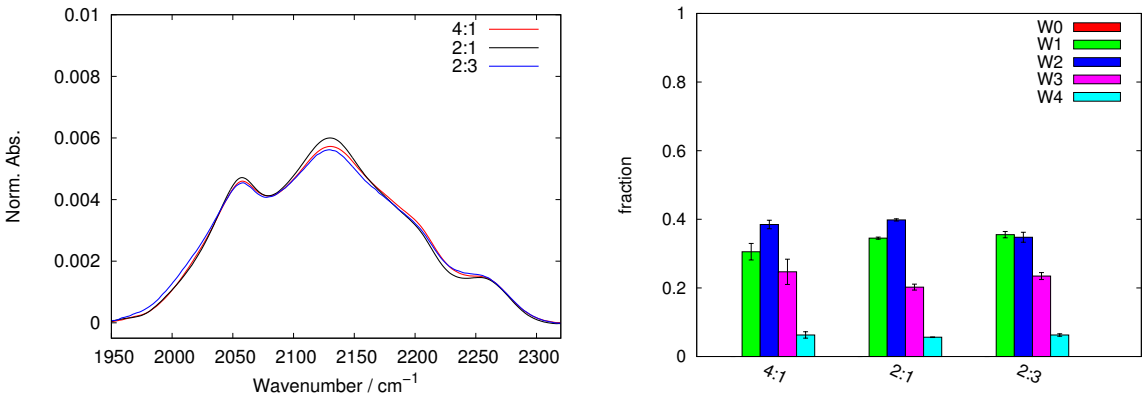

Figure 5.5: Profile of the WAB in trehalose matrices containing KCl at various concentrations (*left*) and population of the sub–bands (*right*).

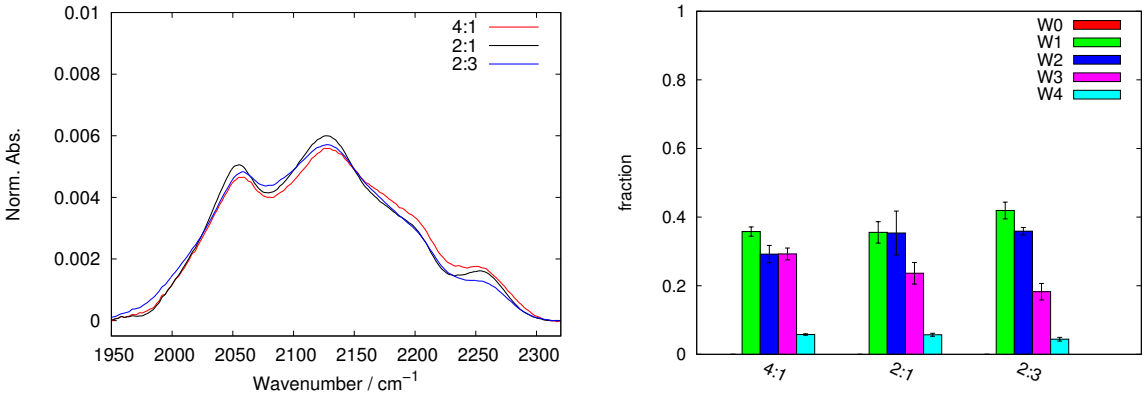

Figure 5.6: Profile of the WAB in trehalose matrices containing KBr at various concentrations (*left*) and population of the sub–bands (*right*).

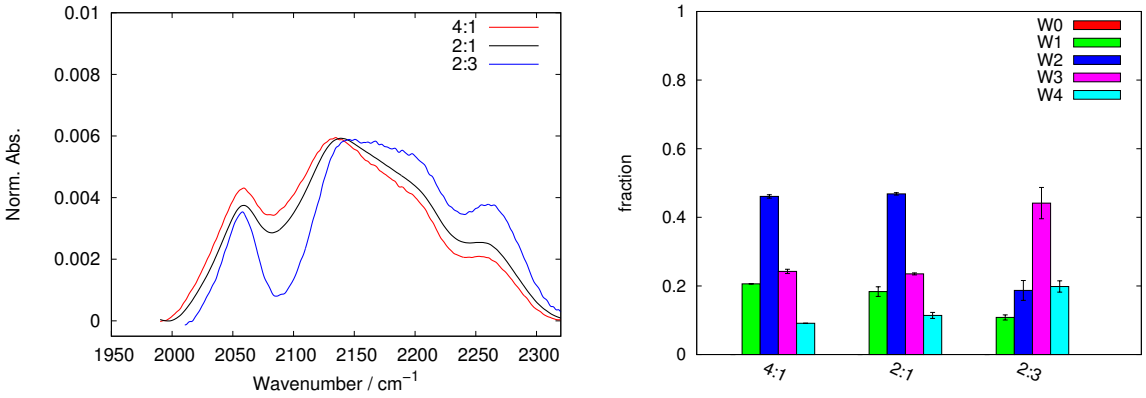

Figure 5.7: Profile of the WAB in trehalose matrices containing KF at various concentrations (*left*) and population of the sub–bands (*right*).

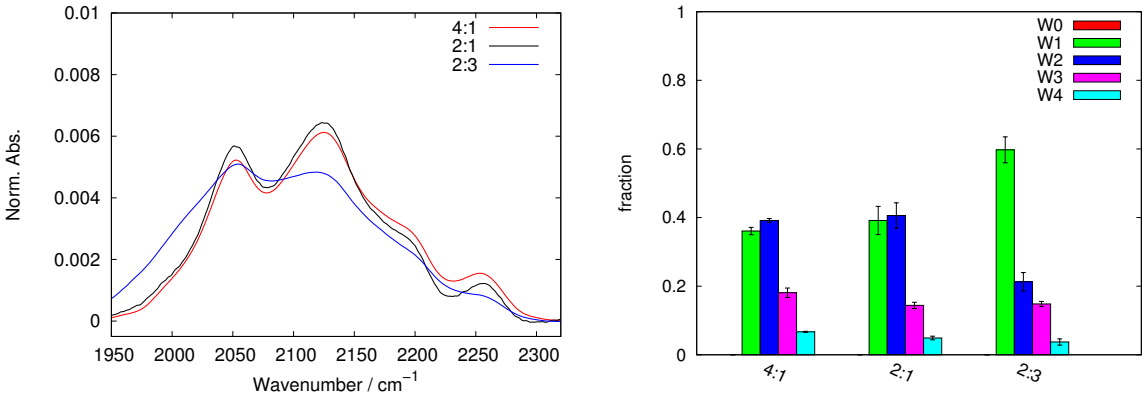

Figure 5.8: Profile of the WAB in trehalose matrices containing KI at various concentrations (*left*) and population of the sub–bands (*right*).

the increasing salt concentration is a slight grewth of W1 with respect to W2, which can be attributed to a weak chaotropic effect of K^+. The KBr case is similar, with stronger effects of concentration with respect to KCl, conceivably due to the weak chaotropic character of both cation and anion.

A different behaviour is found in the presence of KI and KF, considered strongly chaotrope and strongly kosmotrope respectively. For both, matrices with trehalose:salt ratios 4:1 and 2:1 have shape and population very similar to each other, while large deviations are present in matrices with the 2:3 ratio. As it could be expected from the sub–band assignments, high concentration of KF has a very large population of W3 and W4 sub–band (2/3 of total). W2, the bulk–like water component, ranks only third in population. Therefore the strong structuring KF enhances considerably the "structured" components W3 e W4, depressing W2 and W1, which stand for less organized water. In the same way, high concentration of KI enhances W1, which reach a population close to 60% of the total, making to reduce the other components. The behaviour of these two salts again concurs to confirm the dependence of the WAB sub–bands on the Hofmeister effects, and the assignments previously reported.

Another confirmation can be found investigating on more complex, and stronger, kosmotropic and chaotropic salts. Perchlorate (ClO_4^-) is a known chaotropic ion, stronger than I^- [121]. In fig. 5.9 it is shown that this ion induces high populations of W1 and W0, also at relatively low concentrations. Beside the same confirmation for W1, it hints that W0 is also related to non–structured environments, as it could be expected considering the low frequency of the sub–band. By relying on this assignment, it can be strengthened the proposed assignment for Li^+ and Cs^+, i.e. that W0 corresponds to water forced to a destructured environment or close to less polar part

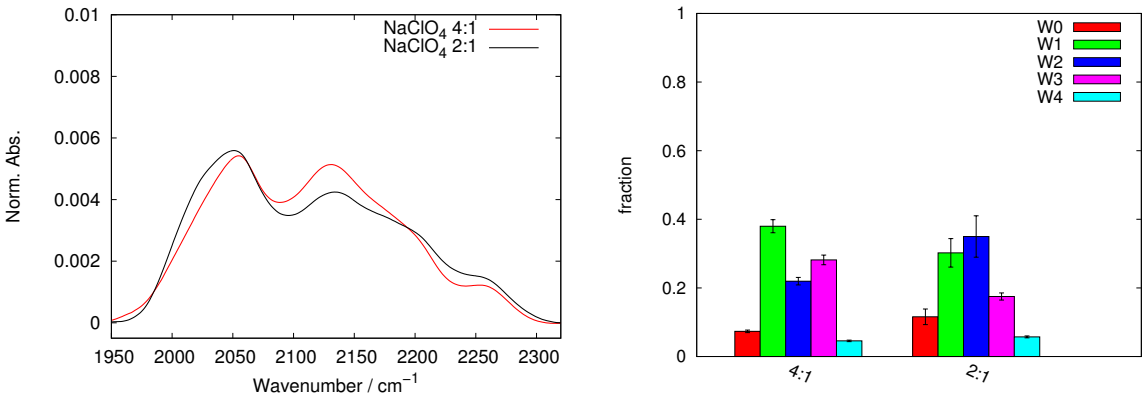

Figure 5.9: Profile of the WAB in trehalose matrices containing $NaClO_4$ (*left*) and population of the sub–bands (*right*).

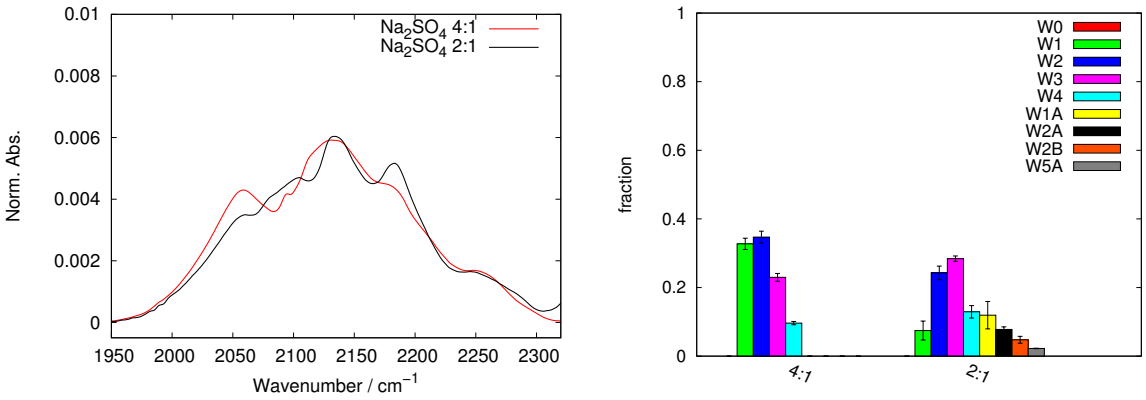

Figure 5.10: Profile of the WAB in trehalose matrices containing Na_2SO_4 (*left*) and population of the sub–bands (*right*).

of the trehalose molecule.

Sulfate ion (SO_4^{2-}) is among the most kosmotropic ions known, able to structure hundreds of water molecule around a single sulphate ion. Its effect on WAB appears much less marked than for perchlorate: at 4:1 ratio the increase in population of high frequency components is very small (see fig. 5.10). However, raising sulphate concentration does not only cause a noteworthy increase of these components, but also the formation of a large number of sub–bands by splitting the original components in two or three. This behaviour is similar to what can be observed upon partial crystallisation (cfr. fig. 5.1). It can be explained admitting that high concentrations of sulphate can structure the matrix up to generate crystalline or crystal–like domains, with water ordered in different ways giving different sub–bands. This again can be considered a

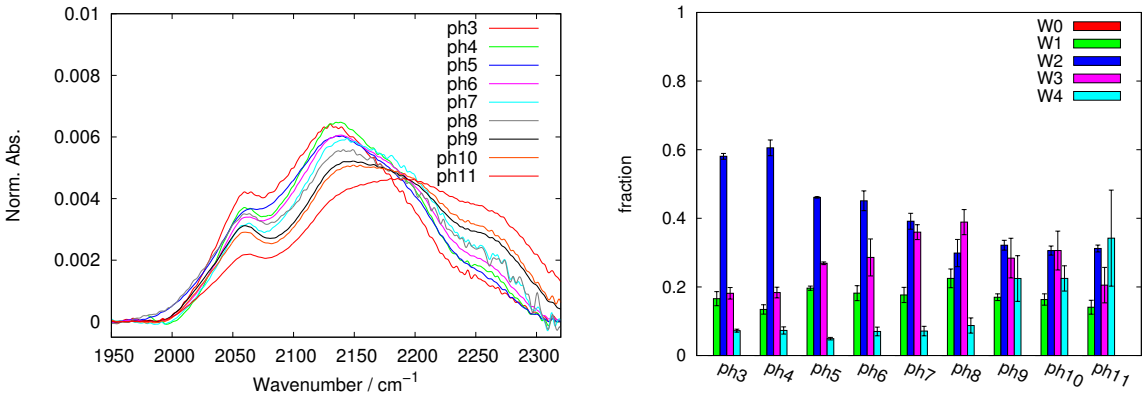

Figure 5.11: Profile of the WAB in trehalose matrices containing potassium phosphate with a ratio trehalose:phosphate 2:1, at various pH from 3 to 11 (*left*) and population of the sub–bands (*right*). The exact species present (H_3PO_4, KH_2PO_4, K_2HPO_4, K_3PO_4) depend on pH solution.

confirmation of the sensitivity of WAB to water stucture.

Also the effect of pH points out a direct relation with water structuring. The systems reported in fig. 5.11 were prepared by adding mixtures of phosphoric acid and its potassium salts with a ratio 2:1 trehalose:(total salt). The specific pH was obtained by regulating the exact composition of the mix: H_3PO_4+KH_2PO_4 at different ratios for pH = 3-5, KH_2PO_4+K_2HPO_4 for pH = 6-9, K_2HPO_4+K_3PO_4 for pH=10-11.

A low pH, which corresponds to high concentrations of the less kosmotropic species $H_2PO_4^-$ and to a rapid exchange of hydrogen bonds, is connected with high populations of W2 component. Raising pH makes to grow the population of more kosmotropic phosphate species, together with W3, and then W4 sub–bands. The pH variation does not alter significantly the population of W1 component, but its effect can be envisaged as an interconversion between W2 and W3-W4 components. This means that, rather than an ordering of the the whole HB network, pH acts by stregthening and ordering the bulk–like fraction of water.

Table 5.4: Assignment of WAB sub–bands.

W0	Strongly destructured
W1	Destructured
W2	Weakly structured *Bulk like*
W3	Structured
W4	Strongly structured *Ice like*

By summarizing the results on the trehalose–salt systems, it has been possible to deduce the assignment in table 5.4: W0 and W1 corresponds to water molecules in destructured environments, the former present only when strong structure–breakers are present; W2 to water with a level of order similar to liquid water, i.e. bulk–like water; W3 and W4 to more structured water, the latter reaching levels similar to a crystal, i.e. ice–like water.

5.2 The WAB in myoglobin–trehalose–cosolute systems

The comparison of band shapes in matrices with and without embedded protein provides data on the effects the presence of the protein plays on the matrix structure. The study of some myoglobin–trehalose–water systems in the presence of Hofmeister salts have substantially confirmed the behaviour already seen in matrices without protein. The concentration of salts in these samples was comparable with the previous ones, although formally the salt:trehalose ratio is doubled, as protein containing samples have roughly the same mass of trehalose+myoglobin and half the amount of trehalose (see section 4.1).

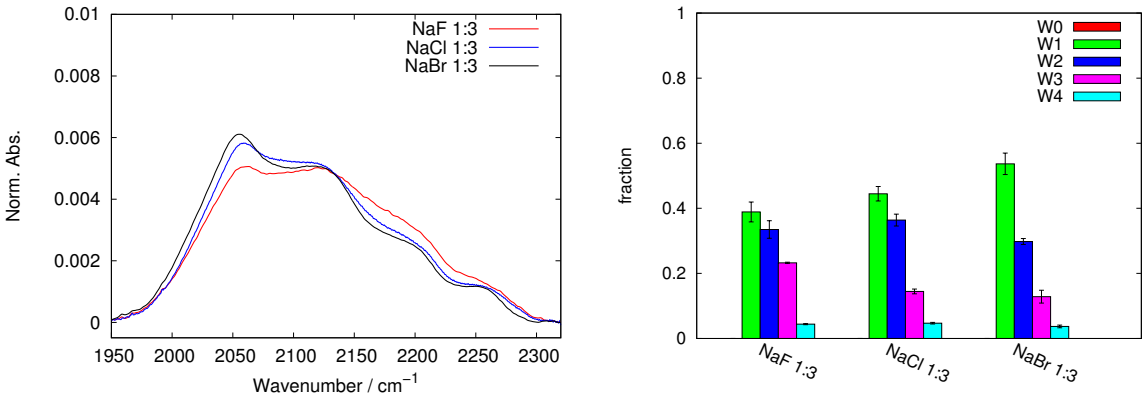

Figure 5.12: Profile of the WAB in myoglobin+trehalose matrices containing sodium halides with a trehalose:salt ratio 1:3 (*left*) and population of the sub–bands (*right*).

In the presence of sodium halides (see fig. 5.12), the effect of the anions is the same noticed in matrices without proteins, with W1 more populated for bromide, and W4 more populated for fluoride, both with respect to chloride. However the comparison between matrices with and without proteins shows two main differences: 1) notwithstanding the high concentration of the salts with respect to trehalose in the samples reported, the effect appears to be lower than what observed in matrices without protein; 2) the population of the sub–bands appears considerably shifted toward low frequency components. This indicates that the protein has a net chaotropic character that can compensate the effects even of strong kosmotropic ions, like fluoride.

With perchlorate and sulphate ions the chaotropic effect of the protein is always evident (see fig. 5.13). With sulphate the population of W1 band is high; large population of W2 and W3 are also present, alongside with a doubling of W1 band. With perchlorate the chaotropic effects of

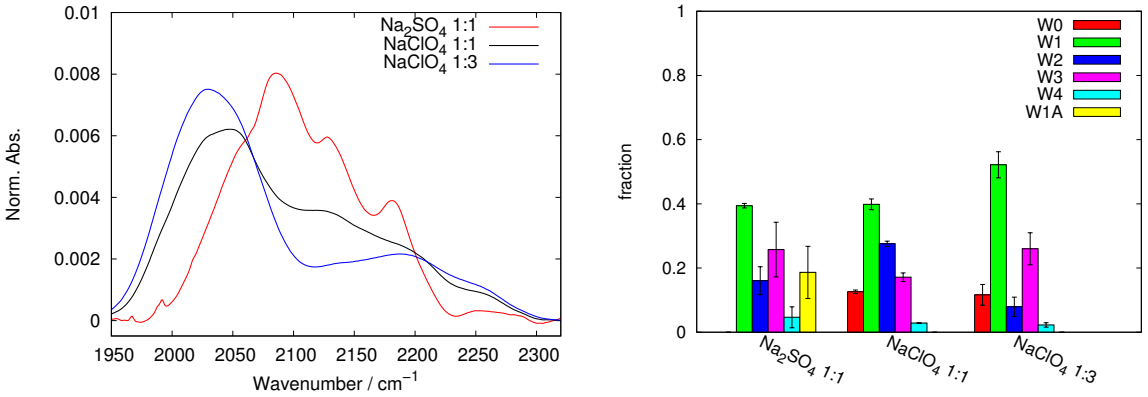

Figure 5.13: Profile of the WAB in myoglobin+trehalose matrices containing either sodium perchlorate or sodium sulphate(*left*) and population of the sub–bands (*right*).

salt and protein add, giving rise to samples with fractions of W0 + W1 above 60% of the total and a distinctive shape for WAB, which appears bifurcated with two separated peaks.

5.3 Myoglobin–saccharide systems

The classification of sub–bands performed in binary trehalose–salt systems has been used to deepen the knowledge of matrices of other saccharides. The normalised profiles of the WAB for trehalose, sucrose, maltose and raffinose are reported respectively in figures 5.14, 5.15, 5.16, 5.17, while the peak frequencies for the sub–bands are reported in table 5.5. In each figure, the normalised profiles of the WAB for saccharide–water systems are reported alongside the WAB for myoglobin–saccharide–water systems dried under high vacuum at 80°C, i.e. in their glassy state, and hydrated at 60% relative moisture, i.e. in their rubbery state.

The development of water–sugar interactions induces a breaking of a number of sugar–sugar HBs proportional to the number of hydroxyls engaged in the sugar–sugar bonding and the generation of new sugar–water HBs. Such a number of HBs is then determined both by the number of hydroxyls available in the sugar molecule (larger in the trisaccharide than in disaccharides) and by the spatial orientation of carbohydrate hydroxyls, which should permit the formation of the new bonds. This implies that carbohydrate with same molecular weight (and same HB donor/acceptor groups), but different spatial orientation of hydroxyls generate different spectra [119].

When comparing high and low hydration samples, a characteristic trend is present irrespective of the saccharide: in the former the band loses its saccharide–specific features and approaches the shape it has in pure water [98]. The population of W2 sub–band is in every case

Table 5.5: Peak positions for WAB components in saccharide (P′r) and protein+saccaride matrices (dry and hydrated).

	Trehalose			Sucrose			Maltose			Raffinose		
	P′r	dry	hydr.	P′r	dry	hydr.	P′r	dry	hydr.	P′r	dry	hydr.
W1	2058	2057	2059	2055	2047	2058	2051	2056	2059	2052	2048	2049
W2	2133	2122	2132	2119	2104	2132	2143	2111	2138	2125	2096	2120
W3	2196	2189	–	2183	2183	–	2194	2188	–	2190	2190	2201
W4	2262	2264	2274	2250	–	2270	2260	2263	2275	2249	2257	2258

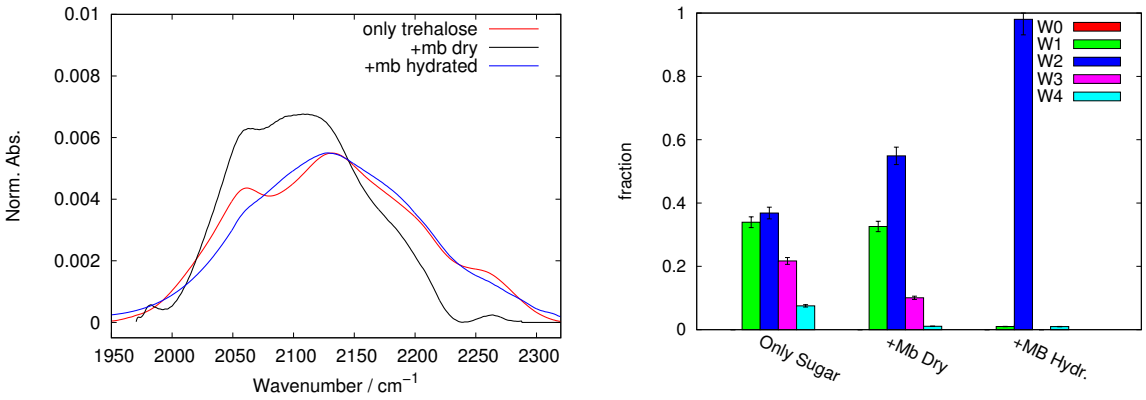

Figure 5.14: Profile of the WAB in various trehalose and myoglobin+trehalose matrices at two different hydrations (*left*) and population of the sub–bands (*right*).

above 90% of the total, with small amounts of W1 or, in the case of raffinose, W3 and W4. This might arise both from the higher contribution of water–water interactions on the band and from a higher mobility of the water molecules, expected for a non–glassy system, i.e. a bulk–like behaviour.

WAB profiles in dry conditions are instead strongly dependent on the type of saccharide, as they arise from different patterns of population of HB local structures. In particular, in the three disaccharides here reported the band is divided in at least four components, whose frequency is roughly the same in trehalose and maltose, but whose population differs. In sucrose the frequencies of the sub–bands are instead lower.

A different behaviour can be noticed in raffinose (see fig. 5.17): the WAB shape in this saccharide is totally dominated by W2 independent of the hydration or of the presence or the

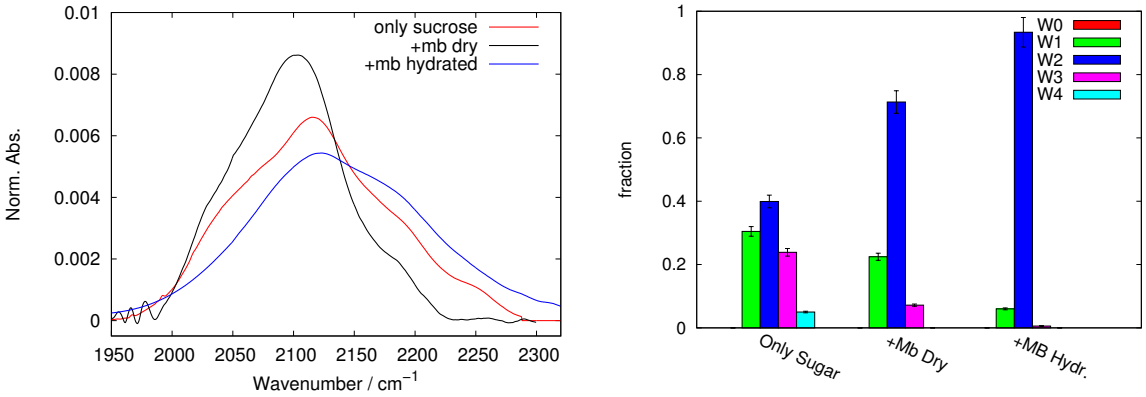

Figure 5.15: Profile of the WAB in various sucrose and myoglobin+sucrose matrices (*left*) and population of the sub–bands (*right*).

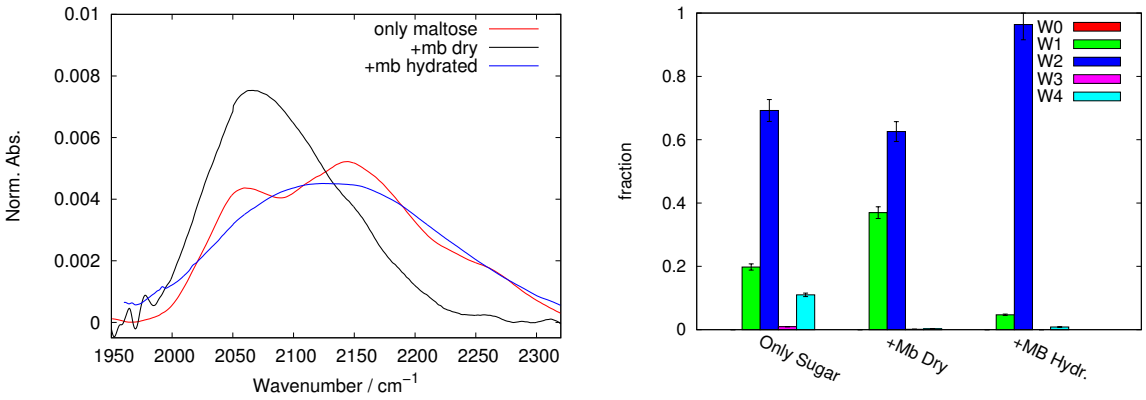

Figure 5.16: Profile of the WAB in various maltose and myoglobin+maltose matrices (*left*) and population of the sub–bands (*right*).

absence of protein. The difference between dry and hydrated samples is an overall red–shift of W2. The peculiarity of raffinose behaviour likely arises from the much large hydration capacity of this sugar, with respect to disaccharides. The distribution of water molecules is not strongly altered with hydration; water is not distributed in different populations as in the other sugars, but instead likely performs bulk–like interactions with the matrix, whose strength is altered by hydration. Low hydration forces water in disordered structures, but in this case instead of producing a separated population of water in a distinct chaotropic environment, it drifts apart W2 peak frequency from the $\sim$2130 cm^{-1} frequency of liquid water. In this light, the behaviour of sucrose can be considered intermediate between raffinose and the other two disaccharides.

This difference among disaccharides is confirmed by the comparison of the band profile in binary and ternary systems in dry conditions. In trehalose and maltose (fig. 5.14 and 5.16) the

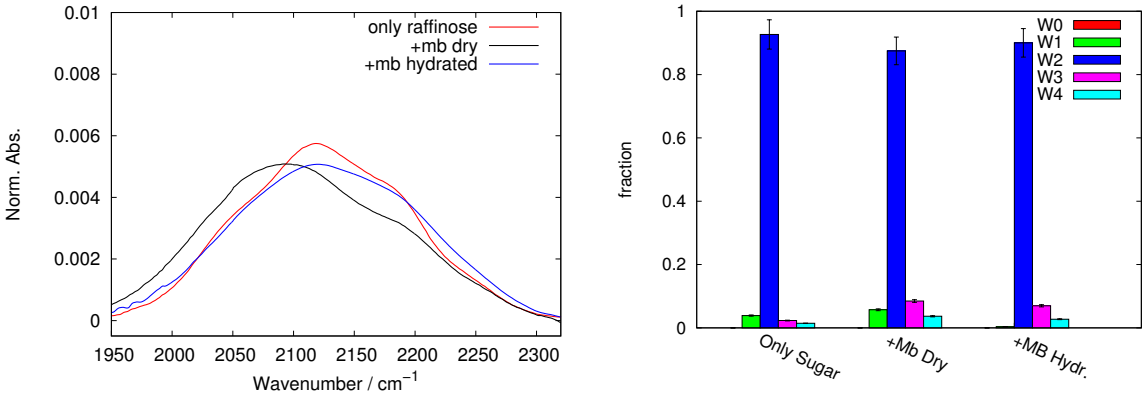

Figure 5.17: Profile of the WAB in various raffinose and myoglobin+raffinose matrices (*left*) and population of the sub–bands (*right*).

band shape undergoes a huge change, indicating that the introduction of protein strongly alters the distribution of HB structures. In both cases one can notice an increase in the low frequency components at the expense of the high frequency ones; the main component is always W2, which also undergoes a red shift. At the same time, W4 almost disappears along with an increase of W1 (see fig. 5.16). The structure–breaking effect of myoglobin therefore involves both the set–up of a separate population of water molecules and the modification of W2 frequency.

At variance, in sucrose (fig. 5.15) the band shape show smaller changes; as for the sub–bands populations, W2 increases to a larger extent than in trehalose and maltose, by depleting all the other components. At the same time it red–shifts to a larger extent with respect to the other disaccharides. Although not easily visible, a similar behaviour is present in raffinose. This agrees with what observed above: protein introduction has overall a chaotropic effect, which can also induce a significant increase of a subpopulation of water in a chaotropic environment, as seen in maltose, while it alters the detailed properties of an averaged water population (W2 sub–band) in raffinose; sucrose has an intermediate behaviour. The presence of the protein has therefore a weak influence on the latter matrices: they do not change substantially its HB networks to better host the protein, but simply reduces the average strength of the HBs. This might reduce the effectiveness toward bioprotection. The different behaviour of sucrose with respect to trehalose is in agreement with reported neutron scattering results, which propose that a larger amount of perturbed HBs establishes in very concentrated trehalose solutions, with respect to sucrose analogous [20], whereas higher average mean square displacements are found in sucrose [122].

The larger population of the low–frequency W1 component in maltose, with respect to the homologous disaccharides, indicates a stronger modification of the distribution of water population toward chaotropic environments, i.e. destructured HB networks. This could indicate an even more intimate interaction of water with the protein in maltose. It would be therefore possible to put the four sugars in an order of HB network resistence to perturbation upon adding protein (raffinose $>$ sucrose $>$ trehalose $>$ maltose). For the disaccharides, this order is the same obtained for the occurrence of inhomogeneities in the matrix (see chapter 7).

The study of COB support these results, from the point of view of the protein. It has been reported that a shoulder appears in the low frequency side of the spectrum of sucrose and raffinose matrices, which corresponds to a fourth A substate [42, 43]. This substate would arise from heme pocket structural modifications induced by sucrose–like units [38]. Here it could

be added that the strong and scarcely alterable HB network in sucrose and raffinose could be a supporting factor, or else another cause, for the deformation of the protein, which is forced to adapt to the matrix HB network. This, at variance with trehalose and maltose, in which the host matrix friendly adapts to protein insertion.

5.4 Measurements at variable hydration: an "optimal" protein–saccharide ratio

Besides water content, the properties of the saccharide amorphous matrices are noticeably variable also with the protein/sugar ratio. It has been already proposed that an optimal ratio between preserver sugar and preserved protein can be identified to grant both the maintenance of the glassy state and the conservation of the biomolecule [123, 124].

Here data for protein+saccharide systems at different ratios from 10:1 to 160:1 (or 320:1) saccharide:protein (S/P) are reported in figures 5.18, 5.19, 5.20, 5.21, 5.22. In each figure the profile of both COB and WAB are reported. In table 5.6 the residual water amounts after dehydration are reported together with the r_A values (see section 4.1). The latter value is used as a rough estimate of the relevance of the interactions of residual water molecules with non–water HB forming groups.

From the data in table 5.6 is evident that different S/P ratios give different water content,

Table 5.6: Water/saccharide (W/S) ratio and r_A for components in protein+saccharide systems at various saccharide/protin ratios (S/P). For raffinose the S/P ratio is renormalised to an equivalent disaccharide, the real values are 2/3 of the reported value.

	Trehalose		Sucrose		Maltose		Lactose		Raffinose	
S/P	W/S	r_A	W/S	r_A	W/S	r_A	W/S	r_A	W/S	r_A
10	3.8	3.0	0.8	20.6	1.2	9.6	2.0	7.4	1.2	18.7
20	1.8	7.8	0.4	39.2	0.5	23.5	0.4	21.2	1.0	19.4
40	0.3	27.5	0.3	19.5	0.3	27.5	0.2	39.1	0.3	68.0
80	1.4	6.0	2.2	5.2	1.2	8.0	2.1	7.9	2.1	6.5
160	2.0	8.7	3.3	5.2	2.4	7.8	3.2	6.8	5.6	4.2
∞	3.0	6.4	0.8	19.5	4.0	5.9	5.3	5.4	6.8	4.6

even though the sample is treated in the same way. At a specific S/P ratio the water content reaches a minimum. This ratio, in the limit of the analysis here performed, is the same in all the systems and corresponds to 40:1 disaccharide:protein (or 27:1 raffinose:protein), i.e. roughly a equal mass ratio between myoglobin and sugar. At this ratio myoglobin performs the most complete substitution of water in the sugar–dominated HB network. Lower ratios imply a network dominated by myoglobin: in this case a complete coating of the protein by the sugar is not granted, and further water is needed to saturate the HB capacities of protein and matrix. This is particularly evident in the case of trehalose, which need more water at high protein concentration with respect to the other sugar.

An increase in residual water content is evident also at high saccharide:protein ratios, beyond 40:1. In this case, when the matrix becomes more and more sugar–dominated, the protein is unable to substitute all the water necessary, and a certain amount of water has to remain in the matrix. This is particularly evident in the case of raffinose, whose increase in water content is higher than the other sugars, in agreement with raffinose higher equilibrium water content. This increase in water content leads generally to values lower than what found for sugar–only matrices (∞ line in table 5.6). An exception is sucrose, whose matrices without protein have lower water content than matrices containing low amounts of protein. This can be explained by considering that stable sucrose crystals are anhydrous, hence removing the protein it is possible that dehydration induces the formation of anhydrous nano–crystalline domains (see chapter 7), leading to reduction in water content. This has been also confirmed with a myoglobin+sucrose sample with a S/P ratio 320:1. Its water content (W/S = 1.1) is intermediate between the sample without protein and with S/P = 160.

The analysis of r_A shows a non–monotonic behaviour with changing composition, which closely parallels the water content. This is expected as lower water content should obviously correspond to higher interactions with non–water hydrogen bonding groups. For all the saccharides r_A maximum is therefore observed at S/P$\simeq$40, except for sucrose, whose maximum is at lower S/P ratio ($\simeq$20). This means that in sucrose the interaction of residual water with other groups is stronger at higher myoglobin ratio with respect to the other saccharides, i.e. more myoglobin has to be added to produce a strong perturbation of the matrix (see section 4.1). This confirms, in some way, what previously found about the resistance to perturbation of the sucrose matrix to protein insertion.

It must be noticed that trehalose show steeper variations around the minimum water content.

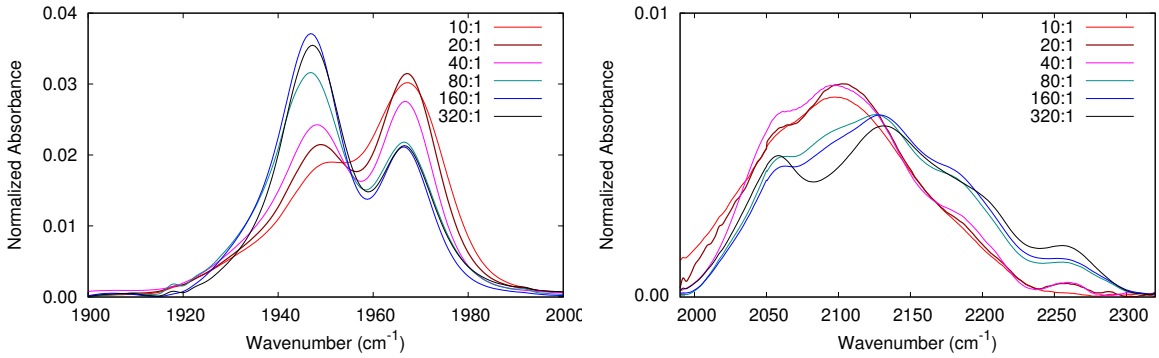

Figure 5.18: Profile of COB (*left*) and WAB (*right*) in protein+trehalose matrices with various sugar:protein ratio.

With respect to other saccharides, at low concentrations trehalose tends to better retain or absorb water. This can be suggested to have a role in biopreservation, allowing trehalose to oppose dehydration until it reaches an "optimal" concentration to maximize the interaction with protein, after which the system is stable also at very low water content.

The profiles of COB and WAB have a common behaviour with the S/P ratio, irrespective of the saccharide. The curves appears in almost every case separated in two groups. This is particularly evident with WAB, where for trehalose, sucrose and maltose the groups are constituted by very similar curves. In lactose and raffinose matrices a less sharp "transition" is evident.

The first group of curves is constituted by samples with S/P ratio equal to 10, 20 and 40. The WAB has in these cases a higher fraction of low frequency components, and it is very dissimilar from the shape it has in samples without protein. The second group is constituted by samples with high S/P ratio (80, 160 and, if present, 320), whose WAB has a higher fraction of high frequency components and appears similar to the one in matrices without protein.

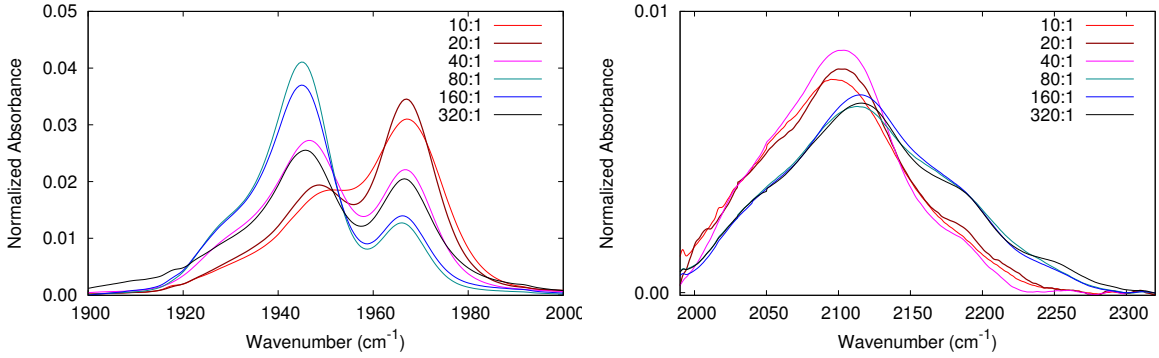

Figure 5.19: Profile of COB (*left*) and WAB (*right*) in protein+sucrose matrices with various sugar:protein ratio.

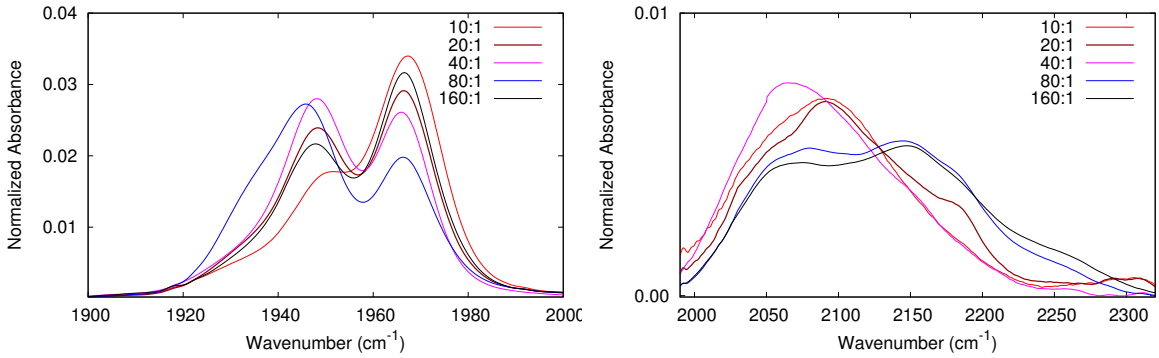

Figure 5.20: Profile of COB (*left*) and WAB (*right*) in protein+maltose matrices with various sugar:protein ratio.

From these data it is possible to deduce that the properties of the matrices do not vary continuously with increasing protein concentration, but undergo a change, which is also abrupt for trehalose, sucrose and maltose, at a S/P ratio between 40 and 80. Above the transition ratio the shape of the WAB is similar to the system without protein, hence it is possible to suggest that the matrix is dominated by the sugar. Below the transition ratio, at variance, the matrix, as perceived by water molecules, is dominated by the presence of the protein. The occurrence of high fractions of low frequency sub–bands indicates that water is forced to a larger extent in a chaotropic environment (plausibly the protein surface), strengthening the idea of an extensive saccharide–protein–water interaction at high protein concentrations.

The same transition can be observed, although less distinctively, in the COB, indicating that the alteration of the matrix is mirrored by simultaneous alteration of the protein heme pocket. The transition seen in the COB appears more gradual than the one observed in WAB, and is different among the different sugars. The jump between S/P = 40 and 80 is still evident in

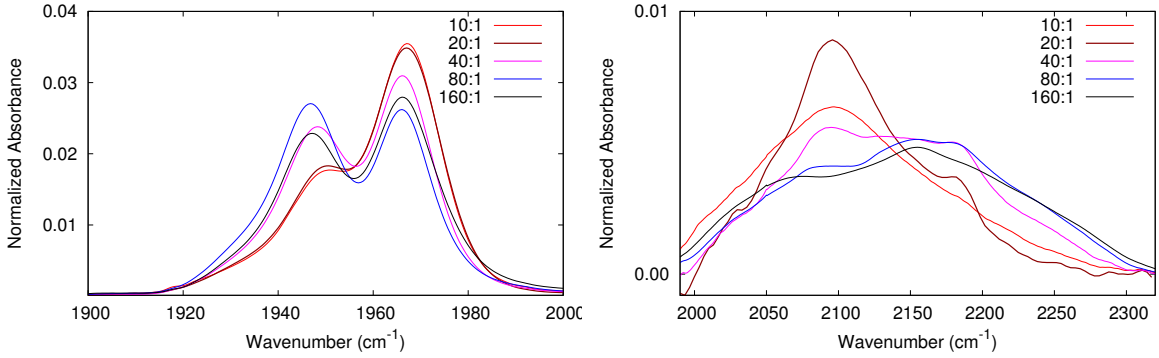

Figure 5.21: Profile of COB (*left*) and WAB (*right*) in protein+lactose matrices with various sugar:protein ratio.

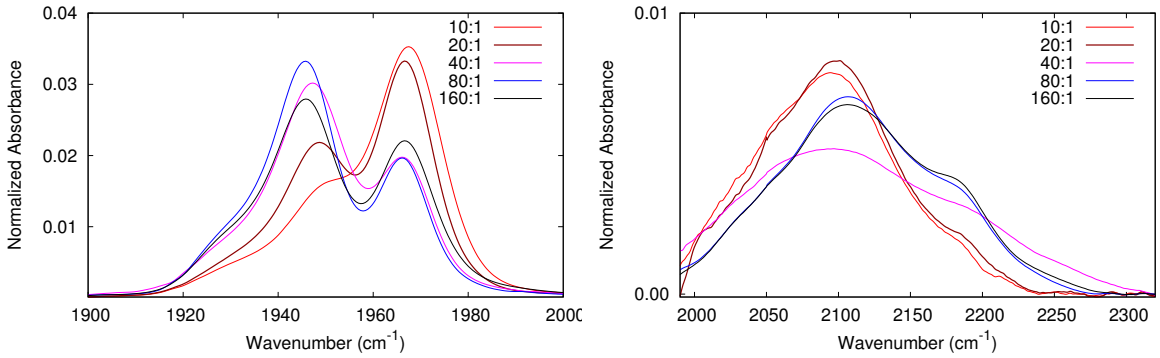

Figure 5.22: Profile of COB (*left*) and WAB (*right*) in protein+raffinose matrices with various sugar:protein ratio. The reported S/P ratio is renormalised to an equivalent disaccharide, for sake of comparison with the other sugars. The real values are 2/3 of the reported value.

trehalose, while in lactose and raffinose it is shifted between 20 and 40; in maltose it is even between 10 and 20; in sucrose S/P = 40 has an intermediate curve, which could be put forward as a "midpoint". These differences hint that, although a relation should be present between the alteration of the matrix and of the protein, this is not straightforward as the common concept of slaving would indicate.

From the point of view of the heme structure, it should be noticed that at high sugar concentration the fraction of A_1 substate, which is the most stable in natural conditions, is higher. Myoglobin is therefore better hosted in systems with high S/P ratio. This should not be surprising as in these conditions the protective effect of the saccharide sums up to a relatively high water content, which would allow myoglobin to adopt and keep a more stable conformation. At variance, the importance of systems with low S/P ratio is that they can withstand very low hydration: in these conditions myoglobin is subject to higher stress, which is reflected in the increase of A_0 substate, but it is not subject to denaturation, as the COB area is roughly the same in all the system studied.

The shift in COB transition with respect to WAB one occurs always on the side of larger protein content. Hence three concentration ranges exist: in the sugar–rich side (S/P $\gtrsim$ 80) the matrix is dominated by the sugar, and in turn it maintains the protein in an unstressed form (matrix slaving on protein); in the protein–rich side (S/P $\lesssim$ 20-40, depending on the sugar) the matrix is dominated by the protein, which converserly appears deformed by the increase of A_0 substate (protein slaving on the matrix); in the intermediate concentration range a mixed behaviour is present, with the matrix dominated by the protein, but still enough sugar, able to preserve the unstressed form of the protein (protein–matrix coupling).

FTIR data for samples with variable S/P ratios therefore confirm the existence of an "optimal" sugar/protein ratio, at which the components of the system are more strongly interacting and the system can withstand lower water content. This ratio does not correspond to a system in which the protein is less perturbed, as this happens at higher sugar content, when the system is more hydrated.

In this respect, it should be noticed that, from an applicative point of view, it is not a good strategy to increase the sugar content hoping to improve the preservation properties. In all the saccharides, with the noteworthy exception of trehalose, the samples with S/P = 160 have a lower fraction of A_1 than the samples with S/P = 80. In the former systems it is likely that extensive sugar domains without protein set up, which might perturb the structure of protein–containing domains simultaneously present, hence act as a perturbing factor also for the protein. Above a certain level, the matrix becomes similar to a sugar–only matrix, to which the protein must adapt. This is particularly evident in sucrose at 320:1 ratio, where nanocrystallisation is easy to happen, and A_1 fraction is largely reduced (see fig. 5.19. The exception of trehalose could be proposed as another factor promoting trehalose effectiveness, as trehalose has the ability to better host the protein in a larger concentration interval. It should be however noticed that also trehalose exhibits the same behaviour, only at much higher S/P ratio, as can be viewed with a sample with S/P = 320 (see fig. 5.18).

5.5 Measurements at variable temperatures: dynamics and coupling

The thermal alterations of both the matrix and the embedded protein have been evaluated by using the *SD*s, calculated for the WAB (SD_{WAB}) and of the COB (SD_{CO}). A detail must be clarified about *SD* definition reported in section 4.1. In previous works [41–43], these alterations were already evaluated from a well reproducible thermal behaviour of *SD*, which monotonically increased from 20 to 300 K. Therefore the lowest temperature measured was, almost naturally, chosen as the reference temperature, assuming it corresponds to a sample in which all dynamics is blocked. Although slight deviations from this trend were observed in the range 20-170 K in very dry samples of glucose, maltose and raffinose, this effect was almost within the experimental error, and was safely neglected. At variance, the thermal behaviour of SD_{WAB} in some maltose and raffinose samples in the absence of protein shows a more pronounced off–trend

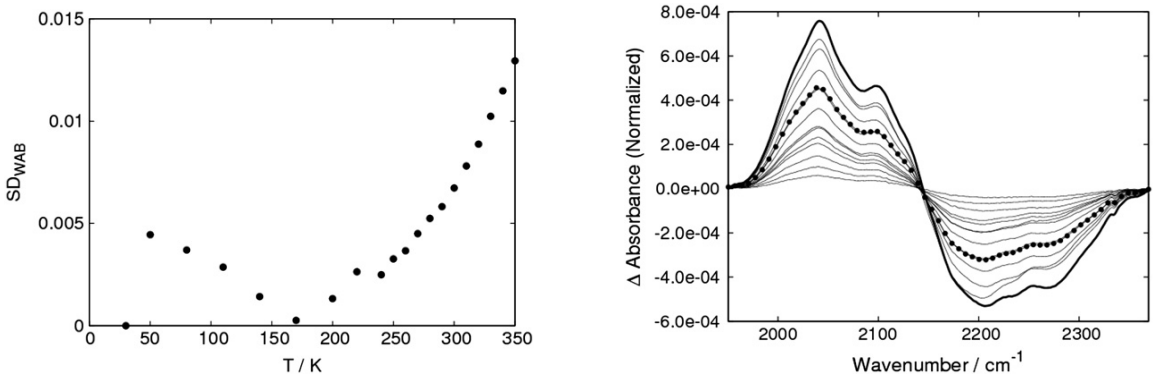

Figure 5.23: SD_{WAB} profile for an amorphous sample of maltose without protein which show strong non–monotonicity (*left panel*) and difference between the spectrum at 300 K and the various spectra at other temperatures for the same sample (*right panel*). Note that the difference increases by lowering T down to 50 K (thick curve). The curve referring to 20 K is almost superimposed to the one referring to 170 K and is evidenced by points for sake of clearness.

behaviour, and it exhibits a maximum, well above the experimental error, between 20 and 170 K (see fig. 5.23, left panel). The presence of a maximum in *SD*s is not easily explanaible in terms of thermal alteration of the sample structure. It is therefore necessary to verify if this behaviour originates from a real similarity among the spectra at temperature above and below the maximum, or derives from an error hidden in calculations.

As shown in fig. 5.23, right panel, which report the difference between the spectrum at 300 K and the various spectra at different T, the plots of the differences 300-20 K and 300-170 K are superimposed: the spectrum at 20 K is therefore more similar to the spectrum at 170 K than to the spectrum at 50 K. No similarity was observed among the spectra in the temperature range 50-170 K and the spectra at temperatures above 170 K, even if they exhibit very close SD values (because equal SD values not necessarily corresponds to overlapping spectra). The differences between the normalized spectrum at 300 K and all the other measured spectra monotonically increase in the range 300-50 K, whereas they decrease from 50 K down to 20 K (see fig. 5.23, right panel).

The use of the lowest temperature as reference is an arbitrary choice, justified because it is expected to have the the largest difference with respect to the spectra at higher temperatures, i.e. to be an “extreme”. However, the above analysis shows that this is not necessarily true, but that the spectrum at 50 K in the sample of maltose has the largest difference with all the spectra at both higher and lower temperatures. This peculiar temperature is not a priori defined and can change among the samples. The *SD* reported hereinafter are calculated with respect to the latter

as reference temperature. The obtained values are similar to what observed with the minimum temperature as reference, except for the presence of a short interval, at low temperature, in which the slope of *SD* vs. T is negative.

A similar behaviour was previously reported for the low temperature (T $<$ 160 K) iron atom mean square fluctuations in myoglobin crystal obtained by Mössbauer experiments [126, 127], and for the Debye–Waller (DW) factors of both protein atoms and crystallographic water in crambin [128], in the range 100-180 K. In the latter case, the thermal behaviour of the DW factor was attributed to the temperature dependence of the excess vibrational entropy of water involved in cooperatively rearranging regions, introduced in the Adam–Gibbs theory to explain some peculiar properties of glass forming liquids [128]. These could be also at the basis of non–monotonicity of *SD*s.

The prominence of this low temperature deviation in maltose systems well agrees with SAXS (see chapter 7) and MD results [56], which suggest that maltose—water glassy systems are inhomogeneous systems in which maltose molecules cluster, leading to the presence of water domains capable of independent rearrangements. The less likely occurrence of extended clustering in the presence of high concentrations of protein accounts for the smaller deviations observed in protein–containing systems. Moreover, the low temperature negative slope is expected to disappear with hydration, due to the loss of compartmentalization. Unfortunately, a similar behaviour is unlikely to be experimentally observed, as hydrated samples not containing protein are not stable toward crystallisation during thermal cycles, but it has been observed that the small deviations detected between 100 and 140 K in maltose, raffinose and sucrose samples containing protein fully disappear following hydration. This clustering model could also explain why not all the samples have this feature: the formation of clusters is likely dependent on the specific history of the sample.

The SD values calculated in this way are shown in figures 5.24, 5.25, 5.26 and 5.27 for trehalose, sucrose, maltose and raffinose, respectively. In each figure the *SD* values for both dry and hydrated samples have been reported, alongside SD_{WAB} values for samples without protein.

In dry samples both SD_{CO} and SD_{WAB} have very low values up to $\sim$200 K for all the sugars. This indicates lack of structural changes in the protein as well as in the matrix and implies that, within our sensitivity, only harmonic atomic motions are present in both. Above 200 K a very small increase is evident for both *SD*s, stemming from interconversion among very low tiers substates.

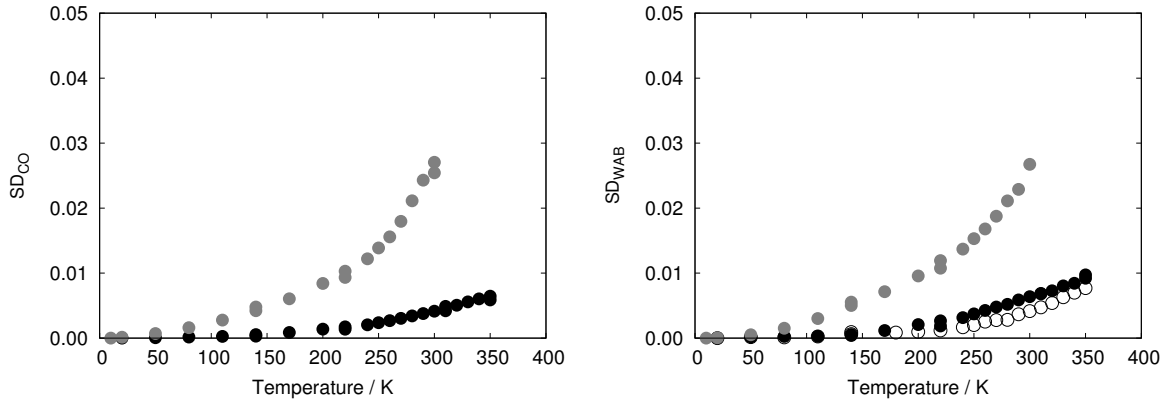

Figure 5.24: Spectra distance, calculated for WAB (SD_{WAB}, *right panel*) and COB (SD_{CO}, *left panel*) for trehalose matrices. Data refer to dry (black symbols) and hydrated (grey symbols) samples containing protein, as well as to dry samples without myoglobin (open symbols, only in the right panel) [41, 43, 98].

The SD_{WAB} for samples without protein (empty points in the figures) has values comparable with dry ternary samples. In trehalose and sucrose, the thermal evolution of SD_{WAB} is almost identical in the presence and in the absence of protein. Taking into account that the presence of the protein clearly affects the population of the components of the WAB (see section 5.3), while SD_{CO} and SD_{WAB} (both with and without protein) have similar behaviour, it is possible to infer the presence of a strict protein–matrix coupling from the point of view of the dynamics; this relation could not be so strict for what concern the alteration of structure, as suggested by data in section 5.4.

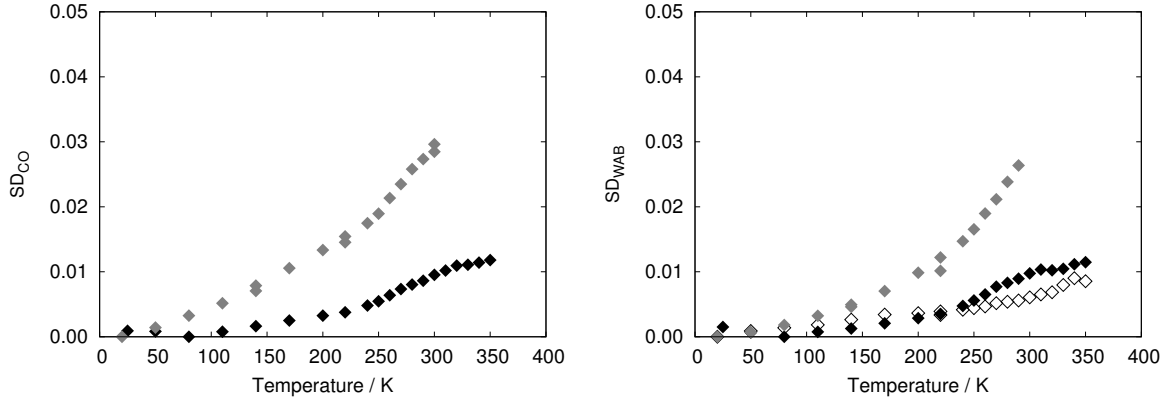

Figure 5.25: Spectra distance, calculated for WAB (SD_{WAB}, *right panel*) and COB (SD_{CO}, *left panel*) for sucrose matrices. Data refer to dry (black symbols) and hydrated (grey symbols) samples containing protein, as well as to dry samples without myoglobin (open symbols, only in the right panel) [42, 43, 98].

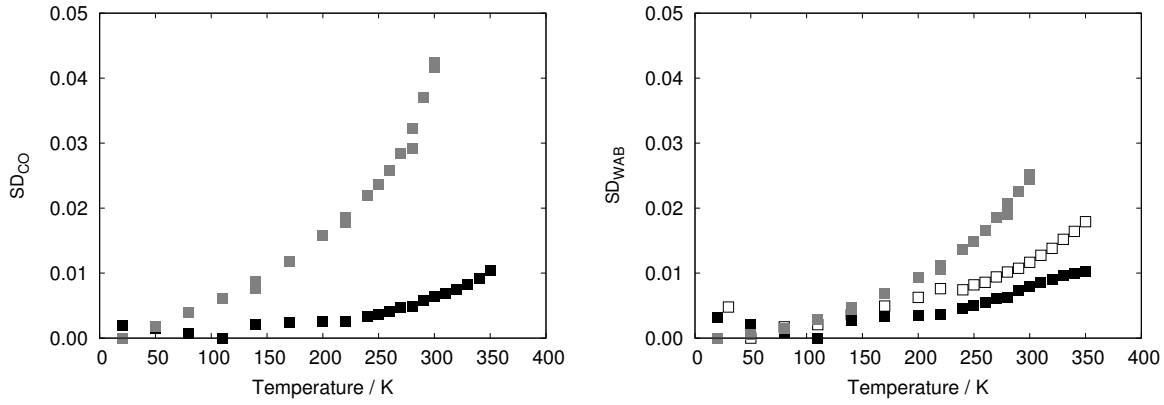

Figure 5.26: Spectra distance, calculated for WAB (SD_{WAB}, *right panel*) and COB (SD_{CO}, *left panel*) for maltose matrices. Data refer to dry (black symbols) and hydrated (grey symbols) samples containing protein, as well as to dry samples without myoglobin (open symbols, only in the right panel) [43, 98].

SD_{WAB} for maltose and raffinose samples without protein is, at variance, consistently above the value for dry samples containing myoglobin. SD_{WAB} value for raffinose sample, in particular, is also above all the values the other systems without protein. To explain this result it must be taken into account that the raffinose and maltose matrices without protein retain a large amount of water (see table 5.6, ∞ line). In protein–containing samples, the high concentration of embedded protein plays a cohesive effect on the matrix, interacting directly with the saccharides and allowing a strong water release and, therefore, a reduction of the matrix dynamics.

Hydrated samples containing protein show, in every case, values higher than dry samples, for both SD_{CO} and SD_{WAB}. The plots have a rather linear trend up to 200 K and change (increase) slope above such temperature for all the disaccharides. The low temperature linear behaviour in SD_{CO} indicates that large scale dynamics of protein is hindered, but low tier conformational interconversions might take place. The same behaviour in SD_{WAB} plot suggests an analogous hindrance of the dynamics of water, hence of the whole saccharide matrix.

Above $\sim$200K, i.e. above the transition from a glassy to a rubbery state, as showed by DSC measurements [52, 53] (see also chapter 2), the collapse of the HB network and the onset of translational displacement of protein–bound water allow protein large scale motions [41, 42, 125] (see also chapter 6). It is worth noting that the onset of large scale interconversions, as detected by FTIR, almost coincides with the onset of protein non–harmonic motions as detected by Elastic Neutron Scattering [65].

In hydrated systems, the different SD_{WAB} plots for the disaccharide matrices are roughly

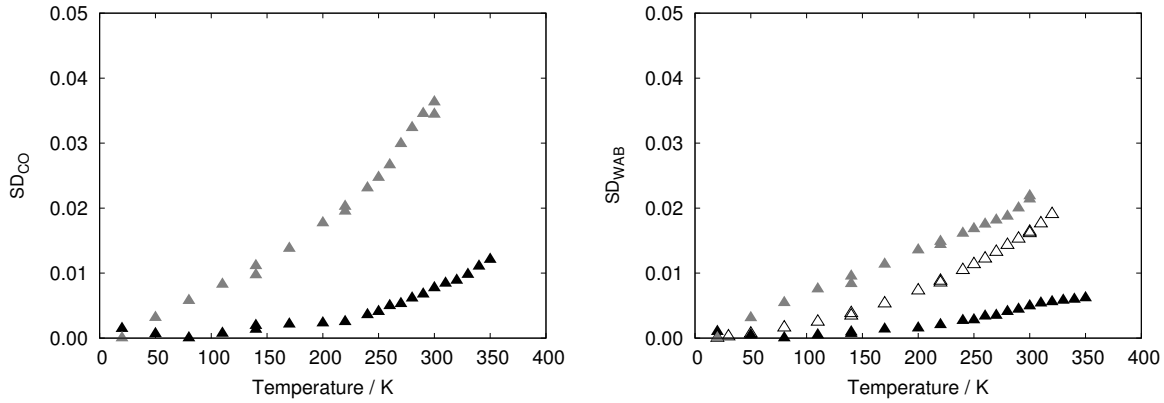

Figure 5.27: Spectra distance, calculated for WAB (SD_{WAB}, *right panel*) and COB (SD_{CO}, *left panel*) for raffinose matrices. Data refer to dry (black symbols) and hydrated (grey symbols) samples containing protein, as well as to dry samples without myoglobin (open symbols, only in the right panel) [43, 98].

superimposable [43]; this confirms again that the substantial similarity of the hydrated saccharide matrices, already put forward by the similar shapes of WABs (see section 5.3), holds true also for the thermal structural rearrangements. The only matrix with a different behaviour is the raffinose one (fig. 5.27): the low–temperature trend extends, in this system, in the whole temperature range. Such a behaviour could be attributed to the large fraction of water molecules raffinose is able to bind. This, conceivably, makes the water–sugar interactions to restrain the water molecules motional freedom, avoiding the onset of large scale motions, and water diffusion processes which are at the basis of the increase of slope in SD_{WAB} at high temperature.

At variance, the different SD_{CO} plots in hydrated samples are not overlapping over the whole temperature range, suggesting differences in the heme pocket thermal dynamics with respect to the matrix dynamics; hence a weakening of dynamical coupling is observed in dry samples. This in line with the different protein–water–sugar structures at the interface observed by MD simulation in different sugar systems [38, 39]. These MD results also pointed out that the fraction of protein–bound water molecules which is also bound to the sugar (or bridging water molecules), over the total number of protein-bound water, is higher in trehalose (73%) than in sucrose (66%) or maltose (68%). This fraction of water molecules shared between protein and sugar could determine the strength of the constraints imposed by the matrix on the protein; then, it could rationalize the larger local freedom for the protein internal motions in sucrose and maltose with respect to trehalose. The fraction of water molecules bridging different sugar molecules, irrespective of their interaction with the protein, is 70%, 66%, and 63% for trehalose,

maltose, and sucrose, respectively; this suggests that trehalose is more able to form structures in which water and sugar molecules cross–connect through the whole system [41], i.e. even far from the protein surface. The result is also in line with simulative and experimental data on binary mixtures, indicating that the presence of trehalose sizably modifies the HB network and the water dynamics by tightly binding water molecules [19, 102].

Chapter 6

MD Results

6.1 Water dynamics in Myoglobin–trehalose systems

The effects of homologue disaccharides on the protein structure/dynamics and the protein–solvent coupling have been already studied with MD simulations on MbCO embedded in trehalose–water matrix at 89% w/w ($\sim$2.3 water/sugar) and 50% w/w ($\sim$19 water/sugar) at 300K [37], corresponding to a glassy system and a liquid solution, respectively [7].

These simulation showed that internal protein dynamics is very reduced in the glassy system (average backbone atoms MSFs 0.04 Å^2), while it is almost unaffected by the presence of trehalose in the liquid solution, where the value of the MSFs averaged on all the backbone atoms is 0.24 Å^2. This value is in good correspondence with the values of 0.23 Å^2 [61] or 0.26 Å^2 [36] found in MD simulations of carboxy–myoglobin in a water solution. Similar results were obtained from simulations of lysozyme in a trehalose aqueous solution (18% w/w, 90 water/trehalose): the calculated fluctuations for the Cα atoms show no significant difference in the presence or absence of trehalose, the corresponding averages over the protein residues being 1.02 Å^2 and 0.98 Å^2, respectively [129].

Vitkup et al. [61] performed a MD simulation of MbCO in water, in which water molecules were kept at 180 K, while the embedded protein was maintained at 300 K; this mimicked a "high viscosity solvent" uniformly surrounding the protein. The MSFs resulted of very low amplitude and uniform over the whole chain. The profile of MSFs versus protein residues, obtained in the simulation in trehalose–water systems at 89%, resulted very similar to the one reported by Vitkup et al. in the case of "cold solvent". It has been also suggested [125] that, in protein–water systems, water translational motions, which allow complete exchange of protein–

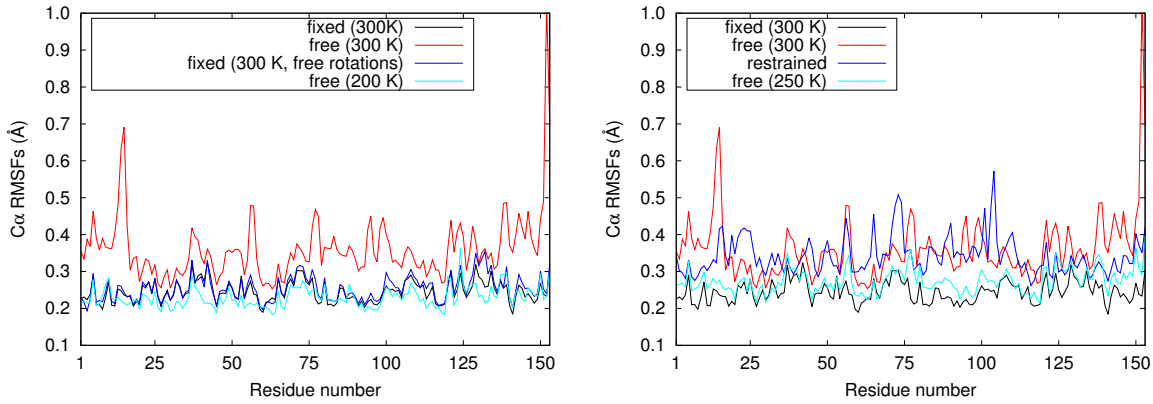

Figure 6.1: RMSFs of C_α atoms as a function of residue number, calculated over 10ns trajectories. *Left Panel:* Comparison between samples with free water, fixed water (both translation and rotation) and fixed water (only translation). *Right Panel:* Comparison between samples with free water, fixed water (both translation and rotation) and water restrained by a harmonic potential.

bound water molecules by translational displacement, are necessary for large–scale fluctuations, e.g. interconversion among high tier substates and structural relaxations.

These studies pointed out that reducing the dynamics of the solvent/matrix as a whole has a strong effect on the dynamics of the protein. For a binary matrix composed of trehalose and water, it is possible to disentangle the effects of the two components by shutting down the dynamics of one of them. To this aim, in this work simulations of MbCO have been performed in a trealose–water 89% w/w system of larger size than the ones already studied [37], with constraints imposed on the water molecules. This has been made either by blocking both the translational and the rotational motions of the molecules, or by blocking only translations, while allowing the water molecule to rotate.

The root mean square fluctuations of C_α atoms on the ten of nanoseconds time scale with free or fixed water molecules at 300 K are shown in fig. 6.1. It clearly appears that the dynamics of myoglobin is severely impaired in the systems with fixed water molecules. In the latter the average RMSFs value reduces of about 30% of the value of the free system at the same temperature. Moreover, data in figure 6.1 show that the RMSFs of the two fixed systems are roughly superimposable; allowing water rotations produces very small effect, within the error. This suggests that the hindering of water translational diffusion is the primary mechanism in the reduction of protein atomic fluctuations throughout the protein, even in trehalose–water matrices. The extent of the reduction is similar to that of a system at 200 K in which all water degrees of freedom are preserved (fig. 6.1, left panel, cyan curve). The average of the RMSFs

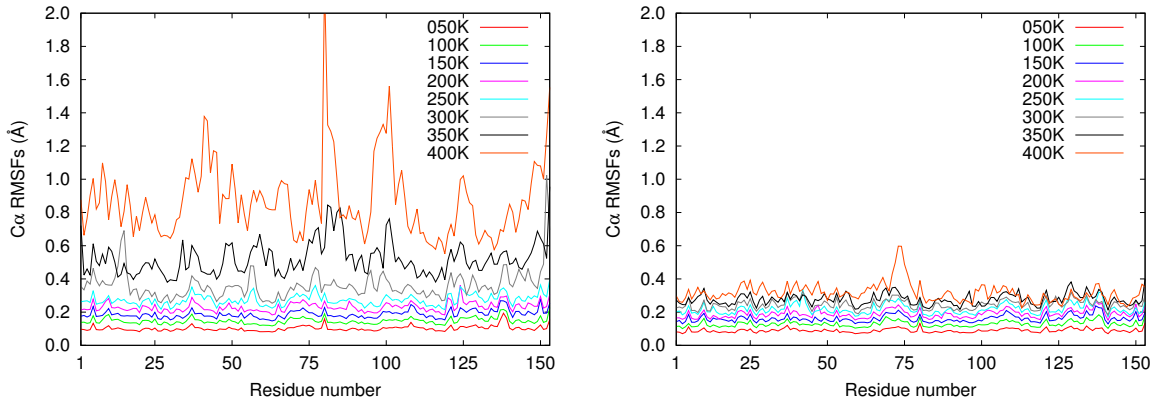

Figure 6.2: RMSFs calculated on the myoglobin α carbon atoms as a function of residue number at various temperatures. Free water (*left panel*) and fixed water systems (both rotations and translations, *right panel*).

along the protein chain is $\sim$0.25 Å($\sim$0.06 Å^2), pointing out that inhibiting water translational displacement at room temperature corresponds to slow down the nanosecond protein dynamics to the one measured on the 100 ps time scale [37].

By imposing a harmonic potential to restrain the water translational motion it has been possible to mimic a temperature reduction effect on water molecules. By reducing water dynamics to an extent analogous to the one of a free system at 250 K, the result is just a damping of the largest fluctuations, but the general profile (see fig. 6.1, left panel, blue curve) is more similar to the one of the free system at 300 K than at 250 K (cfr. fig. 6.1, left panel, red and cyan curves). The average RMSFs values in the case of the harmonic restraint (0.34 Å) is very similar to the value of the free system at 300 K (0.36 Å). At variance with Vitkup results, in a bicomponent solvent it is not possible to modulate protein dynamics by simply, artificially, cooling down one of the components (water in this case).

To sum up, water translations appears to have a strong effect on the protein dynamics. Water effects appear stronger than the trehalose ones, by taking into account that water is present in relative small amount (the matrix is 89% trehalose).

The RMSFs for Cα atoms at variable T are shown in fig. 6.2, while the RMSFs for the glycosidic oxygen in the trehalose molecule are shown in fig. 6.3. In fig. 6.4 the average RMSFs as a function of the temperature are shown, for all the system components.

RMSFs for MbCO C_α in the free water system show a linear increase with temperature below 250 K (a temperature close to the so–called protein dynamical transition in this kind of matrices [65]), followed by a slight increase in slope, which becomes large above 350 K,

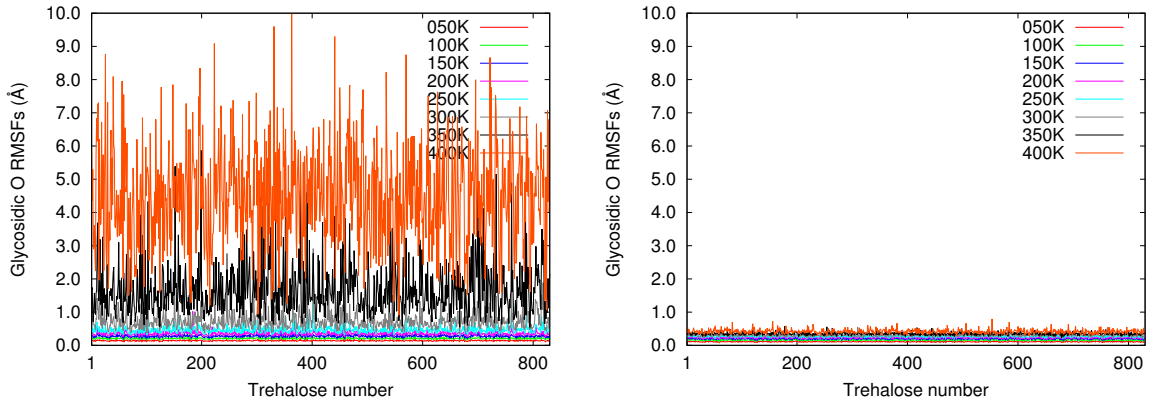

Figure 6.3: RMSFs calculated on trehalose glycosidic oxygen for the various trehalose molecules at various temperatures. Free water (*left panel*) and fixed water systems (both rotations and translations, *right panel*).

i.e. after the glass transition temperature of the system [52].

In the fixed water systems the C_α RMSFs have consistently lower values with respect to the corresponding free water systems, as expected. The reduction is about 20% of the free water value in the 50-250 K, then rapidly increases up to reach about 80% at 400 K. It is noteworthy that RMSFs vs. T plots are linear in the whole temperature range, with no transition at the protein dynamical transition temperature or at the matrix glass transition temperature. The protein dynamics appears uniformly reduced with no specific domain showing significant flexibility, except for the EF loop (see fig. 6.2, right panel), which appears to increase its dynamics at 400 K. As for the lateral chain atoms, they have generally higher flexibility than the C_α atoms, but they show proportionally the same dampening. A difference, which shed light on the origin of the impaired dynamics, can be noticed by looking at the RMSFs of the carboxylate group atoms of glutamate (GLU) and aspartate (ASP) residues. Previous simulations showed that sugar is preferentially bound to these groups in the protein, hence they should experience the largest effects played by the matrix [39]. Actually, the reduction in the dynamics of these groups upon fixing the water molecules is larger than other protein atoms classes. This is particularly true at the highest temperatures, where in the free water system ASP and GLU carboxyl atoms have overall highest flexibility, because of the interaction with the solvent.

As for the matrix dynamics (see fig. 6.3), the temperature behaviour of trehalose atoms show the usual differences between the free water and fixed water conditions; the effects are much more pronounced than in the protein. RMSFs in the fixed water system are $\sim$30-40% lower than the free water system, in the range 50-200 K (see fig. 6.4, middle panel). Very large RMSFs

are found above the glass transition temperature in the free water system, while the dynamics remains of the order of magnitude of the protein one if water translations are blocked. The temperature behaviour of the glycosyl oxygens or of the hydroxyls is similar, the latter having larger flexibility.

Water dynamics is the handle utilised to modulate the dynamics of the whole system, hence its behaviour is trivial if fixed (0 everywhere), while a very large mobility is present if no constraint are imposed (see fig. 6.4, lower panel), where water can also undergo diffusion.

From these data, it appears that the dynamics of the three components is strongly coupled. At 150 K and below, RMSFs for water, trehalose and protein are of the same order of magnitude suggesting that the whole system is subject to harmonic motions. At higher temperatures all the components increase their dynamics, to a larger and larger extent with increasing temperature, with RMSFs(water) $>$ RMSFs(trehalose) $>$ RMSFs(protein); the order of temperature at which anharmonic motions set up is above 150 K for water, above 200 K for trehalose and above 250 K for myoglobin. Blocking water motions has an effect extremely strong on trehalose, whose dynamics is severly hindered because it is intimately bound to water. The effect on the protein is smaller, i.e. just a reduction of the large scale motions, which set up at high temperature (T $>$ 250 K).

The comparison of the dynamics of water

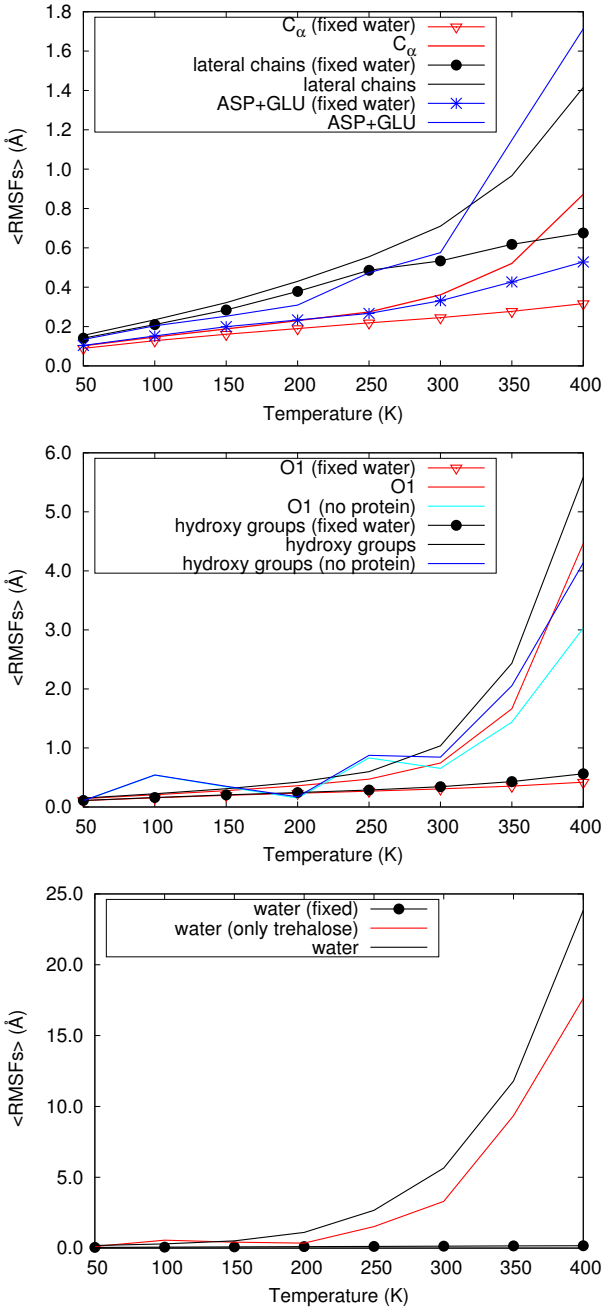

Figure 6.4: RMSFs as a function of temperature for protein atoms (*upper panel*), trehalose atoms (*middle panel*) and water molecules (*lower panel*).

and trehalose molecules between systems with and without myoglobin shows larger RMSFs in the presence of protein (see fig. 6.4, middle and lower panel), supporting the idea that protein and matrix influence themselves. A question could arise, if this protein effect on the matrix depends on direct interactions which establishes at the protein surface, i.e. if the effect of the protein is limited to its immediate surroundings only, or if a dependence of the dynamics on the distance from the protein exists. An answer can be found by calculating the RMSFs of water and trehalose glycosidic oxygen atoms in shells of progressive thickness around the protein (from 3 to 18 Å; in fig. 6.5 only two representatives cases are reported, for sake of clarity).

The fixed water systems do not show any difference, the already impaired dynamics has no dependence on the distance from the protein, as expected for a harmonic solid. The plots for the free water systems (see fig. 6.5, lines without symbols) show instead that the matrix components close to the protein have lower RMSFs than the values averaged over all the system. This behaviour is apparently contrasting with the previous result (see fig. 6.4, middle and lower panel), i.e. protein insertion enhances the dynamics of the matrix; indeed, one would suppose that the protein should mainly affect in this direction the first shells of molecules around itself.

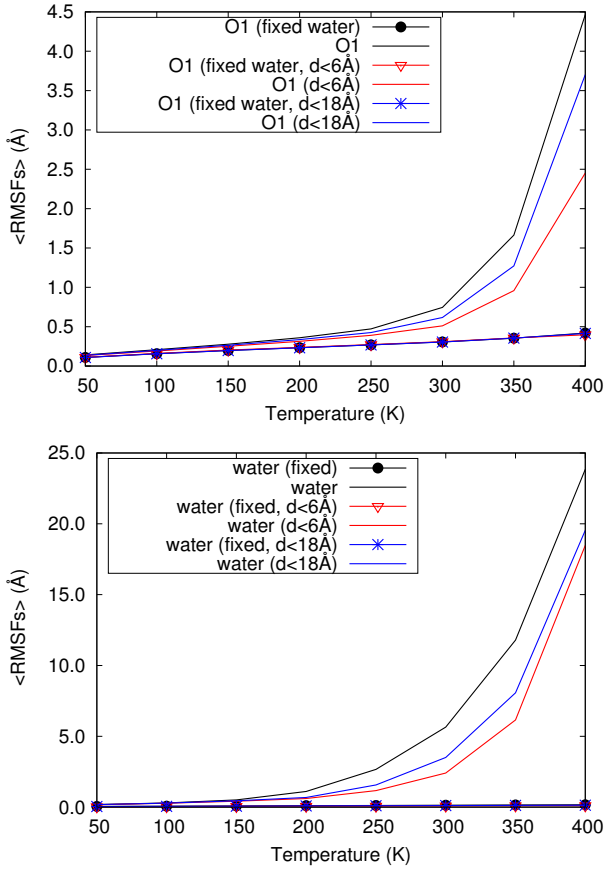

Figure 6.5: RMSFs as a function of temperature for trehalose glycosyl oxygen atoms (*upper panel*) and water molecules (*lower panel*), analysed in shells of 6 and 18 Å from the protein.

This can be rationalized by assuming a different origin for the two effects. While in experiments protein–sugar interactions make to release water, which is lost during dehydration procedures (see section 5.4), simulated systems have the same water content in the presence and in the absence of protein. In this case, the water "excess" released by direct protein–trehalose interaction is not lost; at equilibrium, it could be conceivably spread throughout the whole matrix, and not necessarily confined at the protein interface. Therefore, it can be

supposed that the simulated protein–containing system is more comparable with a trehalose–water system slightly more hydrated. Taking this in consideration, it is not surprising that matrix components have overall larger RMSFs in protein–containing systems, in particular at high temperature, where water dynamics is larger and diffusion may take place. That said, the reduction of the matrix RMSFs close to the protein surface is then merely an effect of direct interactions with the protein. The layers of matrix surrounding the protein acts therefore as a dynamical "joint" between the two subsystems that, at high temperature, have largely different dynamics.

As a counterpart, it is possible to study the effect of water dynamics on the protein as a function of the distance from the protein surface. This was done by simulating systems with water molecules fixed or free only up to a definite distance from the protein surface. The explored thickness of the frozen/free water shell was up to 12 Å, at steps of 3 Å. The results are reported in fig. 6.6, 6.7, 6.8 and 6.9.

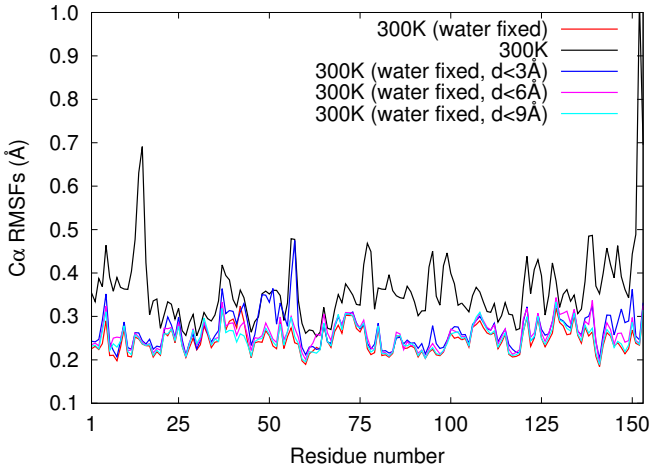

Figure 6.6: RMSFs calculated on the myoglobin C_α as a function of residue number for systems with fixed water molecule up to a definite distance from the protein.

Results show that only the first layers of water around the protein are really needed to modulate protein dynamics (see fig. 6.6). The C_α RMSFs per residue have negligible differences in all the systems with water blocked within 6 Å, irrespective of the state of water above 6 Å. If only the water within 3 Å is fixed, the only region with larger flexibility is the CD loop/D helix. Protein dynamics is therefore inhibited essentially by blocking water within 3 Å. This could be highlighted by plotting the average RMSFs as a function of the thickness of frozen water layer (see fig. 6.7, upper panel). Protein atoms RMSFs are constant if water within 3 Å is fixed, having the same value they would have if all the water molecules were fixed. Interestingly, RMSFs for ASP and GLU lateral chains reduces to a larger extent than the other protein atoms, and a slight reduction can also be noticed between 3 and 6 Å.

Note that, if, conversely, the first shells contain free water in a bulk of fixed water (see fig. 6.7, lower panel), full restoration of protein dynamics is not achieved: by increasing the

thickness, the C_α RMSFs increase regularly but they do not reach the value they have in fully free systems even with a 12 Å thick layer. By analysing ASP and GLU residues, the increase in RMSFs is in two steps: the first on releasing the first 3 Å layer, because of the direct bond with these residues; the second at 12 Å, when the dynamics, at least for these residues, approach the one in the fully free system.

Water far from the protein surface, instead, would contribute only to the suppression of matrix dynamics. The RMSFs of matrix components reduce with a roughly linear trend with increasing thickness of frozen water, with a larger slope for water than for trehalose (see fig. 6.8). By analysing the matrix atoms in shells around the protein, it can be observed that, if large parts of bulk matrix is included in the average (analysis of all atoms or atoms within 18 Å from the protein surface), the trend is always linear for both the components. At variance, if we take into account only the shells close to the surface, we observe a reduction of the slope in trehalose, already evident for atoms closer than 9 Å; the slope values are intermediate between the value observed in the protein case (see fig. 6.7, upper panel) and the one observed in the bulk trehalose. This hints anew that the layers of matrix close to the protein have an intermediate behaviour between the bulk matrix and the protein, acting as a junction. In the case of water, this slope reduction is not noticeable; the value goes sharply to zero when the analysed thickness is smaller than the fixed water shell one.

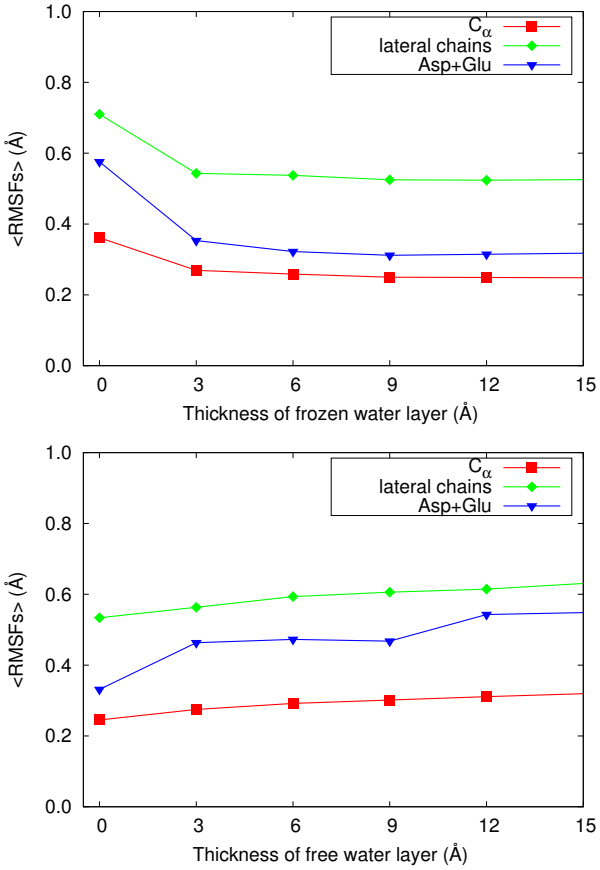

Figure 6.7: Average RMSFs of protein atoms as a function of thickness of frozen water in a bulk with free water (*upper panel*) and as a function of thickness of free water in a bulk with fixed water (*lower panel*).

Results so far discussed are better summarized in fig. 6.9. In this case each curve corresponds to a simulated system, while in the x axis is reported the thickness of the shell used for

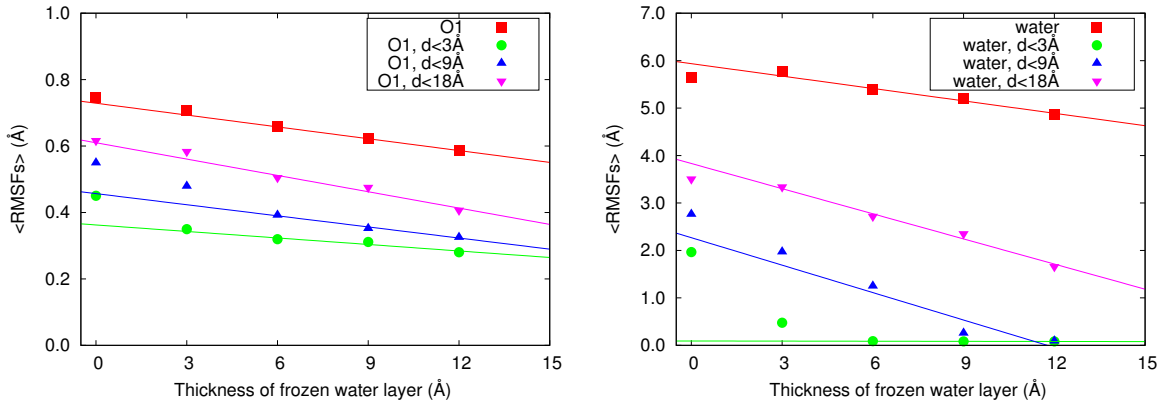

Figure 6.8: Average RMSFs as a function of thickness of frozen water in a bulk with free water. Trehalose glycosidic oxygen atoms (total and within a given distance from the protein, *left panel*), and water molecules (total and within a given distance from the protein, *right panel*).

the analysis. Fixing the water in definite shells causes both trehalose and water dynamics to reduce within that shell (see fig. 6.9, upper panels). However, a residual dynamics remains for both trehalose and water: RMSFs do not reach the values of a fully fixed system because of the presence of water which can diffuse through the shell border.

An interesting feature is present in the plots in which a free water shell is progressively released in a fixed water bulk (see fig. 6.9, lower panels). As expected, the RMSFs are reduced both at the protein surface, as above discussed, and beyond the border of the free water shell. This leaves with an intermediate region in which the matrix dynamics show enhanced mobility, this in particular in the case of water, as already observed in protein–water systems [130]. This feature is much more evident in the case of large free water shells (12 or 9 Å thick), where the thickness is large enough to accomodate matrix molecules not influenced from either the protein surface or the fixed water bulk. Work is in progress to understand if this feature could be attributed to confinement effect due to the presence of both the protein and fixed water bulk, acting as a wall.

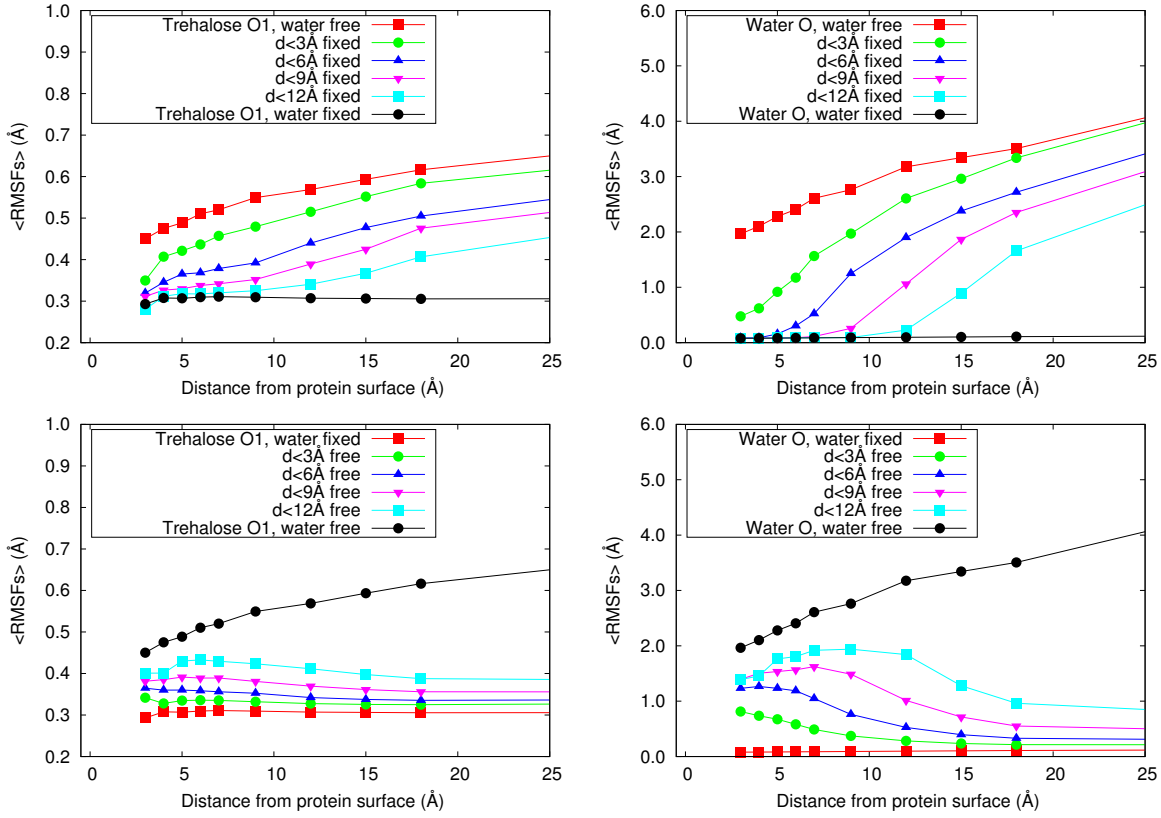

Figure 6.9: Average RMSFs calculated in shell of increasing thickness from the protein surface. Trehalose glycosidic oxygen atoms *left panels*; water molecules *right panels*. Shells with frozen water in a bulk with free water (*upper panels*); shells with free water in a bulk with fixed water (*lower panel*).

Chapter 7

SAXS Results

The four disaccharides studied with FTIR have been investigated also with SAXS. The SAXS patterns of trehalose and sucrose amorphous systems are shown in fig. 7.2, while the same for maltose and lactose are shown in fig. 7.3. The fitting procedure used is reported in fig. 7.1 In each figure both the curves for MbCO–containing (with sodium dithionite) and *met*–Mb–containing (without sodium ditionite) samples are reported, as well as the reference curves for the samples without protein. The study both in the presence and in the absence of sodium ditionite was judged necessary because the sulphur atoms have a high electron density, hence high contrast. This causes an intensification of the signal of areas containing ditionite, which is expected to be uniformly diffused in the matrix. The presence of ditionite would therefore exhalt the matrix features in these systems, while samples without ditionite should allow the study of the system without possible perturbation induced by the salt.

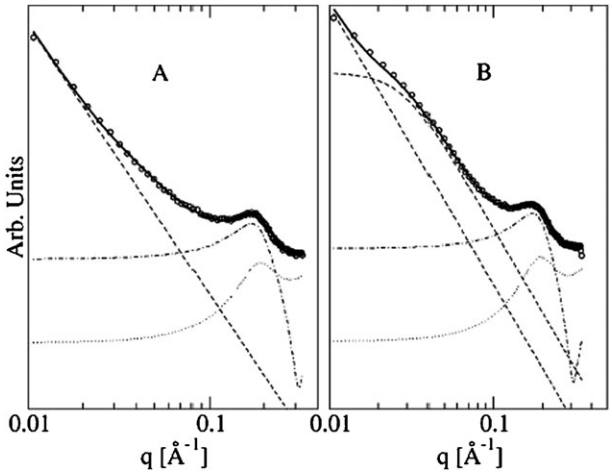

Figure 7.1: Fitting of SAXS patterns for protein–containing samples. *Left:* Curves for a sample without matrix inhomogeneities, only Porod and protein contribution are present. *Right:* Curves for a sample with matrix inhomogeneities, also a Debye contribution is needed.

As evident from the figures, the SAXS patterns for the reference samples in the presence and in the absence of dithionite are roughly equivalent: the salt is likely to be homogeneously

distributed in the sugar matrix. The double logarithm plots of $I(q)$ vs. q exhibit, for the all the binary disaccharide–water sample, the Porod q^{-4} behaviour (see fig. 7.1), which is already evident at the lower bound (q = 0.01 Å^{-1}), and extends in the whole q range investigated. According to the Porod law, this behaviour stems from the presence of domains with homogeneous electronic density, whose size is larger than ∼500 Å [117]. Such domains are supposed to originate from microscopic cracking of the samples.

Only in the case of sucrose a second feature, corresponding to ∼35 Å domains, can be identified in the reference sample in the presence of dithionite. Following what previously reported, we attribute it to local nanocrystallisation [93]. This is indeed expected in extremely dehydrated sucrose samples, since the most stable crystalline form of this saccharide is anhydrous [131], and agrees with previous FTIR results [42]. A confirmation of sucrose nanocrystallisation can be the rather common finding of a crystallographic peak at q ≃ 0.15 Å^{-1}, indicative of the presence of sucrose crystals. Although these crystallised samples have not been used for the analysis, their existence prove that sucrose crystallisation at very low hydration is a common phenomenon with respect to other saccharides. Hence nanocrystallisation is to be expected in sucrose samples, even if larger crystals does not form. For sake of clarity in fig. 7.2 a sample without

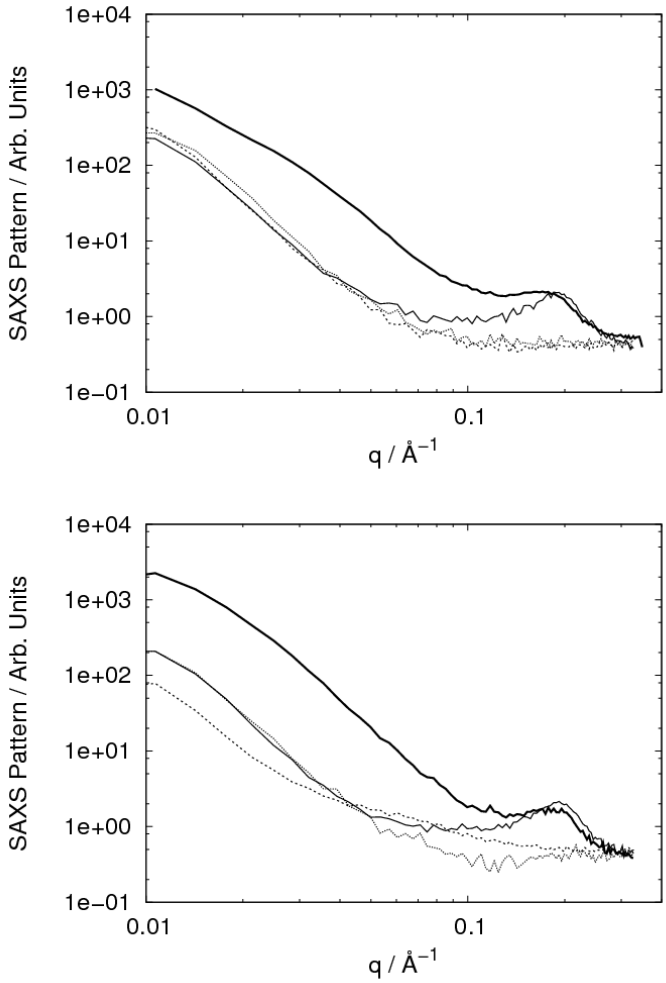

Figure 7.2: SAXS patterns for non-reducing disaccharides (Trehalose, *upper panel*, and Sucrose, *lower panel*). Solid thick line, samples containing MbCO; solid thin line, samples containing *met*–Mb; dotted line, reference sample without $Na_2S_2O_4$; dashed line, reference sample with $Na_2S_2O_4$.

crystallographic peak is reported.

The scattering curves of all the protein–containing samples in fig. 7.2 and 7.3 show a structure appearing in the q range 0.1-0.4 Å^{-1} that can be ascribed to myoglobin. The protein dimension, drawn from the fitting, resulted ∼14 Å in all the the samples, in agreement with the literature [115, 132]. Furthermore, because of the high protein concentration, a peak, arising from interference among Mb molecules, is observed at ∼0.3 Å^{-1}. These peaks have been fitted assuming additivity for the scattering contributions from the different structures, using the Percus–Yevick function in the decoupling approximation as $S(q)$ (see fig. 4.3) and assuming for the protein a spherical form factor [117, 118].

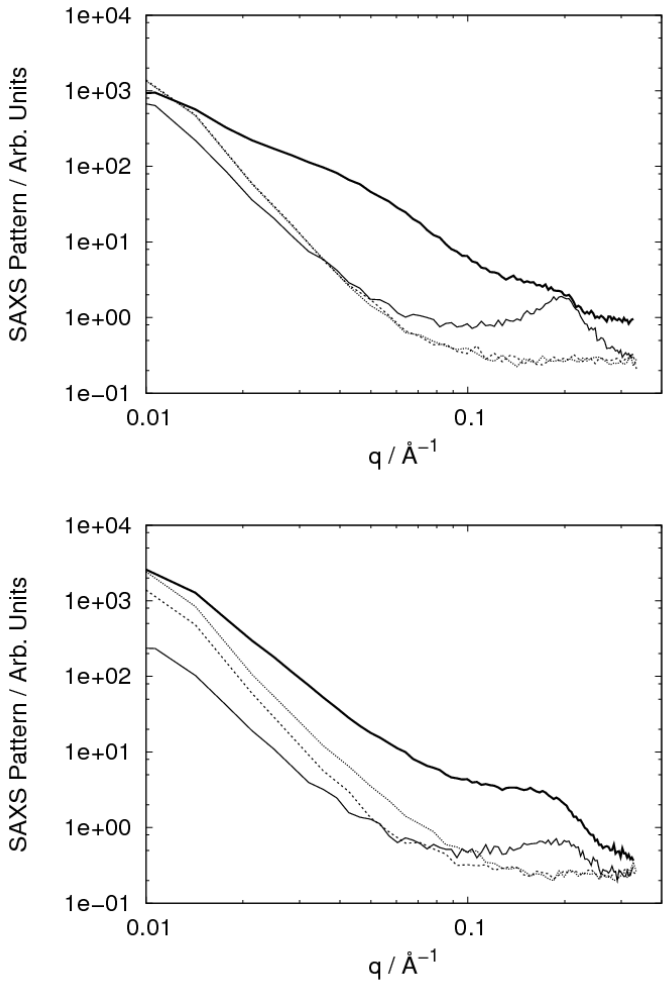

Figure 7.3: SAXS patterns for reducing disaccharides (Maltose, *upper panel*, and Lactose, *lower panel*). Solid thick line, samples containing MbCO; solid thin line, samples containing *met*–Mb; dotted line, reference sample without $Na_2S_2O_4$; dashed line, reference sample with $Na_2S_2O_4$.

The average distance among myoglobin molecules, d, resulted to be between 29 and 31.5 Å^{-1} for the various samples (see table 7.1). Although the d values are slightly smaller for *met*–Mb samples than for MbCO ones, the difference is too small to draw conclusions on differences in the protein behaviour. The only difference which can be noticed is the lower value for d in lactose samples. Since no sizable difference in the protein behaviour is noticeable for this sugar, beside the low fraction of interacting protein η, it can be suggested that lactose samples may undergo partial phase separation, which would reduce the avalaible sugar interacting with the protein, thus making the protein molecules to

Table 7.1: Some parameters obtained from the data fitting. d is the protein–protein average distance, η is the volume fraction of the interacting protein and D is the average dimension of the inhomogeneities. (*) Calculated only on the samples showing the low-q feature.

Sample	d / Å	η	D / Å
MbCO-Treh.	31.4 ± 0.4	0.337 ± 0.012	150 ± 10
met–Mb-Treh.	30.5 ± 0.2	0.386 ± 0.009	—
MbCO-Sucr.	30.9 ± 0.4	0.307 ± 0.009	180 ± 20 (*)
met–Mb-Sucr.	30.7 ± 0.2	0.378 ± 0.010	—
MbCO-Malt.	31.2 ± 0.6	0.27 ± 0.04	60 ± 10
met–Mb-Malt.	30.3 ± 0.2	0.383 ± 0.012	—
MbCO-Lact.	29.4 ± 0.2	0.201 ± 0.016	120 ± 20
met–Mb-Lact.	29.1 ± 0.3	0.313 ± 0.018	—

reduce their separation distance [133].

Concerning the η values (see table 7.1), the most striking effect is the difference between the values in MbCO and *met*–Mb samples. For all the sugar the value is consistently higher for all the samples in the absence of dithionite, and it is almost equal for trehalose, maltose and sucrose. In the presence of dithionite, η value is consistently lowered, with a different extent in the different sugars, and its values are in the order Trehalose $>$ Sucrose $>$ Maltose $>$ Lactose.

η values, which in the Percus–Yevick approximation stand for the volume fraction of the supposedly spherical particles, can be connected to the protein preservation in these system. Actually, upon denaturation the protein might unfold, and stop to contribute to the structure factor. This hypothesis has been confirmed by measuring some MbCO samples in trehalose matrices prepared by heating the solution at 80 °C for different amount of time before the drying procedure. Trehalose is not able to protect myoglobin in solution, hence this procedure allowed us to obtain samples with partially to totally denatured protein. By increasing the denaturation, the protein interference peak initially lowers and broadens until disappearance, while the η values progressively reduces [94].

Sodium dithionite is a chemically active substance, both oxidizing and reducing, that can alter or interfere with the embedded protein, due to the high concentration of our sample. The lowering of η values in matrices containing sodium dithionite can therefore be interpreted as

a partial degradation of the embedded protein in these systems, whose extent would be different in the different disaccharides. The comparison of the η values thus confirms that trehalose is the most efficient preserver. At variance, maltose and lactose have the lesser protective effect, probably because they are reducing sugars, able to undergo the Maillard reaction with the protein [52].

Moreover, the case of lactose matrices is peculiar, as η values are consistently lower than the other sugars, both in the presence and in the absence of $Na_2S_2O_4$. Once more this behaviour can be ascribed to the reported phase separation of lactose [133], which would reduce the amount of sugar available per protein, thus impairing the lactose protective effect.

It must be pointed out that all the effects are here attributed to the presence of $Na_2S_2O_4$, and not on the different binding state of myoglobin. Actually, measurements on Mb samples containing $Na_2S_2O_4$, but neither treated with CO nor dried under CO atmosphere, gave results very similar to MbCO samples (see fig. 7.4), supporting the attribution.

Beside the protein signal, in the MbCO samples, but not in the *met*–Mb ones, a further, broad feature, corresponding to a large structure, is evident within the 0.01-0.1 $Å^{-1}$ q range. This was fitted by the Debye function (see section 4.3) giving a distribution of domains, with an electronic density different from the background, whose average dimension is reported in table 7.1. Interestingly in the *met*–Mb samples the Porod law is enough to fit the part of the curve at $q < 0.1$. The average dimension D of the local inhomogeneities is heavily dependent on the specific saccharide. In particular, it appears that the inhomogeneities dimension grows in the order Sucrose > Trehalose > Lactose > Maltose.

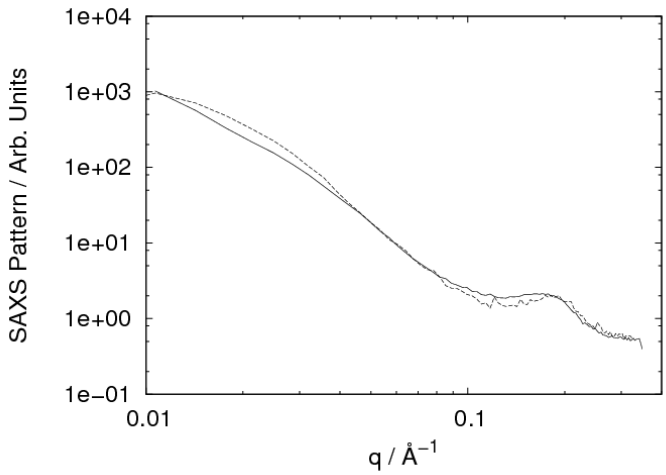

Figure 7.4: Comparison between the SAXS patterns for MbCO (solid line) and Mb without CO (dashed line) in trehalose matrices containg $Na_2S_2O_4$.

Because of the intrinsic uncertainity of water content in these samples, the exact dimension of the domains has a quite large error, in particular in the cases of sucrose and lactose. These

data support the idea that the occurrence of inhomogeneities is a general phenomenon in highly concentrated protein–saccharide systems.

Progressive hydration of the trehalose–myoglobin samples (see fig. 7.5, samples H1 and H2) causes a shift of the low q signal toward still lower q values, accompanied by a broadening of the structure, which moves the signal beyond our instrumental resolution. Such behaviour suggests that water must play a considerable role in the structure of the observed domains. At variance, hydration leaves the high q signal, ascribed to the protein, almost unaltered; this points out that no alteration in protein structure takes place, at least for most of the protein molecules. Further hydration (see fig. 7.5, samples H3 and H4) makes the low q signal to disappear and the distance among proteins to increase to $\sim$ 45 Å, a distance compatible with the presence of at least a hydration layer surrounding the protein, and then disappear. The sample H3 hence approaches a hydration level close to the minimum needed for the onset of the protein function, while H4 corresponds to a largely hydrated sample in which all correlations between protein molecules are lost [93].

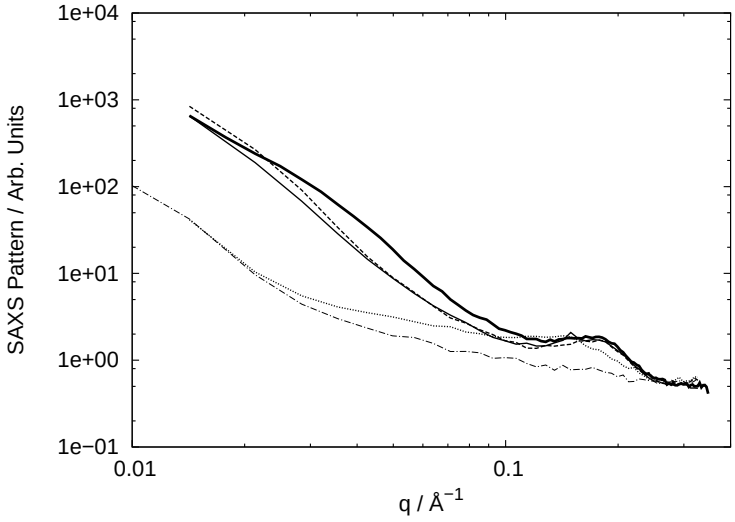

Figure 7.5: SAXS experimental patterns for trehalose–MbCO matrix at various hydrations: the water content is increasing along the order thick line (dry sample), dashed line (H1), thin line (H2), dotted line (H3), dot-dashed line (H4).

About the origin of this feature, the simplest model, in line with the data, would suggest the presence of protein–rich domains (protein clusters) standing out against a sugar–rich background. However, taking into account the large volume of myoglobin molecules and the large protein molar fraction, as compared to saccharide and water, it follows that in these samples, the overwhelming volume fraction ($\sim$80%) consists of protein molecules. Concentration of all the protein in domains with $60 < D < 180$ Å, which occupy less than 50% of the overall volume[1] , would be non–physical as it needed an extreme "compression" of the protein; this consideration

[1]To be observed as objects against the background, their volume must be below the background volume, otherwise the roles of background and object are reversed (Babinet Principle).

rules out the above model for the observed low q domains. Moreover, to obtain a reliable model it is worth noting that:

- The hypothesis that the observed domains are protein–rich regions, with slightly larger protein concentration than the environment, contrasts with the increase in domain size with hydration. Indeed, incoming water should preferentially link to the more hydrophilic sugar molecules, thus widening the sugar rich background rather than the domains;

- The hypothesis that the observed domains differ from the background only in water content (gel–like structure) is ruled out because of the very low sample water; indeed, even assuming all the water in the sample concentrated at the domains, these could not be such to produce liquid–like structures observable against the background;

- The shape and position of crystallographic peaks for saccharide nanocrystals is different, and, moreover, traces of crystallisation have been found only for sucrose, while the low q domains are more common in the other matrices than in sucrose; this would rule out the assignment of the observed domains to nanocrystalline phases.

Hence, local differences in protein/sugar ratio can be suggested as origin of this signal. In particular, protein–rich regions constitute the SAXS background against which protein–poor domains are observable. These domains, mainly constituted by sugar and water connected by extensive hydrogen bond (HB) network, would be stabilised by the partial seclusion of strong HB–maker saccharide from the weak HB–maker protein. In hydrated samples (H1 and H2), the protein background shows no significant differences with respect to dry samples, as pointed out from the unaltered protein–protein distance and protein size. This behaviour is rationalized by considering that the incoming water has to preferentially concentrate at the hydrophilic "sugar rich/protein poor" domains. Further hydration (H3 and H4) makes the domains signal disappear and the protein signal broaden and shift (H3), before disappearing (H4). Such behaviour can be attributed to a change in the structure of the sample above a water threshold: the larger water availability makes to increase the hydration of the protein and leads to the merging of the domains with the background (a sort of "melting").

Although surprising, the absence of this low–q signal in the samples without dithionite[2] can be explained in the frame of the above model. The protein–poor fraction is more polar than the background, due to the higher concentration of the strong HB–maker saccharide molecules,

[2]Please note that also in this case the presence of CO does not alter significantly the SAXS curve, see fig. 7.4.

and it seems, indeed, to bind preferentially water. The same argument can be applied to ionic molecules or salts: they should preferentially concentrate in the most polar regions of the sample. We can therefore suggest that also $Na_2S_2O_4$ ions (as well as its ionic degradation products) should be more likely present in the protein–poor inhomogeneities. This results in an increase of electron density contrast against the background, because of the presence of suphur atoms, hence in a magnification of the inhomogeneities signal that would not be otherwise detectable. Another, equally sound, explaination would be that the high salt concentration induces the "nucleation" of inhomogeneities, by stabilising the protein poor areas. We cannot solve this issue basing only on the present data, but, from an applicative point of view, this is only of secondary importance, as natural matrices have generally quite high concentrations of salts. Local inhomogeneities would therefore be present in all the samples, in the presence of sodium dithionite, although we cannot rule completely out their presence also in the absence of salt, even if they are not evident [94].

The difference in average dimension of the domains might originate from a difference in composition of the same domains. In this respect it is interesting to notice the difference between the inhomogeneities in maltose and sucrose. The MbCO–maltose system has the smallest inhomogeneities, whose average size is only slightly larger than protein size. It should be noticed that studies on analogous maltose systems at a molecular scale, with both simulative and experimental techniques, supported the idea that maltose-water system are inhomogeneous due to maltose clustering [43,56]. Due to the small dimension of the here reported inhomogeneities, it is arguable that they are simply maltose clusters.

At variance, the case of sucrose system is more complex. Firstly it must be pointed out that not all the sucrose samples, which did not crystallise, have the low q feature. Out of 15 measured MbCO–containing sucrose samples, only 8 showed the broad feature, and only in 4 cases it is undisputedly evident. A fitting restricted only on the samples actually showing the feature led to an average dimension of 180 $Å^{-1}$ for the inhomogeneities, very close to the resolution limit of the instrument. It could be hypohesized that in a fraction of the sucrose samples D is too large and only the tail of the Debye function falls within the resolution limit of the instrument, giving patterns that can be fitted with the Porod law only.

Moreover, it must be considered that the scale factor obtained for the Debye function in sucrose samples is, in average, much lower than the value obtained in trehalose (2900 vs. 1700). Hence, either there are only few inhomogeneities or their contrast is low, i.e. the difference in

local concentration between the domains and the background is small. This will contribute to the difficulties in the identification of the inhomogeneities in MbCO–sucrose systems [94].

To sum up, the model exploited from SAXS data depicts, for systems containing myoglobin, the presence of protein–poor domains embedded in a protein–rich background. In the latter the protein is locked into its environment through a HB network involving saccharides and water, whereas the protein–poor domains are mainly constituted by regions of saccharides and water connected by the same networks, in which few to no myoglobin molecules are embedded. Going from maltose to sucrose, they turn from high–contrasted, almost sugar–only, small domains into low–contrasted large domains, which likely have only a little difference in concentration with the background. Trehalose and lactose systems lay inbetween these extremes. The occurrence, and the nature, of these inhomogeneities, in our interpretation, lies on the different hydrogen bonding properties of the disaccharides. However, unduly importance should not be credited to the specific nature of the saccharide, the main properties relying in the HB networks it forms, which could also be modulated by other components of the systems as well as other drying procedures. In this respect it must be noticed that a similar inhomogeneous structure, obtained from Small Angle Neutron Scattering measurements, has been recently reported in frozen solutions of lysozyme, both containing and not containing saccharides [134], suggesting that the segregation is a general feature of these high concentrated protein solutions.

These results support a mechanism for saccharide bioprotection, or another factor increasing its effectiveness, based on water–buffering action, that would contrast the moisture variation by preferentially absorbing water molecules, and then slowly “melting” in a homogeneous phase above a certain hydration level. This gentle transition would prevent a random onset of function [93, 135, 136]. The different effectiveness of the various disaccharides arise, however, from a delicate equilibrium of many different properties of the disaccharide, the water buffering action being only one of them [94].

Chapter 8

Conclusions

The results obtained with the three techniques utilised in the present studies allow to have a description of the solid amorphous sugar matrices, of their mechanism of preservation and of the peculiarity of trehalose.

Based on some of the hypotheses currently present in the literature, which ascribe a noticeably role in the biopreservation to the specific interactions among sugar, water and embedded biostructures, large effort has been here devoted to the study of the properties of the HB network which establishes in saccharide amorphous matrices, and its relation with embedded myoglobin (used as a probe molecule).

This work was preceded by the identification and characterisation of a suitable marker for the study of HB network. This was found in the Water Association Band, or WAB, already used in the literature in the study of saccharide amorphous matrices [41–43, 137]. This infrared band has a noteworthy dependence of the environment of the water molecule, and is structured in dry saccharide solid matrices. The first step in this study was the identification of the populations of water molecules, which give rise to the sub–bands, taking also into account the limitations imposed in a study of a FTIR band of water, which prevent to assign these populations to single, well–defined, structures [97].

WAB was fitted in terms of five recurring sub–bands, which are present in most of the saccharide solid samples. The assignment of these components to families of water molecules was done by studying the behaviour of this band upon hydration and crystallistation, and with modification of the HB properties, making a conscious use of Hofmeister salts. These salts can have a structure–making or structure–breaking activity, and therefore they modify the HB network by enhancing or depressing local order. Addition of Hofmeister salts to trehalose

matrices made the population of the sub–bands to change accordingly to the nature of chaotrope or kosmotrope of the added salt. This allowed to assign the five components to either chaotropic (disordered) or kosmotropic (ordered) environment, and further define two of the components as bulk–like or ice–like water. This assignment has been proven valid also with matrices with embedded myoglobin; the protein was found to have a chaotropic nature, as expected due to the weak HB it can establish with the environment.

Once characterised the different components, the WAB was utilised to deepen the knowledge of other saccharide matrices, with and without protein, in comparison with trehalose. In this way, it has been shown that water in different dry saccharide matrices behaves differently, although with a general distribution in populations caused by the simultaneous presence of strengthened and weakened HB in different domains; this at least for the homologous disaccharides.

The different saccharide matrices also reacts differently to myoglobin introduction. In maltose and trehalose, the chaotropic effect of protein causes a transfer of population among different water classes, i.e. different environments, by increasing the components related to enhanced destructuration. At variance, in sucrose and raffinose, protein insertion causes more a perturbation of a single, bulk–like, averaged water population, with less effective partition in sub–populations. These differences flatten out upon hydration, where the WAB profile approaches the shape it has in water and very hydrated systems.

These findings from FTIR are in very good agreement with the results of SAXS measurements. These latter show that dry saccharide matrices containing myoglobin are not as homogeneous as one would suppose from macroscopic observation. The presence of random sugar–rich domains in a protein rich background was put in evidence, with different properties in different saccharide matrices. In trehalose and maltose these domains are small and high contrasted, being plausibly composed of hydrated sugar, or mainly sugar, clusters, whose presence has already been reported in the literature for maltose [56]. The presence of these domains could be at the basis of the permanence of different classes of water molecules in these matrices. In sucrose, at variance, only large and low–contrasted inhomogeneities seem to be present, which can be described as region with lower concentration of myoglobin with respect to its surroundings. This mesoscopic structure is mirrored, at molecular level, by the higher population of the bulk–like component of WAB in this matrix, which however undergoes overall a significant frequency red shift. Also the loss of structure which appears in WAB of hydrated samples reflects in the

progressive disappearance of the inhomogeneities showed by SAXS.

By combining the results of FTIR and SAXS, it has been therefore possible to put the disaccharides in order of matrix resistence to partition in domains with different protein:trehalose ratio and different structural order, as probed by water, upon adding protein: sucrose $>$ trehalose $>$ maltose. This is also supported by the study of the C–O stretching band, or COB, which put in evidence that the protein undergoes stronger stress conditions in sucrose and raffinose, as showed by the appearance of an unusual fourth substate.

The properties of the matrix were showed to be also dependent on the concentration ratio saccharide:protein. This dependence is not monotonous, but instead a quite sharp transition is evident between a sugar dominated regime and a protein dominated one. This transition is present also in the COB, indicating that there is a direct influence of the matrix on the protein. However, it has been shown that the COB transition is shifted at larger protein content. This indicated that three regions could be found: 1) a sugar–rich one, where sugar is the dominant component and the protein is found in an unstressed form, retaining a quite large amount of water to account for the saccharide hydration; 2) a protein–rich regime, in which the matrix is dominated by the presence of the protein, which conversely is under stress and where water retaining is necessary to hydrate the protein; 3) an intermediate zone, where a protein–dominated matrix is present together with a relatively well preserved protein. In this region the water content may reach minimal values and, such notwithstanding, the matrix is able to preserve the protein. It can be suggested that this region represents an "optimal" value for the biopreservation process and, at the same time, the one at which protein–matrix coupling establishes to a larger extent.

Beside the structural results, this coupling can be put forward also with the temperature dependence of the protein and the matrix bands. In dry systems the coupling is tight, while it is considerably weakened in hydrated samples, where the substantial similarity of the thermal behaviour of the different disaccharide matrices is opposed to different behaviours for the protein. This has been related to the different protein–disaccharide–water structures, which form at the protein–matrix interface, and with different fractions of water molecules bridging protein and saccharides, which would determine the strength of the constraints imposed on the protein, as reported by MD simulations [38, 39].

The importance of water, and in particular of the water present at the interface of the protein, was examined more in depth with MD simulations. Results pointed out that water dynamics is

the key factor for the whole matrix and protein dynamics. Shutting down water dynamics makes to reduce the protein large scale dynamics at high temperature. The dynamics dampening of the matrix is even larger: matrix atoms RMSFs reduce to the same order of magnitude of RMSFs of protein atoms, i.e. the entire system behaves like an harmonic solid. The influence of water in the system has been found to be mostly related to its ability to have translational motions, as no difference was noticed by acting on the water rotational degrees of freedom, in agreement with Tarek and Tobias [125]. By restricting the water motions in specific shells of different thickness around the protein, it has been possible to show that the fundamental role in controlling protein motions is devolved upon the water molecules closer to the protein (up to 3-6 Å from the protein surface), which in turn have a reduced dynamics because of the interactions with the protein. A similar behaviour has been noticed also for trehalose, even if at a reduced extent.

To sum up, FTIR spectra and MD simulations, at the atomistic level, and SAXS measurements, on a supramolecular scale, depict a structure for the protein–saccharide–water matrices, in which an extended water–saccharide HB network encompasses the whole system. The rigidity and dynamics of this network are modulated by water dynamics and content. Its effect on the embedded protein is controlled by water and sugar laying in the first shells around the protein. The thermal behaviour of the embedded protein and of the matrix result coupled and both the components concur in defining the whole system thermal properties, in agreement with DSC results [52, 53].

The comparison among various sugars matrices points out that, despite the structural similarity, saccharides interact with water and protein in different ways, giving different patterns of water populations and leading also to different mesoscopisc structures in the amorphous matrices.

This study suggested many different hints for understanding the better biopreserving properties of trehalose. Trehalose shows stronger interactions both with water and the protein, leading to a stronger protein–matrix coupling; at the same time the trehalose HB network appears ready to undergo changes upon protein addition, which produce less stress conditions for the protein. Through partitioning in domains, trehalose can have a water–buffering action, useful to prevent random onset of large biomolecular dynamics, and function, in different regions of the sample. At low concentration trehalose matrices are even able to absorb more water than the other saccharides, favouring a slow dehydration of the system during the process of trehalose production.

When dehydrated, instead, it has minimal tendency to crystallise, which would be detrimental to the preservation of biomolecules and biological structures, and can withstand high temperatures without onset of degradative processes such as Maillard reaction [52, 55].

All these properties concur to determine the trehalose preservation properties, nevertheless none of them can be called the “mechanism” of working of trehalose.

Bibliography

[1] L.M. Crowe, Lesson from nature: a role of sugars in anhydrobiosis, Comp. Biochem. Physiol. A 132 (2002) 505-513.

[2] J.H. Crowe, Trehalose as a "chemical chaperone": fact and fantasy, Adv. Exp. Med. Biol. 594 (2007) 143-158.

[3] M. Uritani, M. Takai, K. Yoshinaga, Protective effect of disaccharides on restriction endonucleases during drying under vacuum, J. Biochem. 117 (1995) 774-779.

[4] K.C. Fox, Biopreservation. Putting proteins under glass, Science 267 (1995) 1922-1923.

[5] J.L. Holovati, M.I.C. Gyongyossy–Issa, J.P. Acker, Effects of trehalose–loaded liposomes on red blood cell response to freezing and post–thaw membrane quality, Cryobiology 58 (2009) 7583.

[6] J.H. Crowe, L.M. Crowe, A.E. Oliver, N. Tsvetskova, W. Wolkers, F. Tablin, The Trehalose Myth Revisited: Introduction to a Symposium on Stabilization of Cells in the Dry State, Cryobiology, 43 (2001) 89-105.

[7] J. Green, C.A. Angell, Phase relations and vitrification in saccharide-water solutions and the trehalose anomaly, J. Phys. Chem. 93 (1989) 2880-2882.

[8] J.F. Carpenter, J.H. Crowe, An infrared spectroscopic study of the interaction of carbohydrates with dried proteins, Biochemistry 28 (1989) 3916-3922.

[9] P.S. Belton, A.M. Gil, IR and Raman spectroscopic studies of the interaction of trehalose with hen egg white lysozyme, Biopolymers 34 (1994) 957-961.

[10] S.N. Timasheff, Protein hydration, thermodynamic binding, and preferential Hydration, Biochemistry 41 (2002) 13473-13482.

[11] J.G. Sampedro, S. Uribe, Trehalose-enzyme interactions result in structure stabilization and activity inhibition, Mol. Cell Biochem. 256 (2004) 319-327.

[12] M.V. Galmarini, R. Baeza, V. Sanchez, M.C. Zamora, J. Chirife, Comparison of the viscosity of trehalose and sucrose solutions at various temperatures: Effect of guar gum addition, LWT–Food Sci. Technol. 44 (2011) 186-190.

[13] S.D. Allison, B. Chang, T.W. Randolph, J.F. Carpenter, Hydrogen bonding between sugar and protein is responsible for inhibition of dehydration–induced protein unfolding, Arch. Biochem. Biophys. 365 (1999) 289-298.

[14] G. Caliskan, A. Kisliuk, A.M. Tsai, C.L. Soles, A.P. Sokolov, Influence of solvent on dynamics and stability of a protein, J. Non–Cryst. Solids 307310 (2002) 887893.

[15] W.F. Wolkers, H. Oldenhof, M. Alberda, F.A. Hoekstra, A Fourier transform infrared microspectroscopy study of sugar glasses: application to anhydrobiotic higher plant cells, Biochim. Biophys. Acta-Gen. Subj. 1379 (1998) 83-96.

[16] S.H. Gaffney, E. Haslam, T.H. Lilley, T.R.J. Ward, Homotactic and heterotactic interactions in aqueous-solutions containing some saccharides experimental results and an empirical relationship between saccharide solvation and solute interactions, J. Chem. Soc. Faraday Trans. 84 (1998) 2545-2552.

[17] F. Sussich, C. Skopec, J. Brady, A. Cesàro, Reversible dehydration of trehalose and anhydrobiosis: from solution state to an exotic crystal?, Carbohydr. Res. 334 (2001) 165-176.

[18] C. Branca, S. Magazù, G. Maisano, P. Migliardo, Anomalous cryoprotective effectiveness of trehalose: Raman scattering evidences, J. Chem. Phys. 11 (1999) 281-288.

[19] S. Magazù, G. Maisano, F. Migliardo, C. Mondelli, Mean-square displacement relationship in bioprotectant systems by elastic neutron scattering, Biophys. J. 86 (2004) 3241-3249.

[20] S. Magazù, F. Migliardo, M.T.F. Telling, Structural and dynamical properties of water in sugar mixtures, Food Chem. 106 (2008) 1460-1466.

[21] S.L. Lee, P.G. Debenedetti, J.R. Errington, A computational study of hydration, solution structure, and dynamics in dilute carbohydrate solutions, J. Chem. Phys. 122 (2005) 204511.

[22] S.B. Engelsen, C. Monteiro, C. Hervé de Penhoat, S. Pérez, The diluted aqueous solvation of carbohydrates as inferred from molecular dynamics simulations and NMR spectroscopy, Biophys. Chem., 93 (2001) 103-127.

[23] M.T. Cicerone, C.L. Soles, Fast Dynamics and Stabilization of Proteins: Binary Glasses of Trehalose and Glycerol, Biophys. J. 86 (2004) 3836-3845.

[24] A. Hédoux, J-F. Willart, R. Ionov, F. Affouard, Y. Guinet, L. Paccou, A. Lerbret, M. Descamps, Analysis of sugar bioprotective mechanisms on the thermal denaturation of lysozyme from Raman scattering and differential scanning calorimetry investigations, J. Phys. Chem. B 110 (2006) 22886-22893.

[25] J.-A. Seo, A. Hédoux, Y. Guinet, L. Paccou, F. Affouard, A. Lerbret, M. Descamps, Thermal Denaturation of Beta-Lactoglobulin and Stabilization Mechanism by Trehalose Analyzed from Raman Spectroscopy Investigations, J. Phys. Chem. B 114 (2010) 6675-6684.

[26] A. Lerbret, F. Affouard, P. Bordat, A. Hedoux, Y. Guinet, M. Descamps, Low-frequency vibrational properties of lysozyme in sugar aqueous solutions: a Raman scattering and molecular dynamics simulation study, J. Chem. Phys. 24 (2009) 245103.

[27] A. Hédoux, F. Affouard, M. Descamps, Y. Guinet L. Paccou, Microscopic description of protein thermostabilization mechanisms with disaccharides from Raman spectroscopy investigations, J. Phys.–Condens. Matter 19 (2007) 205142.

[28] A. Hédoux, J.F. Willart, L.Paccou, Y.Guinet, F.Affouard, A.Lerbret, M. Descamps, Thermostabilization Mechanism of Bovine Serum Albumin by Trehalose, J. Phys. Chem. B 113 (2009) 6119-6126.

[29] A. Lerbret, F. Affouard, P. Bordat, A. Hédoux, Y. Guinet, M. Descamps, Slowing down of water dynamics in disaccharide aqueous solutions, J. Non–Cryst. Solids 357 (2011) 695-699.

[30] L. Cordone, M. Ferrand, E. Vitrano, G.Zaccai, Harmonic Behavior of Trehalose-Coated Carbon-Monoxy-Myoglobin at High Temperature, Biophys. J., 76 (1999) 1043-1047

[31] L. Cordone, G. Cottone, S. Giuffrida, G. Palazzo, G. Venturoli, C. Viappiani, Internal dynamics and protein-Matrix coupling in trehalose coated proteins, BBA-Proteins Proteomics 1749 (2005) 252-281.

[32] L. Cordone, G. Cottone, S. Giuffrida, Role of residual water hydrogen bonding in sugar/water/biomolecule systems: a possible explanation for trehalose peculiarity, J. Phys.–Condens. Matter 19 (2007) 205110.

[33] A. Lerbret, F. Affouard, A. Hédoux, S. Krenzlin, J. Siepmann, M.C. Bellissent-Funel, M. Descamps, J. Phys. Chem. B. 116 (2012), 11103-11116.

[34] F. Francia, M. Dezi, A. Mallardi, G. Palazzo, L. Cordone, G. Venturoli, Protein-matrix coupling/uncoupling in "dry" systems of photosynthetic Reaction Center embedded in trehalose/sucrose: the origin of trehalose peculiarity. J. Am. Chem. Soc. 130 (2008) 10240-10246.

[35] A. Savitsky, M. Malferrari, F. Francia, G. Venturoli, K.laus Möbius, Bacterial Photosynthetic Reaction Centers in Trehalose Glasses: Coupling between Protein Conformational Dynamics and Electron–Transfer Kinetics as Studied by Laser–Flash and High–Field EPR Spectroscopies, J. Phys. Chem. B 114 (2010) 12729-12743.

[36] G. Cottone, L. Cordone, G. Ciccotti, Molecular Dynamics simulation of carboxymyoglobin embedded in a trehalose–water Matrix, Biophys. J. 80 (2001) 931-938.

[37] G. Cottone, G. Ciccotti, L. Cordone, Protein–trehalose–water structures in trehalose coated carboxy–myoglobin, J. Chem. Phys. 117 (2002) 9862-9866.

[38] G. Cottone, S. Giuffrida, G. Ciccotti, L. Cordone, Molecular dynamics simulation of sucrose– and trehalose–coated carboxy–myoglobin, Proteins 59 (2005) 291-302.

[39] G. Cottone, A comparative study of carboxy myoglobin in saccharide–water systems by Molecular Dynamics simulation, J. Phys. Chem. B 111 (2007) 3563-3569.

[40] M.V. Fedorov, J.M. Goodman, D. Nerukh, S. Schumm, Self–assembly of trehalose molecules on a lysozyme surface: the broken glass hypothesis, Phys. Chem. Chem. Phys. 13 (2011) 2294-2299.

[41] S. Giuffrida, G. Cottone, F. Librizzi, L. Cordone, Coupling between the thermal evolution of the heme pocket and the external matrix structure in trehalose coated carboxymyoglobin, J. Phys. Chem. B 107 (2003) 13211-13217.

[42] S. Giuffrida, G. Cottone, L. Cordone, Structure–dynamics coupling between protein and external matrix in sucrose–coated and in trehalose-coated MbCO: an FTIR study, J. Phys. Chem. B 108 (2004) 15415-15421.

[43] S. Giuffrida, G. Cottone, L. Cordone, Role of solvent on protein–matrix coupling in MbCO embedded in water-saccharide systems: a Fourier Transform Infrared spectroscopy study, Biophys. J. 91 (2006) 968-980.

[44] U. Samuni, D. Dantsker, C.J. Roche, J.M. Friedman, Ligand recombination and a hierarchy of solvent slaved dynamics: the origin of kinetic phases in hemeproteins. GENE 398 (2007) 234-248 and references therein.

[45] A.M. Massari, I.J. Finkelstein, B.L. McClain, A.Goj, X. Wen, K.L. Bren, R.F. Loring, M.D. Fayer. The Influence of Aqueous versus Glassy Solvents on Protein Dynamics: Vibrational Echo Experiments and Molecular Dynamics Simulations, J. Am. Chem. Soc. 127 (2005) 14279-14289.

[46] M. Heyden, E. Bründermann, U. Heugen, G. Niehues, D.M. Leitner, M. Havenith, Long–range influence of carbohydrates on the solvation dynamics of waters — answers from terahertz absorption measurements and molecular modeling simulations, J. Am. Chem. Soc. 130 (2008) 5773-5779.

[47] Q. Liu, R.K. Schmidt, B. Teo, P.A. Karplus, J.W. Brady, Molecular Dynamics Studies of the Hydration of α,α–Trehalose, J. Am. Chem. Soc. 119 (1997) 7851-7862.

[48] M. Paolantoni, L. Comez, M. E. Gallina, P. Sassi, F. Scarponi, D. Fioretto, A. Morresi, Light Scattering Spectra of Water in Trehalose Aqueous Solutions: Evidence for Two Different Solvent Relaxation Processes, J. Phys. Chem. B. 113 (2009) 7874-7878.

[49] L. Lupi, L. Comez, M. Paolantoni, D. Fioretto, B. M. Ladanyi, Dynamics of Biological Water: Insights from Molecular Modeling of Light Scattering in Aqueous Trehalose Solutions J. Phys.Chem. B. 116 (2012) 7499-7508.

[50] S. Perticaroli, L. Comez, M. Paolantoni, P. Sassi, L.Lupi, D. Fioretto, A. Paciaroni, A. Morresi, Broadband Depolarized Light Scattering Study of Diluted Protein Aqueous Solutions, J. Phys. Chem. B. 114 (2010) 8262-8269.

[51] C. Schebor, M.F. Mazzobre, M.P. Buera, Glass transition and time-dependent crystallization behavior of dehydration bioprotectant sugars, Carbohydr. Res. 345 (2010) 303-308.

[52] G. Bellavia, G. Cottone, S. Giuffrida, A. Cupane, L. Cordone, Thermal denaturation of myoglobin in water–disaccharide matrixes: relation with the glass transition of the system, J. Phys. Chem. B 113 (2009) 11543-11549.

[53] G. Bellavia, S. Giuffrida, G. Cottone, A. Cupane, L. Cordone, Protein Thermal Denaturation And Matrix Glass Transition In Different Protein–Trehalose–Water Systems, J. Phys. Chem. B 115 (2011) 6340-6346.

[54] D. Voet,J.G. Voet, Biochimica, ed. Zanichelli, Bologna, Italy (1993).

[55] P. Cappelli, V. Vannucchi, Chimica degli alimenti. Conservazione e trasformazioni, ed. Zanichelli, Bologna, Italy (1994).

[56] A. Lerbret, P. Bordat, F. Affouard, M. Descamps, F. Migliardo, How homogeneous are the trehalose, maltose, and sucrose water solutions? An insight from molecular dynamics simulations. J. Phys. Chem. B 109 (2005) 11046-11057.

[57] S. Fischer, D. Hopkinson, M. Liu, A.A. MacLean, V. Edwards, E. Cutz & al., Raffinose improves 24hour lung preservation in low potassium dextran glucose solution: a hystologic and ultrastructural analysis, Ann. Thorac. Surg. 71 (2001) 1140-1145.

[58] K.E. van Holde, P. S. Ho, W.C. Johnson, Principles of Physical Biochemistry, ed. Prentice Hall, Upper Saddle River, New Jersey, USA (1998).

[59] D. Beece, L. Eisenstein, H. Frauenfelder, D. Good, M.C. Marden, L. Reinisch, A.H. Reynolds, L.B. Sorensen, K.T. Yue, Solvent viscosity and protein dynamics, Biochemistry 19 (1980) 5147-5157.

[60] A. Ansari, J. Berendzen, D. Braunstein, B.R. Cowen, H. Frauenfelder, M.K. Hong, I.E.T. Iben, J.B. Johnson, P. Ormos, T.B. Sauke, R. Scholl, A. Schulte, P.J. Steinbach, J. Vittitow, R.D. Young, Rebinding and relaxation in the myoglobin pocket, Biophys. Chem. 26 (1987) 337-355.

[61] D. Vitkup, D. Ringe, G.A. Petsko, M. Karplus, Solvent mobility and the protein 'glass' transition, Nat. Struct. Biol. 7 (2000) 34-38.

[62] F. Librizzi, C. Viappiani, S. Abbruzzetti, L. Cordone, Residual Water modulates the dynamics of the protein and of the external matrix in "trehalose coated" MbCO: an infrared and flash–photolysis study. J. Chem. Phys. 116 (2002) 1193-1200.

[63] S. Abbruzzetti, S. Giuffrida, S. Sottini, C. Viappiani, L. Cordone, Light–Induced Protein–Matrix Uncoupling and Protein Relaxation in Dry Samples of Trehalose-Coated MbCO at Room Temperature, Cell Biochem. Biophys. 43 (2005) 431-437.

[64] F. Librizzi, E. Vitrano, L. Cordone, Dehydration and crystallization of trehalose and sucrose glasses containing carbonmonoxy–myoglobin, Biophys. J. 76 (1999) 2727-2734.

[65] L. Cordone, G. Cottone, S. Giuffrida, F. Librizzi, Thermal evolution of the CO stretching band in carboxy–myoglobin in the light of neutron scattering and molecular dynamics simulations, Chem. Phys. 345 (2008) 275-282.

[66] F. Hofmeister, Zur Lehre von der Wirkung der Salze, Arch. Exp. Pathol. Pharmakol., 24 (1888) 247-260.

[67] K.D. Collins, M.W. Washabaugh, The Hofmeister series and the behaviour of water interfaces. Quart. Rev. Biophys. 18 (1985) 323-422.

[68] M.G. Cacace, E.M. Landau, J.J. Ramsden, The Hofmeister series: salt and solvent effects on interfacial phenomena. Quart. Rev. Biophys. 30 (1997) 241-277.

[69] P. Lo Nostro, B.W. Ninham, S. Milani, L. Fratoni, P. Baglioni, Specific Anion Effects on the Optical Rotation of Glucose and Serine, Biopolymers, 81 (2006) 136-148.

[70] N.V. Nucci, J.M. Vanderkooi, Effects of salts of the Hofmeister series on the hydrogen bond network of water, J. Mol. Liq. 143 (2008) 160170.

[71] Y. Zhang, P.S. Cremer, Interactions between macromolecules and ions: the Hofmeister series, Curr. Op. Chem. Biol. 10 (2006) 658-663.

[72] A. Aroti, E. Leontidis, E. Maltseva, G. Brezesinskii, Effects of Hofmeister Anions on DPPC Langmuir Monolayers at the Air–Water Interface, J. Phys. Chem. B 108 (2004) 15238-15245.

[73] B.W. Ninham, V. Yaminsky, Ion Binding and Ion Specificity: The Hofmeister Effect and Onsager and Lifshitz Theories, Langmuir 13 (1997) 2097-2108.

[74] P. Lo Nostro, L. Fratoni, B.W. Ninham, P. Baglioni, Water Absorbency by Wool Fibers: Hofmeister Effect, Biomacromolecules 3 (2002) 1217-1224.

[75] E. Chiotelli, G. Pilosio, M. Le Meste, Effect of Sodium Chloride on the Gelatinization of Starch: A Multimeasurement Study, Biopolymers, 63 (2002) 41-58.

[76] W. Wachter, W. Kunz, R. Buchner, G. Hefter, Is There an Anionic Hofmeister Effect on Water Dynamics? Dielectric Spectroscopy of Aqueous Solutions of NaBr, NaI, $NaNO_3$, $NaClO_4$, and NaSCN, J. Phys. Chem. A 109 (2005) 8675-8683.

[77] H.J. Bakker, Structural Dynamics of Aqueous Salt Solutions, Chem. Rev. 108 (2008) 1456-1473.

[78] P. Ball, Water as an Active Constituent in Cell Biology, Chem. Rev. 108 (2008) 74-108.

[79] A. Dér, L. Kelemen, L. Fábián, S.G. Taneva, E. Fodor, T. Páli, A. Cupane, M.G. Cacace, J.J. Ramsden, Interfacial Water Structure Controls Protein Conformation, J. Phys. Chem. B 111 (2007) 5344-5350.

[80] J.D. Batchelor, A. Olteanu, A. Tripathy, G.J. Pielak, Impact of Protein Denaturants and Stabilizers on Water Structure, J. Am. Chem. Soc. 126 (2004) 1958-1961.

[81] S. Moelbert, B. Normand, P. De Los Rios, Kosmotropes and chaotropes: modelling preferential exclusion, binding and aggregate stability, Biophys. Chem. 112 (2004) 45-57.

[82] J.M. Broering, A.S. Bommarius, Evaluation of Hofmeister Effects on the Kinetic Stability of Proteins, J. Phys. Chem. B 109 (2005) 20612-20619.

[83] R. Vogel, G.B. Fan, M. Sheves, F. Siebert, Salt Dependence of the Formation and Stability of the Signaling State in G Protein–Coupled Receptors: Evidence for the Involvement of the Hofmeister Effect, Biochemistry 40 (2001) 483-493.

[84] V. Ragoonanan, A. Aksan, Heterogeneity in Desiccated Solutions: Implications for Biostabilizationi, Biophys. J. 94 (2008) 2212-2227.

[85] H. Frauenfelder, F. Parak, R. D. Young, Conformational substates in proteins, Annu. Rev. Biophys. Chem. 17 (1988) 451-479.

[86] J. Vojtěchovský, K. Chu, J. Berendzen, R. M. Sweet, I. Schlichting, Crystal structures of myoglobin–ligand complexes at near-atomic resolution, Biophys. J. 77 (1999) 2153–2174.

[87] D. Eisenberg, W. Kauzmann, The structure and properties of water, Oxford University Press, London, 1969.

[88] J.P. Devlin, J. Sadlej, V. Buch, Infrared Spectra of Large H_2O Clusters: New Understanding of the Elusive Bending Mode of Ice, J. Phys. Chem. A 105 (2001) 974-983.

[89] H.D. Lutz, W. Pobitschka, B. Frischemeier, R.–A. Becker, Lattice Vibration Spectra. XX. Infrared and Raman Spectra of $BaCl_2{\cdot}2H_2O$ and $BaCl_2{\cdot}2D_2O$, Appl. Spectrosc. 32 (1978) 541-547.

[90] B. Wozniak, J. Dera, Light Absorption in Sea Water, Springer Science+Business Media LLC, New York, NY, USA, 2007.

[91] J.–J. Max, C. Chapados, Isotope effects in liquid water by infrared spectroscopy, J. Chem. Phys. 116 (2002) 4626-4642.

[92] V. Razumas, Z. Talaikytė, J. Barauskas, Y. Miezis, T. Nylander, An FT–IR study of the effects of distearoyphosphatidylglycerol and cytochrome *c* on the molecular organization of the monoolein–water cubic liquid–crystalline phase, Vib. Spectrosc. 15 (1997) 91–101.

[93] A. Longo, S. Giuffrida, G. Cottone, L. Cordone, Myoglobin embedded in saccharide amorphous matrices: water-dependent domains evidenced by Small Angle X-Ray Scattering, Phys. Chem. Chem. Phys. (2010) 6852-6858.

[94] S. Giuffrida, M. Panzica, F.M. Giordano, A. Longo. SAXS study on myoglobin embedded in amorphous saccharide matrices, Eur. Phys. J. E 34 (2011) 87.

[95] M. Malferrari, F. Francia, G. Venturoli, Coupling between Electron Transfer and Protein–Solvent Dynamics: FTIR and Laser–Flash Spectroscopy Studies in Photosynthetic Reaction Center Films at Different Hydration Levels, J. Phys. Chem. B, 115 (2011), 14732–14750.

[96] A. Nilsson, A. Holmgren, G. Lindblom, Fourier–Transform Infrared Spectroscopy Study of Dioleoylphosphatidylcholine and Monooleoylglycerol in Lamellar and Cubic Liquid Crystals, Biochemistry, 30 (1991) 2126-2133.

[97] K.A. Sharp, B. Madan, E. Manas, J.M. Vanderkooi, Water structure changes induced by hydrophobic and polar solutes revealed by simulations and infrared spectroscopy, J. Chem. Phys. 114 (2001) 1791-1796.

[98] S. Giuffrida, G. Cottone, E. Vitrano, L. Cordone, A FTIR study on low hydration saccharide amorphous matrices: thermal behaviour of the Water Association Band. J. Non–Cryst. Solids, 357 (2011) 677-682.

[99] K. Haxaire, Y. Maréchal, M. Milas, M. Rinaudo, Hydration of Hyaluronan Polysaccharide Observed by IR Spectrometry. II. Definition and Quantitative Analysis of Elementary Hydration Spectra and Water Uptake, Biopolymers 72 (2003) 149-161.

[100] X. Zhou, P. Hines, M.W. Borer, Moisture determination in hygroscopic drug substances by Near Infrared Spectroscopy, J. Pharm. Biomed. Anal. 17 (1998) 219-225.

[101] E.A. Galinski, M. Stein, B. Amendt, M Kinder, The Kosmotropic (Structure-Forming) Effect of Compensatory Solutes, Comp. Biochem. Physiol. 117A (1997) 357-365.

[102] P.B. Conrad, J.J. de Pablo, Computer Simulation of the Cryoprotectant Disaccharide α,α-Trehalose in Aqueous Solution. J. Phys. Chem. A 103 (1999) 4049-4055.

[103] J.C. Phillips, R. Braun, W. Wang, J. Gumbart, E. Tajkhorshid, E. Villa, C. Chipot, R.D. Skeel, L. Kale, K. Schulten, Scalable molecular dynamics with NAMD, J. Comp. Chem. 26 (2005) 1781-1802.

[104] A.D. MacKerell, Jr., N. Banavalii, N. Foloppe, Development and current status of the CHARMM force field for nucleic acids, Biopolymers 56 (2001) 257–265.

[105] O. Guvench, S.S. Mallajosyula, E.P. Raman, E.R. Hatcher, K. Vanommeslaeghe, T.J. Foster, F.W. Jamison, A.D. MacKerell, Jr., CHARMM Additive All–Atom Force Field for Carbohydrate Derivatives and Its Utility in Polysaccharide and Carbohydrate-–Protein Modeling, J. Chem. Theory Comput., 7 (2011) 3162–3180.

[106] W.L. Jorgensen, J. Chandrasekhar, J.D. Madura, R.W. Impey, M.L. Klein, Comparison of simple potential functions for simulating liquid water, J. Chem. Phys. 9 (1983) 926-935.

[107] T. Taga, M. Senma, K. Osaki, The crystal and molecular structure of trehalose dihydrate, Acta Crystallogr. B 29 (1972) 3258–3263.

[108] X. Cheng, B.P. Schoenborn, Hydration in protein crystals: a neutron diffraction analysis of carbonmonoxymyoglobin, Acta Crystallogr. B 46 (1990) 195-208.

[109] M.P. Allen, D.J. Tildesley, Computer simulation of liquids, Clarendon Press, Oxford, UK, 1987.

[110] U. Essmann, L. Perera, M. Berkowitz, T. Darden, H. Lee, L.G. Pedersen, A smooth particle mesh Ewald method, J. Chem. Phys. 103 (1995) 8577-8593.

[111] J.P. Ryckaert, G. Ciccotti, H.J.C. Berendsen, Numerical integration of the Cartesian equations of motion of a system with constraints: molecular dynamics of n-alkanes, J. Comp. Phys. 23 (1977) 327-341.

[112] G. Ciccotti, J.P. Ryckaert, Molecular dynamics simulations of rigid molecules, Comp. Phys. Rep. 4 (1986) 345-392.

[113] H.C. Andersen, Rattle: a "velocity" version of the shake algorithm for molecular dynamics calculations, J. Comput. Phys. 52 (1983) 24-34.

[114] W. Humphrey, A. Dalke, K. Schulten, VMD – Visual Molecular Dynamics, J. Molec. Graphics, 14 (1996) 33-38.

[115] L.A. Feigin, D.I. Svergun, Structure Analysis by Small Angle X–Ray and Neutron Scattering, Plenum Press, New York, 1987.

[116] P. Debye, H.R. Anderson and H. Brumberger, J. Appl. Phys., 1957, 28, 679-683.

[117] H. Brunberger, Aspect of Small–Angle Scattering, Kluwer Academic Publishers, Dordrecht, NL, 1993.

[118] J.S. Pedersen, Analysis of small–angle scattering data from colloids and polymer solutions: modeling and least–squares fitting, Adv. Colloid Interface Sci., 70 (1997) 171-210.

[119] R. Giangiacomo, Study of water–sugar interactions at increasing sugar concentration by NIR spectroscopy, Food Chem. 96 (2006) 371-379.

[120] P. Westh, H. Kato, K. Nishikawa, Y. Koga, Toward Understanding the Hofmeister Series. 3. Effects of Sodium Halides on the Molecular Organization of H_2O As Probed by 1–Propanol, J. Phys. Chem. A 110 (2006) 2072-2078.

[121] K. Saitow, K. Kobayashi, K. Nishikawa, How are Hydrogen Bonds Perturbed in Aqueous $NaClO_4$ Solutions Depending on the Concentration?: A Near Infrared Study of Water, J. Sol. Chem. 33 (2004) 689-698.

[122] S. Magaziù, F. Migliardo, A. Benedetto, R. La Torre, L. Hennet, Bio–protective effects of homologous disaccharides on biological macromolecules, Eur. Biophys. J., 41 (2011) 361-367.

[123] S.B. Leslie, E. Israeli, B. Lighthart, J.H. Crowe, L.M. Crowe, Trehalose and sucrose protect both membranes and proteins in intact bacteria during drying, Appl. Environ. Microbiol. 91 (1995) 3592-3597.

[124] S.J. Prestrelski, K.A. Pikal, T. Arakawa, Optimization of lyophilization conditions for recombinant human interleukin2 by dried state conformational analysis using Fourier-Transform Infrared Spectroscopy, Pharm. Res. 12 (1995) 1250-1259.

[125] M. Tarek, D.J. Tobias, Role of Protein–Water Hydrogen Bond Dynamics in the Protein Dynamical Transition, Phys. Rev. Lett. 88 (2002) 138101

[126] F. Parak, H. Formanek, Untersuchung des Schwingungsanteils und des Kristallgitterfehleranteils des Temperaturfaktors in Myoglobin durch Vergleich von Mössbauerabsorptionsmessungen mit Röntgenstrukturdaten, Acta Crystallogr., A27 (1971) 573-578.

[127] F. Parak, E.N. Frolov, R.L. Mössbauer, V.I. Goldanskii, Dynamics of metmyoglobin crystals investigated by nuclear gamma resonance absorption, J. Mol. Biol. 145 (1981) 825-833.

[128] M.M. Teeter, A. Yamano, B. Stec, U. Mohanty, On the nature of a glassy state of matter in a hydrated protein: relation to protein function, Proc. Nat. Acad. Sci. USA 98 (2001) 11242-11247.

[129] R.D. Lins, C.S. Pereira, P.H. Hunemberger, Trehalose–protein interaction in aqueous solution, Proteins 55 (2004) 177-186.

[130] P. Ahlström, O. Teleman, B. Jönsson, Molecular Dynamics Simulation of Interfacial Water Structure and Dynamics in a Parvalbumin Solution, J. Am. Chem. Soc., 110 (1988) 4198-4203.

[131] G.M. Brown, H.A. Levy, Further refinement of the structure of sucrose based on neutron–diffraction data, Acta Cryst. B29 (1973) 790-797.

[132] K. Ibel, H.B. Stuhrmann, Comparison of neutron and X–ray scattering of dilute myoglobin solutions, J. Mol. Biol. 93 (1975) 255-266.

[133] Y.H. Lam, R. Bustami, T. Phan, H.K. Chan, F. Separovic, J. Pharm. Sci., 91 (2002) 943-951.

[134] J.E. Curtis, H. Nanda, S. Khodadadi, M. Cicerone, H. J. Lee, A. McAuley, S. Krueger, Small-Angle Neutron Scattering Study of Protein Crowding in Liquid and Solid Phases: Lysozyme in Aqueous Solution, Frozen Solution, and Carbohydrate Powders, J. Phys. Chem. B0 116 (2012) 9653-9667.

[135] A. Cesàro, Carbohydrates: All dried up, Nature Materials 5 (2006) 593-594.

[136] D. Kilburn, S. Townrow, V. Meunier, R. Richardson, A. Alam, J. Ubbink, Organization and mobility of water in amorphous and crystalline trehalose, Nature Materials 5 (2006) 632-635.

[137] S. Giuffrida, R. Troia, C. Schiraldi, A. D'Agostino, M. De Rosa, L. Cordone, MbCO Embedded in Trehalosyldextrin Matrices: Thermal Effects and Protein-Matrix Coupling, Food Biophys. 6 (2011) 217-226.